5-2010

# Plutonium - Humic Acid Stability Constant Determination and Subsequent Studies Examining Sorption in the Ternary Pu(IV) - Humic Acid - Gibbsite System

Trevor Zimmerman
*Clemson University*, Trevorz@clemson.edu

# PLUTONIUM-HUMIC ACID STABILITY CONSTANT DETERMINATION AND SUBSEQUENT STUDIES EXAMINING SORPTION IN THE TERNARY Pu(IV) – HUMIC ACID – GIBBSITE SYSTEM

---

A Thesis
Presented to
the Graduate School of
Clemson University

---

In Partial Fulfillment
of the Requirements for the Degree
Master of Science
Environmental Engineering

---

by
Trevor Nathan Zimmerman
May 2010

---

Accepted by:
Dr. Brian Powell, Committee Chair
Dr. Cindy Lee
Dr. Mark Schlautman

# ABSTRACT

Plutonium has been released to the environment through a variety of intentional and unintentional mechanisms, including atmospheric testing, disposition from weapons manufacturing processes, and subsurface disposal. Therefore, a thorough understanding of the chemical, physical, and biological processes affecting plutonium transport is imperative. It has been shown that humic acid (HA) (a refractory component of natural organic matter (NOM)) can effectively solubilize plutonium (Santschi *et al.*, 2002). Increased solubility may result in enhanced subsurface transport, due to the higher concentration of Pu in the aqueous phase. In contrast, the formation of ternary surface complexes may hinder actinide transport. Solution pH is likely to affect the dominance of one species over another. For these reasons, a better understanding of binary Pu-HA and Pu-mineral and ternary Pu-HA-mineral systems is essential for accurately predicting plutonium fate and transport.

The primary objective of this research was to determine the conditional stability constant for Pu-HA complexes using a hybrid ultra-filtration/equilibrium dialysis ligand exchange (EDLE) technique from pH 4 to 6.5. Ethylenediaminetetraacetic acid (EDTA) was used as a reference ligand to allow the aqueous chemistry of the Pu-HA system to be probed at increased pH, without appreciable metal hydrolysis.

The conditional stability constant for Pu(IV) complexation with Leonardite HA determined as part of this work is $\log\beta_{112} = 6.76 \pm 0.14$. This stability constant is valid over the pH range 4 – 6.5 and I = 0.1 M NaCl, for the equation shown below:

$$Pu^{4+} + HL3 + 2H_2O \leftrightarrow Pu(OH)_2L3^{+} + 3H^{+} \qquad \text{Log } \beta_{112} = 6.76 \pm 0.14$$

where HA is represented by HL3 (a binding site on the HA with a pKa value of 7).

The conditional stability constant for Th(IV) complexation with Leonardite HA was also determined. Over the pH range 4 – 6.5 the value $\log\beta_{112} = 4.63 \pm 0.04$ was calculated (I = 0.1 M NaCl) for the reaction shown below:

$$Th^{4+} + HL1 + 2H_2O \leftrightarrow Th(OH)_2L1^{+} + 3H^{+} \qquad \text{Log } \beta_{112} = 4.63 \pm 0.04$$

where HL1 represents a pKa 3 binding site on the HA.

Preliminary sorption studies using gibbsite were also conducted to evaluate the effects of Pu-HA complex formation on Pu sorption behavior. Enhanced Pu sorption to gibbsite was observed in the presence of HA. Notably, enhanced sorption was observed at low pH (pH 4) which is indicative of ligand promoted sorption. Therefore, despite observations of increased solubility of Pu in the presence of HA, the formation of ternary surface complexes may prevent enhanced subsurface transport. The data from these studies will aid in modeling the fate and transport of Pu in the environment and inform the development of conceptual models describing the influence of ternary surface complex formation on Pu sorption.

# DEDICATION

Dedicated to my wife, Bonnie, with my love and appreciation.

# ACKNOWLEDGMENTS

Thanks to God above all.

To Bonnie, the love of my life, your steadfast support has made so many things possible, my heartfelt thanks.

My gratitude also goes to my advisor, Dr. Brian Powell, who gave me a challenge and showed me the way. Your knowledge, patience, and enthusiasm have been invaluable. Thank you for giving me the opportunity to work with you.

I would like to acknowledge my committee, Dr. Cindy Lee and Dr. Mark Schlautman, your feedback has elevated the caliber of this manuscript tremendously.

To Dr. Timothy DeVol, Dr. Robert Fjeld, Amy Hixon, Michael Lilley, Todd Miller, and the whole radiochemistry group, thank you for your feedback.

I would like to thank my entire family. Scott and Sonja, thank you for your support over the years; Shearer and Bonita, thank you for your encouragement during graduate school; and Grandma and Grandpa Zimmerman, thank you for all our Sunday evening discussions.

Finally, I would like to acknowledge the many baristas who provided the caffeine that made this thesis possible.

TABLE OF CONTENTS

Page

Table of Contents (Continued)

Page

LIST OF TABLES

List of Tables (Continued)

Table Page

LIST OF FIGURES

List of Figures (Continued)

Figure Page

List of Figures (Continued)

Figure Page

List of Figures (Continued)

Figure Page

List of Figures (Continued)

Figure Page

# CHAPTER ONE

## INTRODUCTION

The proliferation of nuclear materials and technology has led to the introduction of anthropogenic radionuclides into the environment. Between July 1945 and September 1992 the United States detonated over 1000 nuclear devices (DOE, 2000). The Nevada Test Site (NTS) alone was the site of more than 900 detonations, resulting in an inventory of radioactive material in excess of $10^8$ Ci (DOE, 2000 and Kersting *et al.*, 1999). Deposition from atmospheric testing, accidental releases (*e.g.*, Chernobyl), and subsequent transport have served to ensure that radionuclides such as Pu are now ubiquitous. Atmospheric testing of nuclear weapons is thought to be responsible for the majority of the Pu found in the environment. It is estimated that approximately 10,000 kg of Pu was released during these tests (Argonne, 2005). As a result of subsequent atmospheric deposition, current Pu levels in surface soils range from about 0.01 to 0.1 picocurie per gram (pCi/g) (Argonne, 2005). Contamination at locations such as weapons manufacturing facilities (*e.g.*, Rocky Flats), nuclear accident sites (*e.g.*, Chernobyl), radioactive waste storage facilities (*e.g.*, Hanford and the Savannah River Site (SRS)), and weapons testing sites (*e.g.*, NTS) are generally observed to be much higher.

The Yucca Mountain Repository is no longer the proposed storage site for nuclear waste in the United States (Hebert, 2009). However, many countries, including the U.S., still view deep geological burial as the only currently viable, long-term radioactive waste disposal option. Regardless of the storage location, or the containment practices

employed, the possible release mechanisms and the processes controlling contaminant transport must be understood. For example, one primary concern with deep geological burial is groundwater facilitated radionuclide transport. Therefore, understanding groundwater flow in and around a storage site is essential. Also, an understanding of the chemical, physical, and biological processes at work in the system of interest is imperative. Processes of interest, which play a critical role in contaminant transport, include oxidation/reduction (redox), complexation, sorption/desorption, and solubility. The purpose of this thesis is to examine the interaction between Pu and humic acid (HA) (a refractory component of natural organic matter) in the context of these various processes. Specifically, the conditional stability constant for the Pu – HA complex will be determined.

# CHAPTER TWO

# BACKGROUND

## NATURAL ORGANIC MATTER

Sposito refers to soils as a "biological milieux teeming with microorganisms" (Sposito, 1989). These microorganisms serve a variety of essential functions such as the production of organic acids which can readily form soluble complexes with metals through a variety of functional moieties such as carboxyl, hydroxyl, and amino groups (Sposito, 1989). These organic acids combine with carbohydrates, amino acids, and other organic matter to produce what is collectively referred to as humus. Another important component of humus is humic substances (HS) which differ from the biopolymers mentioned previously by virtue of their refractory nature (Sposito, 1989). Humic

substances can be further subdivided into three groups using operationally defined criteria. Specifically, HA is the portion of HS that is soluble above pH 2, fulvic acid (FA) is soluble at all pH values, and humin is not soluble in water (Sposito, 1989). HAs are generally larger (*i.e.,* more polymerized) than FAs (Sposito, 1989). It is important to note that given the innate heterogeneity of these materials, their properties can only be discussed generally, as their exact properties will vary depending on the environment from which they were extracted and the extraction procedure used. In general, HS are considered to be large molecules that are highly functionalized, and therefore, exceptionally well suited for complexing metal ions. These functional groups include carboxyl, phenolic and alcoholic hydroxyl, quinone and ketonic carbonyl, amino, and sulfhydryl groups (Sposito, 1989). Despite the innate heterogeneity of HS, model structures have been proposed. Figure 1 is a model HA molecule proposed by Stevenson and Schnitzer (1982). Similarly, Figure 2 contains a theoretical construct of a FA as determined by Buffle *et al.* (1977).

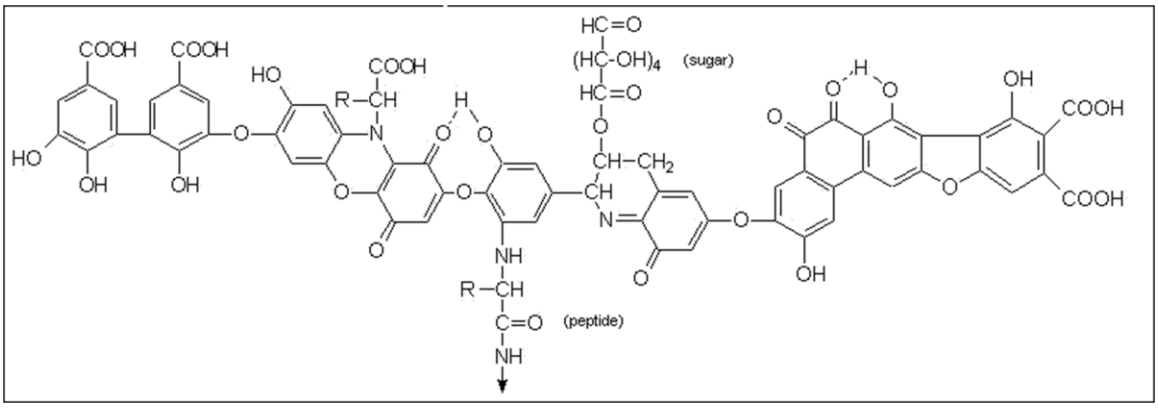


Figure 1: Model structure of HA (Stevenson and Schnitzer, 1982).

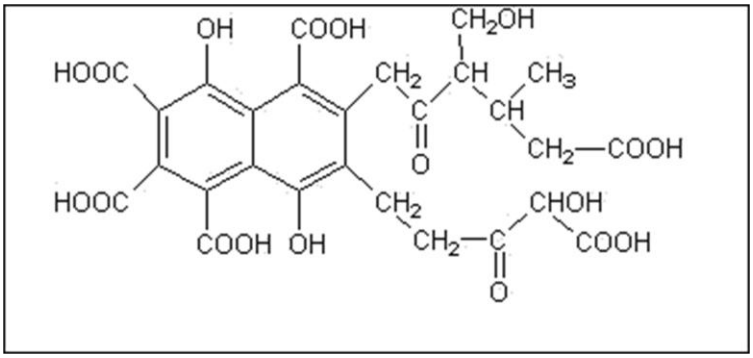


Figure 2: Model structure of FA (Buffle *et al.*, 1977).

Natural organic matter, including HAs and FAs, can have a profound impact on the mobility of radionuclides in both the subsurface and surface waters (Silva and Nitsche, 1995 and Santschi *et al.*, 2002). The formation of metal - HA complexes (*e.g.*, Pu-HA) occurs primarily through carboxylic and phenolic groups on the HA, which effectively solubilize the metal. However, the question remains as to whether increased solubility, as a result of complexation with NOM, will ultimately result in increased transport. Enhanced transport may be hindered by the formation of ternary Pu – NOM – Mineral complexes. Currently, our ability to model the effect of NOM on actinide transport is hindered by a lack of fundamental data (*i.e.*, stability constants). The determination of these values for the Pu – HA complex will be the major focus of this work.

## PLUTONIUM REDOX CHEMISTRY

Given its complex chemistry, wide-spread distribution, and contribution to the radiotoxicity of high-level radioactive waste, Pu represents an especially daunting environmental challenge. Pu may exist simultaneously in four oxidation states (III, IV, V, and VI) (Clark *et al.*, 2006). This unique behavior is driven by similarities between

the electrochemical potentials for the various Pu redox couples. At an acidic pH, the redox potentials for the various Pu oxidation states are similar. As the pH of the system increases, formation of Pu(III) becomes increasingly less likely; while the potentials for IV, V, and VI remain very similar, allowing for their continued coexistence (Choppin, 2003). Table 1 contains the formal electrochemical potentials for the various Pu ions in acidic, neutral, and basic solutions *versus* the standard hydrogen electrode (adapted from Clark *et al.*, 2006).

Table 1: Formal electrochemical potentials for plutonium redox couples

| Couple | Acidic[a] | Neutral[b] | Basic[c] |
|---|---|---|---|
| Pu(IV)/Pu(III) | +0.982 | -0.39 | -0.96 |
| Pu(V)/Pu(IV) | +1.170 | +0.70 | -0.67 |
| Pu(VI)/Pu(V) | +0.913 | +0.60 | +0.12 |
| Pu(VI)/Pu(IV) | +1.043 | +0.65 | +0.34 |
| Pu(V)/Pu(III) | | +1.076 | |
| Pu(VII)/Pu(VI) | | | +0.85 |
| Pu(V)/Pu(IV) | +1.17 | | |

[a] Formal potential in 1M $HClO_4$ solution
[b] pH 8
[c] Determined in 1M NaOH.

Although the redox potentials for Pu(IV,V, and VI) remain similar at *circa* neutral pH values, examination of the Eh – pH diagram below (Figure 5) shows that Pu(VI) only exists in highly oxidizing and/or high pH systems. Pu(VI) may also exist in systems containing relatively high concentrations of carbonate. Therefore, Pu(IV) and (V) are the likely states present in most environmental systems (Choppin, 2003 and Roberts *et al.*, 2008). The specific conditions of the system in question must be considered when determining which oxidation state(s) could be present. For example, Roberts *et al.* (2008) in their study of surface waters, suggest that only Pu(IV) and Pu(V) need to be

considered. In contrast, Buda *et al.* (2008) examined an environmental system in which they claim that only Pu(III) and Pu(IV) should be considered. This opinion is likely driven by the fact that Buda *et al.* (2008) were primarily concerned with far-field transport from the proposed Gorleben nuclear waste repository which contains highly reducing groundwater conditions (Schäfer *et al.*, 2003). Therefore, further discussion will focus on these dominant oxidation states of Pu (*i.e.*, IV and V).

Disproportionation reactions such as:

$$3\ Pu^{4+} + 2H_2O \leftrightarrow 2\ Pu^{3+} + PuO_2^{2+} + 4\ H^+ \quad (1)$$

result in a distribution of oxidation states, which is important since the oxidation state of an actinide has a profound impact on its behavior (*e.g.*, sorption and complexation). However, at environmental concentrations, most disproportionation reactions are not favored. For example, in oxic surface waters, Pu is predominantly present in the pentavalent state, $Pu(V)O_2^+$ (Choppin, 2003). Examination of the disproportionation reaction for Pu(V):

$$2\ PuO_2^+ + 4H^+ \leftrightarrow Pu^{4+} + PuO_2^{2+} + 2H_2O \quad (2)$$

and the resulting equation for the equilibrium constant:

$$K = \frac{[Pu^{4+}][PuO_2^{2+}]}{[PuO_2^+]^2[H^+]^4} \quad (3)$$

shows that Pu(V) disproportionation has an inverse $4^{th}$ order dependence on the hydrogen ion concentration (pH) and an inverse $2^{nd}$ order dependence on $[Pu(V)]_{total}$. Furthermore, in natural, as well as many engineered systems, the presence of various ligands will limit disproportionation by complexing the metal and limiting the metal – metal interactions necessary for disproportionation to occur. Also, Pu(V) has the greatest tendency to disproportionate. Many environmentally significant ligands are known to reduce Pu(V) to (IV), thereby further reducing the likelihood of disproportionation (Andre and Choppin, 2000). For these reasons, disproportionation reactions are generally insignificant in environmental systems.

HA, specifically, has been shown to reduce Pu(V) to (IV). Andre and Choppin (2000) examined initially Pu(V) systems with and without HA. As expected, in the absence of HA, Pu was present primarily in the pentavalent state. In systems containing HA (1 or 10 ppm HA), a significant fraction of the Pu(V) was readily reduced to Pu(IV), in the presence of light (Andre and Choppin, 2000). In the absence of light, Pu(V) reduction was still observed for samples containing 10 ppm HA, though the effect was not as pronounced; approximately 40% of the Pu(V) was reduced to Pu(IV) after 5 days (Andre and Choppin, 2000). Figure 3 shows the percentage of Pu(V) remaining as a function of time and HA concentration in the presence of light.

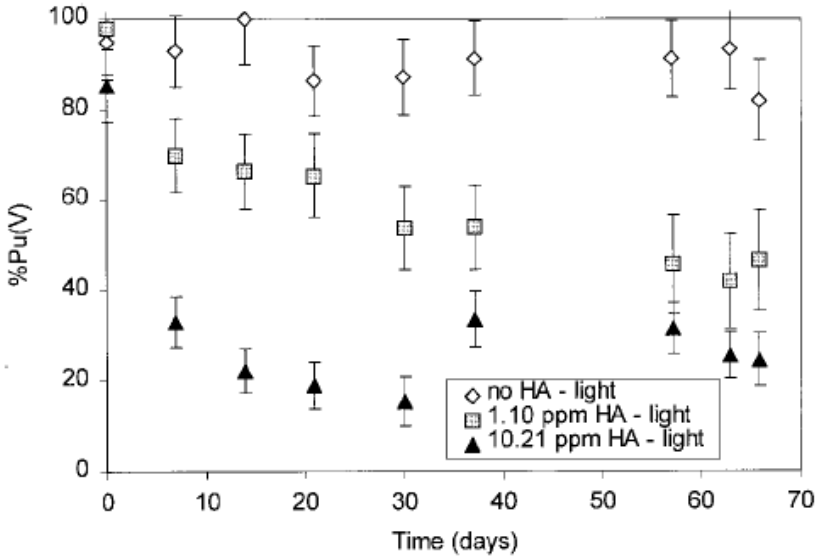


Figure 3: Percentage of Pu(V) remaining as a function of time and HA concentration (Andre and Choppin, 2000).

## HYDROLYSIS

Hydrolysis occurs as the positive charge on the metal ion (*e.g.*, $Pu^{4+}$) polarizes $H_2O$ sufficiently to remove a proton, thus forming a hydrolysis product according to the following reaction:

$$nAn^{z+} + qH_2O \leftrightarrow An(OH)_q^{nz-q} + qH^+ \quad (4)$$

Hydrolysis of the dioxy cation, $Pu(V)O_2^+$, does not occur until the pH is greater than 9. Therefore, Pu(V) will exist as the dioxy cation, $PuO_2^+$ in most environmental systems. In contrast, Pu(IV) hydrolyzes strongly in all but very acidic solutions (*i.e.*, pH ≈ 0). It is possible that Pu(IV) hydrolysis proceeds in a step-wise fashion to yield intermediate hydrolysis products $Pu(OH)_n^{4-n}$ (n = 1, 2, 3, or 4) (Clark *et al.*, 2006). These monomeric Pu species ($2 \leq n \leq 4$) can then undergo irreversible polymerization to yield colloidal species (Clark *et al.*, 2006). X-ray diffraction studies by Soderholm *et al.* (2008) recently

reported that Pu(IV) polymerizes to form well-defined (*i.e.*, crystalline), nanometer-sized particles with the formula $[Pu_{38}O_{56}Cl_{54}(H_2O)_8]^{14-}$; where the excess negative charge is balanced by lithium ions to yield the chemical formula: $Li_{14}(H_2O)_n[Pu_{38}O_{56}Cl_{54}(H_2O)_8]$ (Soderholm *et al.*, 2008). Plutonium solubility studies conducted by Neck *et al.* (2007) found that Pu(IV) colloid formation is independent of pH and occurs at $\log[Pu(IV)]_{total} \geq -8.3 \pm 1.0$ (Figure 4). Therefore, the Pu concentration dependence and pH independence of Pu(IV) colloid formation has been established and a rough concentration limit, or cutoff, for colloid formation ($[Pu]_{total} \approx$ 5E-9 M) has been defined.

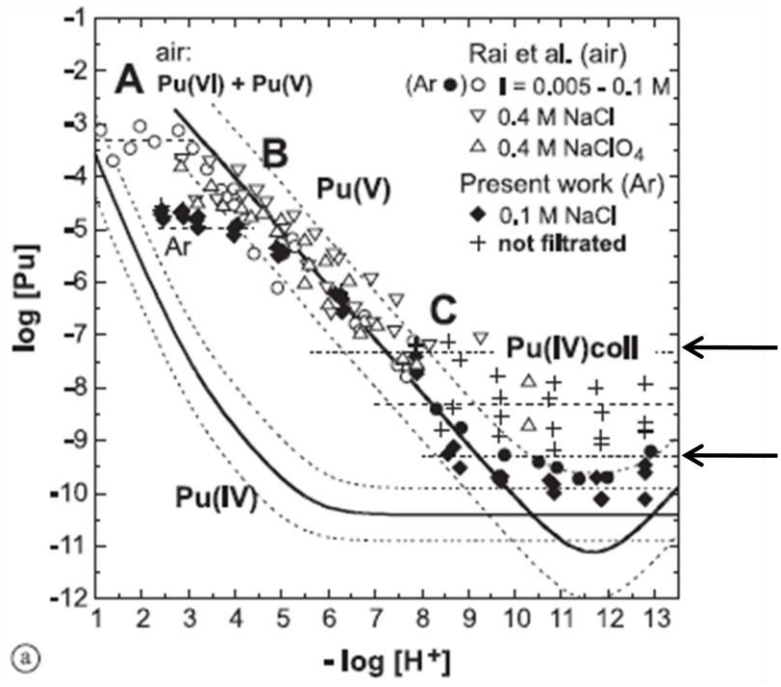


Figure 4: log [Pu] – pH diagram of Pu(IV)/(V) detailing the solubility of Pu and the influence of colloids (Neck *et al.*, 2007). The arrows (and dashed lines) denote the error-range on $[Pu]_{colloid}$.

At Pu concentrations below 5E-9 M, the mononuclear hydrolysis product $Pu(OH)_4$ (aq) will likely form. Figure 5 shows the anticipated speciation of Pu in 0.1 M

NaCl for $[Pu]_{total}$ = 1E-9 M (*i.e.*, below the theoretical colloidal cut-off). Recognize that the aqueous species shown for a given set of conditions is not the only species in solution; it is simply the dominant species (*i.e.*, the complex shown accounts for greater than 50% of the total Pu in solution). Carbonate and other potentially environmentally relevant ligands have been excluded from this modeling effort for clarity.

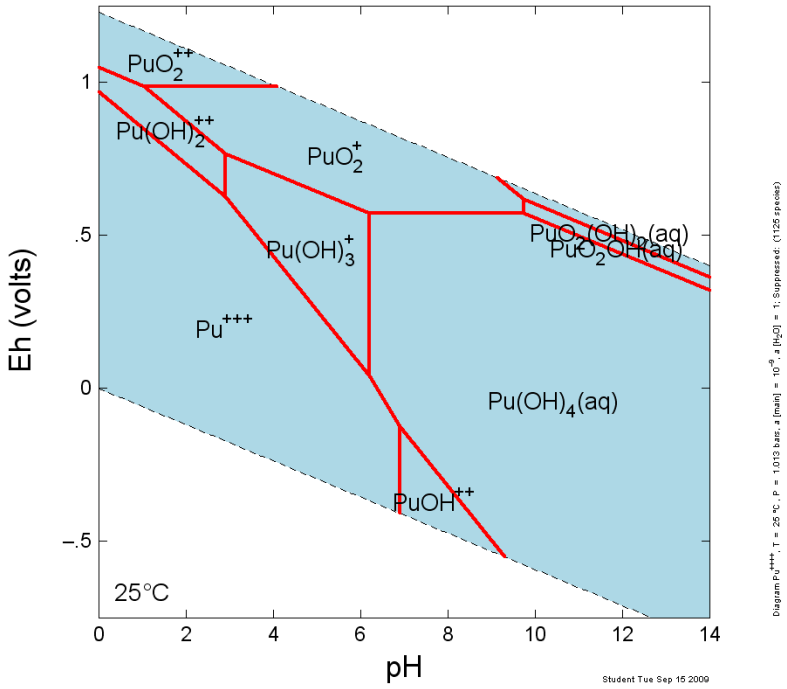


Figure 5: Eh – pH diagram of Pu – $H_2O$ with [Pu] = 1E-9 M; I = 0.1 M NaCl. Mineral formation suppressed. Modeled using Geochemists Workbench ™.

To better illustrate Pu(IV) hydrolysis, a Pu(IV) speciation model is shown in Figure 6, which was prepared using the same parameters used to generate the Eh – pH diagram in Figure 5. In Figure 6, mineral formation was again suppressed (*i.e.*, solids were not allowed to precipitate) to yield a different representation of the data found in Figure 5.

The various intermediate, mononuclear hydrolysis products are formed as the system pH is increased. Above pH ≈ 6.5, $Pu(OH)_4$ is the dominant aqueous species.

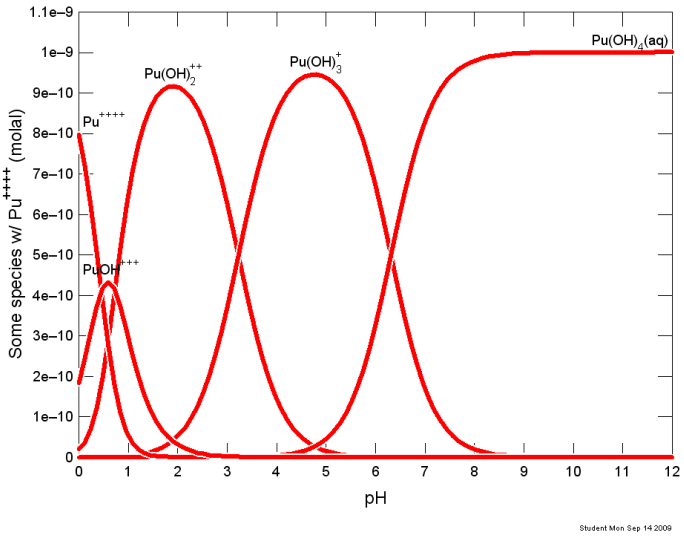


Figure 6: Pu(IV) hydrolysis as a function of pH modeled using Geochemists Workbench™. Mineral formation suppressed; [Pu] = 1E-9 M; I = 0.1 M NaCl.

## SOLUBILITY

The various mononuclear Pu(IV) hydrolysis products can aggregate to form macroscopic precipitates. $Pu(OH)_4$ is only sparingly soluble in water and has a tendency to readily precipitate as an amorphous hydroxide, $Pu(OH)_4$(am) (Neck *et al.*, 2007). Theoretically, $Pu(OH)_4$(s) can lose two waters to form a more thermodynamically favorable and extremely insoluble species, $PuO_2$(s). While thermodynamically favorable, it is highly unlikely that crystalline Pu will form under typical environmental conditions. Given the tendency for Pu(IV) to precipitate, the model used to generate Figure 6 was

modified to allow solids to form (Figure 7). For clarity only the aqueous species are shown.

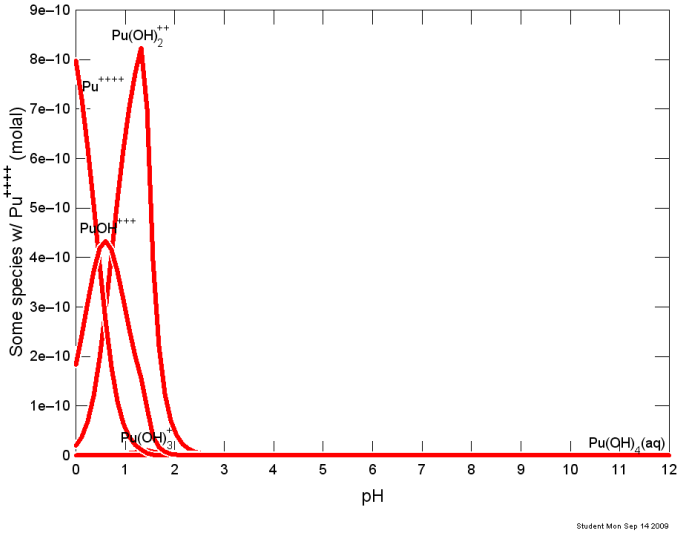


Figure 7: Pu(IV) hydrolysis as a function of pH modeled using Geochemists Workbench$^{TM}$. Precipitation allowed; [Pu] = 1E-9 M; I = 0.1 M NaCl.

The differences between Figure 6 and Figure 7 illustrate the propensity for actinides in the +4 oxidation state to precipitate. When solids are allowed to form (Figure 7) there is very little (approximately $10^{-11}$ M) aqueous Pu above pH 2. It is important to note that these models were generated assuming only Pu, water, and 0.1 M NaCl were present in solution and the concentration of Pu was sufficiently low to negate colloid formation.

Figure 8 shows a schematic summarizing the various redox and solubility processes discussed above.

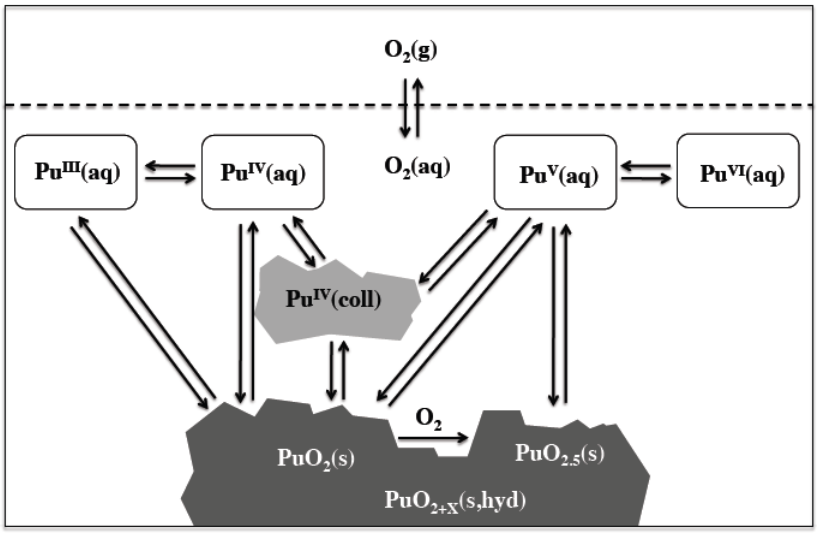


Figure 8: Schematic depicting the various solid – liquid and redox equilibria of Pu in oxygenated water. Adapted from Neck *et al.* (2007).

Although depicted in Figure 8, Pu(III) and Pu(VI) are unlikely to predominate in most environments. As discussed previously, in oxic surface waters, Pu is predominantly in the pentavalent state (Orlandini *et al.*, 1986). However, the aqueous solubility of Pu(V) is limited in large part by the insolubility of Pu(IV). The thermodynamic favorability of the insoluble Pu(IV) – (hydr)oxides, limit the aqueous solubility Pu(V) as noted in Figure 8. This restricts the aqueous solubility of Pu(V) to approximately $10^{-6}$ – $10^{-8}$ M (Choppin, 2003). Similarly, based on a $\log_{10}K_{sp} = -(58 \pm 1)$ as reported by Neck and Kim (2001), the aqueous solubility of Pu(IV) at pH 7 is roughly $10^{-11}$ M. In reality, observed Pu solubilities range from $10^{-8}$ – $10^{-13}$ M due to interactions with ligands, metal hydrolysis, redox instability, and colloid formation (Neck and Kim, 2001).

Neck and Kim (2001) found that the colloidal Pu(IV) species was necessary for modeling the system shown in Figure 8. The Pu(IV) colloid depicted in the aqueous phase would be the nanometer-sized, crystalline particles observed by Soderholm *et al.*

(2008) and discussed previously. These Pu(IV) nanoparticles can aggregate and precipitate to form a solid phase. Although $PuO_2$(s) and $PuO_{2.5}$(s) are shown in Figure 8, these are theoretical constructs necessary for modeling the system shown. In reality the solid phase formed from the precipitation of Pu(IV) and (V) will be some $PuO_{2+x}$ (s, hyd) species (Neck and Kim, 2001).

## COMPLEXATION

As mentioned previously, oxidation state has a significant effect on chemical behavior. It is important to note that overall effective charge does not follow net charge. Actinides in the +5 and +6 oxidation states are present as dioxy cations ($AnO_2^+$ and $AnO_2^{2+}$). The axial oxygen atoms withdraw electron density from the metal ion, thus leading to an effectively higher charge than expected based on stoichiometry. The axial oxygen atoms also restrict the area that is accessible for reaction to this electron poor region, which leads to an effective charge that is greater than the overall charge of the ion. Therefore, the following trend is observed with respect to decreasing effective charge.

$$An^{4+} > AnO_2^{2+} > An^{3+} > AnO_2^{+}$$

$$4 > 3.3 \pm 0.1 > 3 > 2.3 \pm 0.1 \qquad (5)$$

The above trend also shows the decreasing complexation affinity with decreasing effective charge. Similarly, actinides show varying affinity for various organic and inorganic ligands. The following trend examines the relative strength of complexation for common inorganic ligands (Silva and Nitsche, 1995):

$$OH^-, CO_3^{2-} > F^-, HPO_4^{2-}, SO_4^{2-} > Cl^-, NO_3^- \quad (6)$$

The propensity for actinides to undergo hydrolysis requires a competing ligand (*e.g.*, $CO_3^{2-}$) to remove a water from the actinide before forming a bond. Stability constants are a measure of the energetic favorability of a given complexation reaction. Therefore, stability constants, along with mass and charge balances, can be used to predict speciation.

Examination of the same generic actinide hydrolysis reaction used previously (Equation 4) yields the following equilibrium constant:

$$\beta_{nq} = \frac{\left[An(OH)_q^{nz-q}\right]\left[H^+\right]^q}{\left[An^{z+}\right]^n a_{H_2O}} \quad (7)$$

The equilibrium constant (β) above is referred to as the overall- or cumulative-stability constant for a given reaction. This reaction can also be written as a complexation reaction to yield the following complexation constant (K).

$$nAn^{z+} + qOH^- \leftrightarrow An(OH)_q^{nz-q} \quad (8)$$

$$K = \frac{\left[An(OH)_q^{nz-q}\right]}{[An^{z+}]^n[OH^-]^q} \quad (9)$$

Figure 9 shows the cumulative stability constants for the 1:1 reactions of various ligands with the four environmentally relevant oxidation states of Pu. Notice that the data adhere to all of the relevant aforementioned trends.

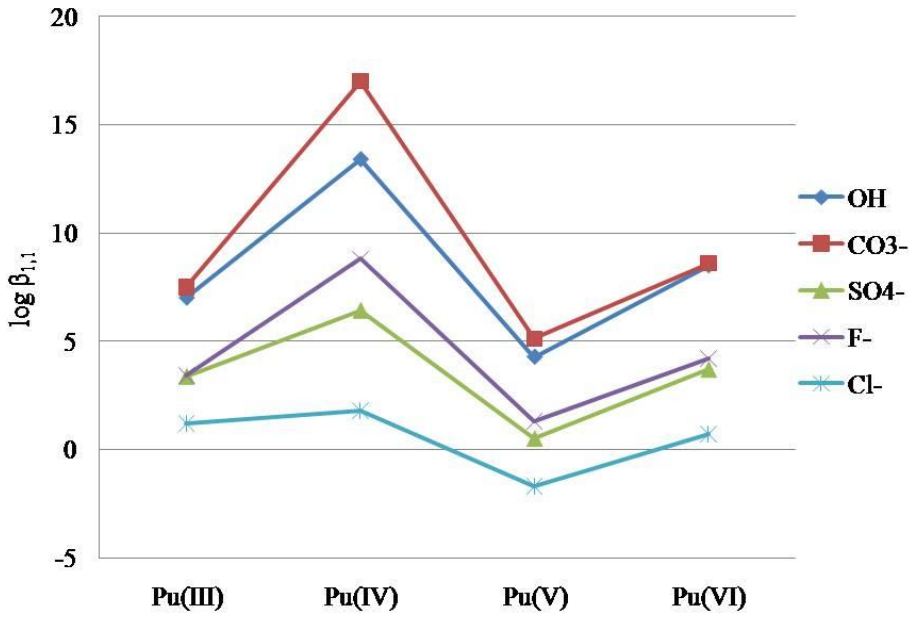


Figure 9: Cumulative stability constants for Pu – inorganic ligand complexes as a function of oxidation state. Adapted from Silva and Nitsche (1995).

Organic ligands such as ethylenediaminetetraacetic acid (EDTA), oxalic acid, and desferrioxamine B (DFO-B) form strong complexes with actinides. Table 2 shows the cumulative stability constants (log β) for representative Pu-organic ligand complexes.

Table 2: Pu – Ligand cumulative stability constants (log β).

| *Ligand* | *Complex* | $Pu^{3+}$ | $Pu^{4+}$ | $PuO_2^+$ | $PuO_2^{2+}$ |
|---|---|---|---|---|---|
| Acetate, $Ac^-$ | $[ML]/[M][L]$ | 2.02 | 5.31 | | 2.2 |
| | $[ML_2]/[M][L]^2$ | 3.34 | | | 3.6 |
| | $[ML_5]/[M][L]^5$ | 16.7 | 22.6 | | |
| $EDTA^{4-}$ | $[ML]/[M][L]$ | 16.1 | 26.4 | 12.3 | 14.6 |
| | $[ML_2]/[M][L]^2$ | | 35.39 | | |
| $Citrate^{2-}$ | $[ML]/[M][L]$ | 8.9 | 15.6 | | |
| | $[ML_2]/[M][L]^2$ | | 29.8 | | |
| $Oxalate^{2-}$ | $[ML]/[M][L]$ | | 8.30 | | |
| | $[ML_2]/[M][L]^2$ | 9.3 | 14.9 | | 9.4 |
| | $[ML_3]/[M][L]^3$ | 9.4 | 23.4 | | |
| | $[ML_4]/[M][L]^4$ | 9.9 | 27.5 | | |

Adapted from Clark *et al.* (2006).

Notice that the values for ligands such as EDTA are many orders of magnitude larger than those for common inorganic ligands (Figure 9). This indicates that organic ligands such as EDTA, citrate, and oxalate will dominate over hydrolysis reactions assuming the ligands are present in a sufficient concentration relative to the metal and the pH is such that the ligand is deprotonated.

Figure 10 shows the predicted fraction of Pu remaining in the aqueous phase, Pu(aq), in the presence and absence of two equivalents of EDTA per equivalent of Pu. The data in Figure 10 indicates that EDTA, when present in sufficient concentrations relative to Pu, can out-compete Pu hydrolysis reactions up to approximately pH 8. In the absence of EDTA, Pu readily precipitates from solution at concentrations greater than 5E-9 M and pH greater than approximately 2 (as shown in Figure 4, Figure 10, and discussed previously).

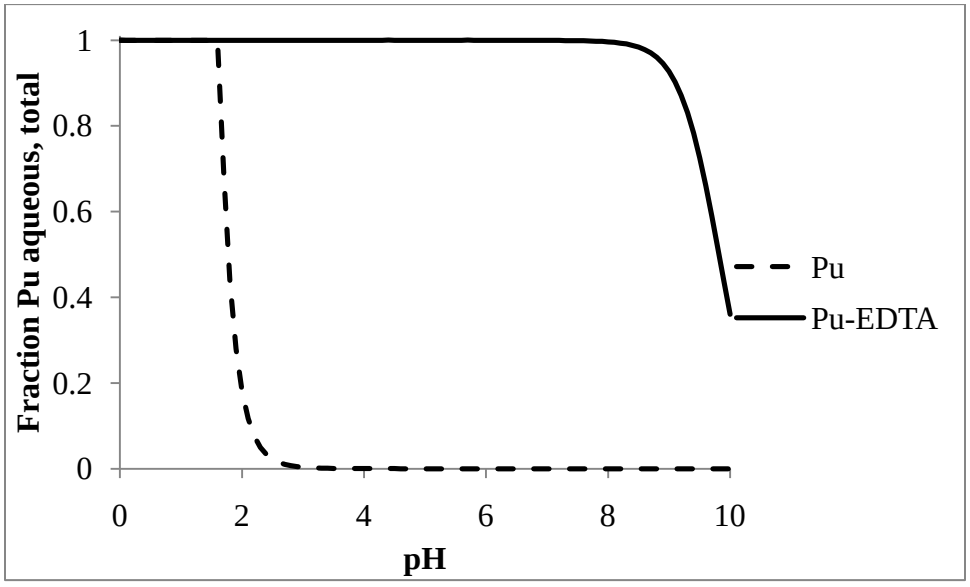


Figure 10: Fraction of Pu(IV) in the aqueous phase in the presence and absence of two equivalents of EDTA per equivalent of Pu ([Pu(IV)] = 1E-5 M). System modeled using Pu-EDTA stability constants from Boukhalfa *et al.* (2004).

It is hypothesized that given the similarities in functionality between ligands such as EDTA and DFO-B, and humic acid, the stability constants for Pu-HA complexes would be on the order of (or greater than) those observed for Pu-EDTA and Pu-(DFO-B) complexes. Stability constants for Pu-HA complexes are sparse in the literature. Therefore, determination of these values will be a major focus of this work.

## SORPTION

### BINARY SORPTION

Because the chemical behavior of actinides with the same oxidation state is similar, Am(III), Th(IV), and Np(V) are often used as surrogates for Pu(III), (IV), and (V), respectively. This approach greatly simplifies matters as the above mentioned redox reactions of Pu can be neglected and data for a specific oxidation state can be obtained. Figure 11 shows how oxidation state affects the sorption of actinides to amorphous silica.

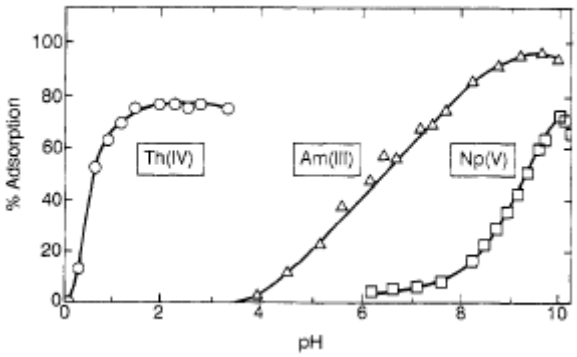


Figure 11: Adsorption of actinides on precipitated amorphous silica (60 ppm $SiO_2$ for Th, and 1200 ppm $SiO_2$ for Am and Np) as a function of pH (Righetto *et al.*, 1991).

In binary metal - mineral systems, metal adsorption generally increases with increasing pH. This trend is shown in both Figure 11 and the Pu-gibbsite system in

Figure 12. In Figure 12, increasing sorption with increasing pH is exhibited most clearly for Pu(V). However, if Th(IV) (Figure 11) is taken as a surrogate for Pu(IV), nearly 80% sorption would be expected at pH greater than 2. This is in fact the case; in Figure 12 Pu(IV) is approximately 80% sorbed at the lower-end of the pH region examined (pH ≈ 3.5). In both cases, Pu sorption to gibbsite was studied in the absence of organic ligands.

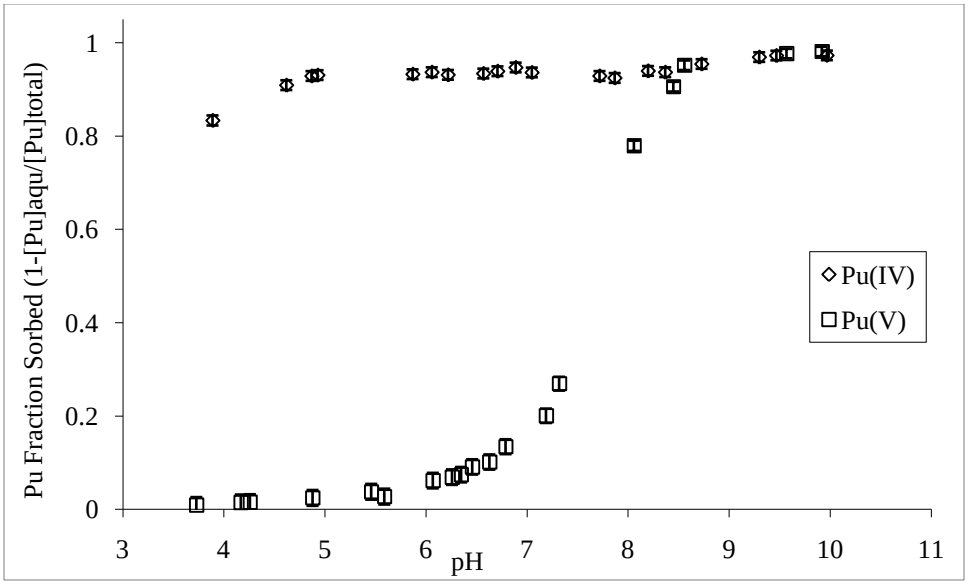


Figure 12: Pu(IV) and Pu(V) sorption to gibbsite after 24 hours (Powell *et al.*, 2008). [α-Al(OH)3] = 10 $m^2$ $L^{-1}$, ionic strength 0.01M (NaCl), $CO_2$(g)-free, $[^{238}Pu]_{total} = 10^{-10}$ M

Enhanced subsurface transport of Pu has been observed for Pu associated with mineral colloids. Kersting *et al.* (1999) documented kilometer scale subsurface transport of Pu-mineral colloids at the NTS. A similar and perhaps more relevant (to the current work) study by Santschi *et al.* (2002) observed Pu migration in surface waters at the Rocky Flats Environmental Technology Site (RFETS) and found that NOM played a significant role in facilitating Pu transport. Santschi *et al.* (2002) observed Pu associated with pseudo-colloids (*i.e.*, Pu associated with a different carrier substrate) such as HA.

Furthermore, these colloids showed enhanced transport during storm runoff events. The correlation between HA concentration and colloidal Pu concentration was further examined under laboratory conditions and found to be significant. Figure 13 shows the influence of HA on the aqueous phase concentration of Pu in RFETS soil suspensions as a function of time (Santschi *et al.*, 2002).

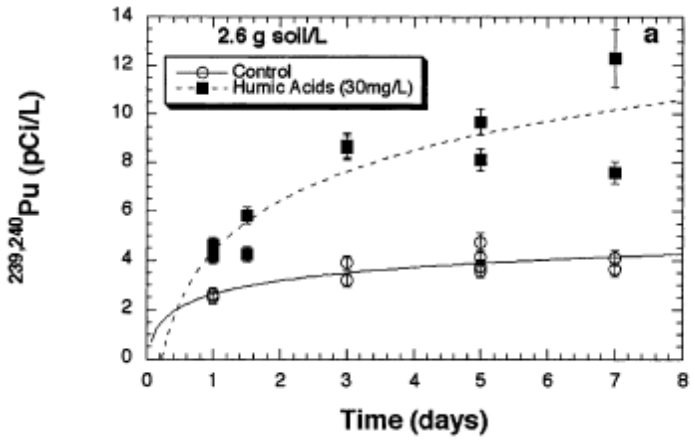


Figure 13: Kinetics of colloidal Pu remobilization with and without addition of Aldrich HA (30 mg C/L) (Santschi *et al.*, 2002).

As mentioned previously, it has historically been assumed that plutonium in the vadose- and saturated-zones would be present as Pu(IV) thereby limiting its mobility. This belief is driven by the fact that Pu(IV) can have an aqueous solubility as low as $10^{-17}$ M (Neck and Kim, 2001). However, complexation with natural organic matter (NOM) appears to increase the solubility of actinides in laboratory studies (Santschi *et al.*, 2002). Increased solubility could indicate enhanced transport, due to the higher mass of Pu in the aqueous phase. Therefore, a better understanding of metal - NOM (*e.g.*, Pu-HA), metal – mineral (Pu-soil, *i.e.*, sorption), and ternary, metal – NOM – mineral (*e.g.*, Pu-HA-soil) systems is essential for accurately predicting actinide fate and transport.

TERNARY SORPTION

While increased solubility could indicate enhanced transport, as discussed above, the formation of ternary, Pu – NOM – solid complexes may limit subsurface transport of Pu. Schindler (1990) describes two types of surface ternary complexes: Type A and Type B complexes. For example, consider a metal-ligand complex (ML) interacting with a mineral surface denoted (≡SOH). The following Type A surface complex may form according to the reaction (hydrating waters removed from metal for clarity):

$$\equiv S\text{-}OH + M\text{-}L^{z+} \leftrightarrow \equiv S\text{-}O\text{-}M\text{-}L^{(z-1)+} + H^{+} \quad (10)$$

or more simply:

$$\equiv S\text{-}O\text{-}M\text{-}L \quad (11)$$

Alternatively, assuming that the ligand molecules are capable of replacing the surface hydroxyl groups, the following Type B surface complex is formed:

$$\equiv S\text{-}OH + M\text{-}L^{z+} \leftrightarrow \equiv S\text{-}L\text{-}M^{(z+1)+} + OH^{-} \quad (12)$$

or more simply:

$$\equiv S\text{-}L\text{-}M \quad (13)$$

Recent work by Powell *et al.* (2010) indicates that both of these surface complexation mechanisms (*i.e.*, Type A and Type B) are essential to describing the partitioning of Pu in the presence of organic ligands. Figure 14 shows the effect of 1-hydroxyethane-1,1-diphosphonic acid (HEDPA), a chelating agent, on Pu(V) sorption to boehmite (γ-AlOOH) (Powell *et al.*, 2010).

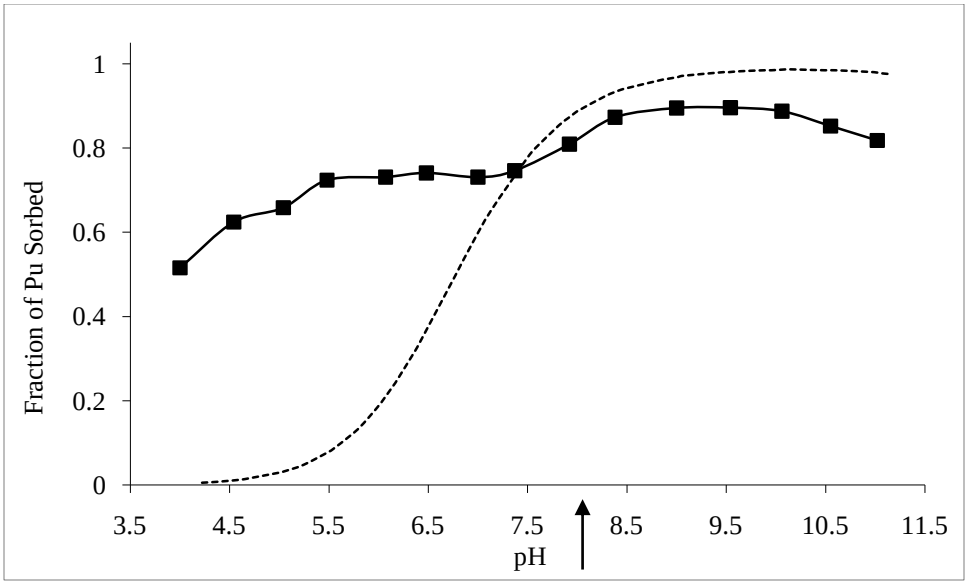


Figure 14: Effect of HEDPA on Pu sorption to boehmite. The boxes indicate the fraction of Pu sorbed in the ternary system, while the smoothed dashed line represents Pu(V) sorption to boehmite in the absence of HEDPA (similar to Figure 10). The arrow denotes the PZC of boehmite. Adapted from Powell *et al.* (2010).

It is apparent that organic ligands play a significant role in the geochemical behavior of Pu through both Type A and Type B ternary surface complexes. Therefore, a fundamental understanding of the influence of ternary complex formation on Pu sorption is necessary to evaluate the chemical, physical, and biological processes affecting the transport of Pu in the subsurface. This is critical for performing comprehensive risk analyses for nuclear waste repositories, which will ensure protection of human and environmental health.

CHAPTER THREE

EXPERIMENTAL APPROACH

EQUILIBRIUM DIALYSIS-LIGAND EXCHANGE

The Equilibrium Dialysis Ligand Exchange (EDLE) technique has been shown to be well suited for determination of the conditional stability constants of metal-HA complexes over a broad range of environmentally significant pH and ionic strength values (Van Loon *et al.*, 1992). The EDLE technique distinguishes between metal bound to a reference ligand (M-$L_n$) and metal bound to HA (M-HA) by employing a semi-permeable membrane. The semi-permeable membrane is selected to allow the M-$L_n$ complex to move freely throughout the system, while the M-HA complex, by virtue of its larger size, is restricted to the inside of the dialysis membrane (Figure 15).

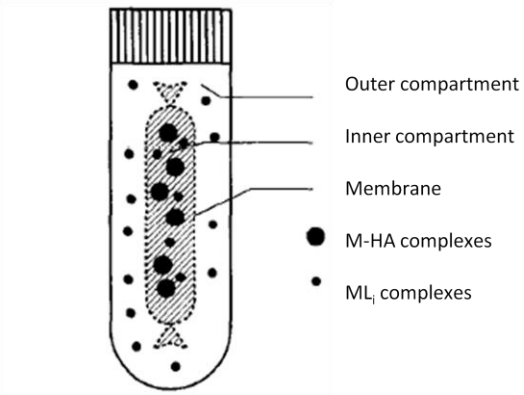


Figure 15: Schematic depicting the experimental setup used in EDLE. The free metal ion, free ligand, and the free HA have been omitted for simplicity (adapted from Glaus *et al.*, 1995).

Selection of an appropriate reference ligand is crucial as it must meet certain size requirements (*i.e.*, the M-$L_n$ complex must be able to pass through the membrane unhindered) and have a stability constant similar to that of the M-HA complex (Van Loon

*et al.*, 1992). Furthermore, it is essential that in the absence of HA, the vast majority of the metal is complexed by the reference ligand to prevent hydrolysis and subsequent precipitation. While it is important that the M-$L_n$ complex be strong enough that hydrolysis of the metal does not occur to an appreciable extent, upon addition of HA, a distribution of the two complexes is required for Equation 14 to be valid (Van Loon *et al.*, 1992). Once these criteria are met, the conditional stability constant for the M-HA complex can be determined using Equation 14 (Van Loon *et al.*, 1992).

$$K_{MHA}=\frac{[MHA]K_{ML}[L]^n}{[ML_n][HA]} \tag{14}$$

Assuming an appropriate reference ligand is selected and the proper concentrations are added, the only unknowns in Equation 14 are the concentrations of metal bound to HA, [M-HA] and metal bound to the reference ligand, [M-$L_n$]. These values can be determined by conducting a mass-balance on the metal in each compartment. Let $C_{in}$ represent the concentration of metal in the inner compartment (*i.e.*, inside of the dialysis membrane) and $C_{out}$ symbolize the metal concentration in the outer compartment. The following mass-balance equations can then be written:

$$C_{in}=[MHA]+[ML_n]+\left[M^{x+}\right] \tag{15}$$

$$C_{out}=[ML_n]+[M^{x+}] \tag{16}$$

Assuming the reference ligand is present in excess relative to the metal, it is assumed that the concentration of free metal [$M^{x+}$] is negligibly small. The above equations then reduce to:

$$C_{in}=[MHA]+[ML_n] \quad (17)$$

$$C_{out}=[ML_n] \quad (18)$$

The concentration of the metal-HA complex can then be determined by difference.

$$[MHA]=C_{in} - C_{out} \quad (19)$$

The above equations can now be used to calculate a conditional stability constant for Pu-HA complexes ($K_{MHA}$).

## ULTRA-FILTRATION

Similarly, ultra-filtration (UF) has been employed for M-HA stability constant determination (Banik *et al.*, 2007). The diagram in Figure 16 depicts the type of UF unit used in complexation studies of this type. The UF approach is conceptually very similar to EDLE in the use of a semi-permeable membrane to separate high molecular weight species (*i.e.,* M-HA) from low molecular weight compounds (*e.g.,* uncomplexed metal ions, $M^{x+}$). UF has the advantage (*versus* EDLE) that the volume inside the dialysis membrane no longer needs to be determined. Thus eliminating the error associated with determining the volume of a flexible dialysis membrane. Furthermore, the time required to equilibrate the system is reduced, since establishing equilibrium between the inner- and outer-compartments (for the M-$L_n$ complex) is not a prerequisite for metal equilibration between the available ligands.

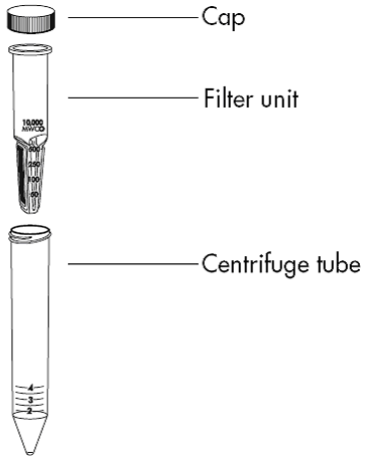


Figure 16: Diagram of a Millipore-Amicon® Ultra-4 centrifugal filter (Millipore, 2010).

Ultra-filtration has previously been used to determine stability constants for M-HA complexes by measuring the $[M^{x+}]_{free}$ in the filtrate (Ephraim and Xu, 1989). However, this approach is not applicable for the Pu–HA system. The formation of Pu-hydrolysis products and subsequent precipitation makes stability constant determination using ultra-filtration as described previously, unreliable under environmentally significant conditions (*i.e.,* pH > 0). Precipitation has the obvious drawback that if Pu is removed from solution, a uniform distribution of Pu, at a known concentration can no longer be assumed. The formation of Pu colloids, as described previously, would confound efforts to determine Pu partitioning between the two ligands. Furthermore, if Pu precipitates from solution, these experiments will be studying the solubilization of Pu by HA as opposed to aqueous complexation of the same species. To address these problems, a hybrid technique will be employed using ultra-filtration and the use of a reference ligand (as done in EDLE). The reference ligand will limit the hydrolysis and

subsequent precipitation of Pu while allowing for ultra-filtration at environmentally relevant pH values.

Previous studies have attempted to mitigate precipitation of the actinide of interest by working at low pH. Banik *et al.* (2007) examined the ternary Pu-HA-kaolinite system and also conducted aqueous Pu-HA complexation studies. Commercially available Aldrich HA (Sigma-Aldrich Company) was used in these experiments. Since it is readily obtainable, Aldrich HA is often used in studies of this type, despite concerns that it does not accurately represent "natural" HAs. Using ultra-filtration, Banik *et al.* (2007) reported stability constants (log β) for Pu(IV)-HA ranging from 6.4 to 8.4 over the pH range: 1.8 - 3. However, there are several problems with this study. First, the pH range of interest was 1.8 - 3 (Banik *et al.*, 2007). Recall that by definition, HA is the fraction of HS that is soluble above pH 2. Therefore, precipitation of HA (and subsequent co-precipitation of Pu) at low pH values is a concern. Also, the authors mention that scatter in the data could indicate the formation of Pu colloids, yet there was no apparent attempt made to limit or quantify the effect of these reactions (Banik *et al.*, 2007). Pu colloid formation would confound these results for the reasons mentioned previously.

Similarly, Buda *et al.* (2008) attempted to determine conditional stability constants for the Pu(IV)–Aldrich HA complex. Buda *et al.* (2008) reported stability constant values (log β) ranging from 6.5 – 7.9 at pH 1.8; 6.7 – 8.3 at pH 2.5; 6.4 – 8.4 at pH 3. There is also scatter in these data that indicates that the HA may have been precipitating and the authors speculate that Pu colloids may have formed (Buda *et al.*, 2008).

While the above studies represent significant progress in this area of research, further study is needed. The use of a suitable reference ligand should mitigate, if not eliminate the precipitation of Pu(IV) and colloid formation. Since we will be working in the pH range: 4 – 6.5, precipitation of the HA (and co-precipitation of Pu) should not be of concern.

In contrast to the approach used by Banik *et al.* (2007) and Buda *et al.* (2008), where the stability constant is normalized to a loading capacity (LC) term, proton-binding will be modeled using the discrete pKa spectrum approach in this study. This technique is similar to that used by Westall *et al.* (1995) to study Co complexation by Leonardite HA. This approach assumes that the HA can be represented by a discrete number of acid sites with a fixed pKa spectrum (*e.g.*, pKa = 4, 6, 8, and 10). From acid-base titration data, the total number of binding sites at each pKa value can then be determined. HA acid-base titration data will allow the use of FITEQL to model proton binding and more accurately determine the number of accessible functional sites.

## PROJECT OBJECTIVES AND TASKS

The objectives of this research can be summarized as follows:

1. Determine the conditional stability constants for Pu-HA complexes from pH 4 to 6.5.
2. Conduct preliminary binary- and ternary-sorption studies to evaluate the effects of Pu-HA complex formation on Pu sorption behavior.

The following tasks served to achieve these objectives.

*Task 1: Method development:*

*Subtask 1.1: HA ultracentrifugation studies:*

Centrifuge filters with molecular weight cut offs (MWCOs) ranging from 1 – 30 kDa (1, 3, 10, and 30 kDa) were evaluated to determine the filter size required to retain the HA. The absence of HA in the filtrate was confirmed using UV-Vis spectroscopy and TOC (Wang *et al.*, 2003).

*Subtask 1.2: Reference ligand selection and evaluation:*

HYSS (a modeling program) was employed to determine which ligands can prevent Pu(IV) hydrolysis over the pH range of interest (*i.e.*, pH 4 – 6.5); EDTA was selected. Subsequently, laboratory studies were conducted to confirm that 100% of the Pu-EDTA complexes are recovered from the UF selected in Subtask 1.1.

*Task 2: Stability constant determination:*

The conditional Pu-HA stability constant was determined over the pH range: 4 to 6.5.

*Subtask 2.1: Proton binding modeling:*

As discussed previously, proton binding was modeled assuming discrete pKa values (3, 5, 7, and 9 were selected). Humic acid titration data were used as input data for the modeling program FITEQL to determine the number of binding sites at each pKa value.

*Subtask 2.2: Ultra-filtration studies:*

Using the reference ligand selected in Task 1, ultra-filtration coupled with inductively coupled plasma – mass spectroscopy (ICP-MS) was used to determine the

concentration of Pu associated with HA and the concentration of Pu bound to the reference ligand over the pH range of interest. These Pu concentrations, combined with the concentrations of proton binding sites on the HA (determined in Subtask 2.1), and the assumption of pKa values for those binding sites, allowed the stability constants for the Pu-HA complex to be determined over the pH range of interest using FITEQL.

T*ask 3: Preliminary sorption studies:*

Sorption isotherms at pH 4 and 6 were generated for the ternary Pu-HA-gibbsite system. These data were then coupled with studies examining metal sorption in the binary, Pu-gibbsite system to explore the influence of HA on Pu sorption to gibbsite.

# CHAPTER FOUR

## MATERIALS AND METHODS

Unless stated otherwise, all chemicals used in this study were ACS reagent grade or higher. Water for all experiments was supplied from a Millipore Super-Q water system (MQ-water). Labware was cleaned by sequential base (0.1 M NaOH) and acid baths (0.1 M HCl), then rinsed at least five times with MQ-water and dried. Leonardite HA, available as a solid (*i.e.,* dehydrated) from the International Humic Substances Society (IHSS), was used in these studies. The HA was rehydrated and converted to the fully-protonated form by dissolving an appropriate quantity of HA in 0.1 M NaCl and then increasing the solution pH to approximately 9. After the HA was fully dissolved (approximately 24 hours) the pH was decreased to approximately 5. The HA was then dialyzed using 1000 molecular weight cut-off (MWCO) dialysis tubing *versus* 0.1 M NaCl for one week with daily renewal of the dialysis solution. Dialysis was used to remove the low-molecular weight and "ash" fraction of the HA. The dialyzed HA stock solution concentration was then quantified using a Shimadzu TOC-V CSH total organic carbon (TOC) analyzer and stored in a cleaned amber glass bottle at 4°C until needed. Attempts to quantify the mass of HA lost during dialysis were hindered by incomplete recovery of the dialyzed solution. In an effort to estimate the fraction lost during dialysis, the initial concentration of HA was compared to the final concentration, as determined using TOC analysis. Based on these data, 21% of the initial material was lost during dialysis. However, it is important to note that this estimate includes "losses" due to

dilution. The IHSS reports the ash content of Leonardite HA as 2.58% (w/w). The IHSS defines "ash" as the inorganic residue in a dry sample (IHSS, 2010).

The loss of low molecular weight material will likely have little influence on the Pu-HA complexation experiments since the number of functional groups per unit mass of HA should remain unchanged. In contrast, the loss of the hydrophilic, low molecular weight, fraction will likely influence the sorption of Pu in the ternary, Pu-HA-gibbsite system. Hydrophobic bonding (*i.e.*, van der Waals attraction forces) has been shown to enhance the adsorption of HA on mineral surfaces (Stumm, 1992).

## ACID-BASE TITRATIONS OF HUMIC ACID

By building on the work of Ritchie and Perdue (2002) and initial titrations conducted as part of this research, the titration parameters and system conditions have been optimized to limit drift and hysteresis. The system was cycled a total of five times using the following criteria between acid/base additions. After an initial addition of 0.1 mL 0.1 N HCl to achieve a desirable starting point (pH ≈ 3.5), the titrations were carried out as follows. Forward (base) titrations were performed using 0.025 mL additions of 0.1 N NaOH; the stability criterion between additions was 0.1 mV $min^{-1}$. Back (acid) titrations were conducted using 0.025 mL additions of 0.1 N HCl. The stability criterion for each back titration was as follows: cycles 1 and 2, 30 seconds before next addition; cycle 3, 10 minutes before next addition; cycle 4, 1 hour before next addition; and cycle 5, 2 hours before next addition. The initial HA concentration was 50 mg C/L as determined using TOC analysis. All titrations were conducted using a Metrohm 836 Titrino titrator, under an inert, Ar(g) atmosphere at 25°C. Before introduction to the

headspace of the titration vessel, the Ar(g) was passed through NaOH to remove $CO_2$(g) and "wet" the gas. The temperature was controlled using a jacketed titration vessel connected to a constant temperature water bath. Additionally, the temperature was continuously monitored using a Metrohm Pt 1000 electrode. The system pH was continuously monitored using a Thermo Fisher Orion Ross Sure-Flow combination electrode calibrated using pH 4, 6, and 10 buffers. The Ross electrode was re-calibrated every 24 hours. Initial experiments found that the electrode had no significant drift over this time-period.

All acid and base additions were recorded. Therefore, the total concentration of $H^+$ ($T_H^{exp}$) in the system can be determined using Equation 20:

$$T_H^{exp} = C_a - C_b + T_H^0 = \Delta T_H + T_H^0 \quad (20)$$

where $C_a$ and $C_b$ represent the total concentrations of strong acid and base added to the system during the course of a titration, and $T_H^0$ represents the concentration of acid or base initially present (*e.g.*, added during HA re-hydration). While $C_a$ and $C_b$ are known, the concentration of $T_H^0$ (mol/L) was determined by modeling the titration data using FITEQL. The consumption of acid and base by water was accounted for by including the dissociation constant of water ($K_w$) in models. All titration data in this thesis were plotted with $\Delta T_H$ on the y-axis vs. pH on the x-axis.

## PLUTONIUM-HA COMPLEXATION

The partitioning of Pu between HA and EDTA was examined using UF, as described in Chapter Three. A NIST traceable $^{242}$Pu(IV) stock solution was used in the

preparation of all standards and samples. Similarly, $^{232}$Th from High Purity Standards was used to prepare both standards and samples containing $^{232}$Th. Complexation studies were conducted with 4.35E-8 M (10 ppb) or 2.60E-7 M (63 ppb) $^{242}$Pu and an additional study with 4.90E-8 M (11 ppb) $^{232}$Th served as a tetravalent oxidation state analog. Regardless of the actinide concentration, samples contained 1E-5M EDTA and 10 mg C/L HA. The ionic strength was 0.1 M with NaCl. The pH of the samples was adjusted using a minimum of 0.1 N HCl or 0.1 N NaOH to produce a distribution of samples over the pH range: 4 - 6.5. All pH measurements were conducted using a Thermo Fisher Ross Sure-Flow semi-micro electrode that had been calibrated using pH 4, 7, and 10 buffers. Samples were prepared in 50 mL polypropylene vials and mixed on an orbital shaker at 25°C. Homogenous aliquots were removed after 24 hours, 1 week, and 2 weeks during the first experiment (2.60E-7 M $^{242}$Pu). This study indicated that equilibrium was established after 1 week, so a single 1.5 week sampling event was used in subsequent experiments (4.35E-8 M $^{242}$Pu and 4.90E-8 M $^{232}$Th).

Preliminary experiments showed that Millipore 3 kDa Amicon® Ultra-4 centrifugal filters achieved complete removal of HA, while allowing greater than 99% recovery of the Pu-EDTA complex (see Appendix A for detailed discussion). These filters employ regenerated cellulose membranes which were compatible with UV-Vis and TOC analysis of the filtrate in HA exclusion experiments (see detailed discussion in Appendix A). Filters were pre-rinsed with approximately 2 mL 0.01 M EDTA prior to filtration. A homogenous 4 mL aliquot was then transferred to a centrifugal filter. Approximately 2 mL of the Pu- or Th-HA solution were passed through the filter as a

pre-equilibration step before the final sample was removed for analysis (see Appendix A for procedure development). Centrifugation was performed on a Beckman GS-6 centrifuge with a swing-bucket rotor at 3000 rotations $min^{-1}$. After separation, the filtrate was diluted to 10 mL using 0.01 M EDTA and the concentrations of $^{242}Pu$ and $^{232}Th$ were determined using a Thermo Scientific X-series II Inductively Coupled Plasma Mass Spectrometer (ICP-MS). Initial scoping experiments found that running samples, standards, and wash solutions through the ICP-MS in 0.01 M EDTA was necessary to overcome the propensity for actinides to hydrolyze and precipitate at high pH and EDTA to precipitate (and co-precipitate the An) at low pH (please see Appendix A for further discussion). $^{238}U$ and $^{232}Th$ were used as internal standards during analysis of samples containing $^{242}Pu$. In Th-HA complexation studies, $^{208}Pb$ was used in place of $^{232}Th$ as an internal standard. In both cases, matrix matched Pu- and Th-EDTA standards were used to calibrate the instrument. Standards prepared contained 0.01, 0.05, 0.1, 1, 5, or 10 ppb Pu or Th. The resulting calibration curve indicated a theoretical detection limit of 15 ppq.

As discussed previously, since the ligands (HA and EDTA) were present in excess relative to the metal, the assumption can be made that the metal was only present as an M-HA or M-EDTA complex. This assumption allows for the following mass-balance equations:

$$C_{in}=[MHA]+[ML_n] \quad (21)$$

$$C_{out}=[ML_n] \quad (22)$$

However, post-experiment comparisons between the expected (*i.e.*, calculated) An concentration and the concentrations measured in un-filtered controls, indicated significant "losses" of the An of interest were occurring. These loses are reflected as a percentage of the theoretical total Pu in Figure 17. This problem highlights another challenge of working with actinides and HAs simultaneously; whether one should use glass or plastic vials for experiments. In contrast to glass, working with plastic vials mitigates An sorption to vial walls, and increases the safety of experiments with radioactive and toxic metals. However, HA adsorbs much more strongly to plastic than glass. Since plastic vials were used in these experiments, and the pH range of these experiments is consistent with the pH range where HA sorption would be expected, we assumed that the differences observed between calculated and measured (using un-filtered controls) Pu concentrations can be attributed to HA sorption to the vial walls. Based on this assumption, the above mass-balance equations become:

$$C_{total} = [MHA]+[ML_n]+ [MHA]_{sorbed} \quad (23)$$

$$C_{filtrate} = [ML_n] \quad (24)$$

Since the An is still complexed with the HA , the formation of surface complexes does not hinder the complexation experiments, assuming the initial An concentration is based on calculated, as opposed to measured (un-filtered samples) concentrations. Therefore, the concentration of metal bound to the HA was calculated using Equation 25:

$$[MHA] = C_{total,\ calculated} - C_{filtrate,\ measured} \quad (25)$$

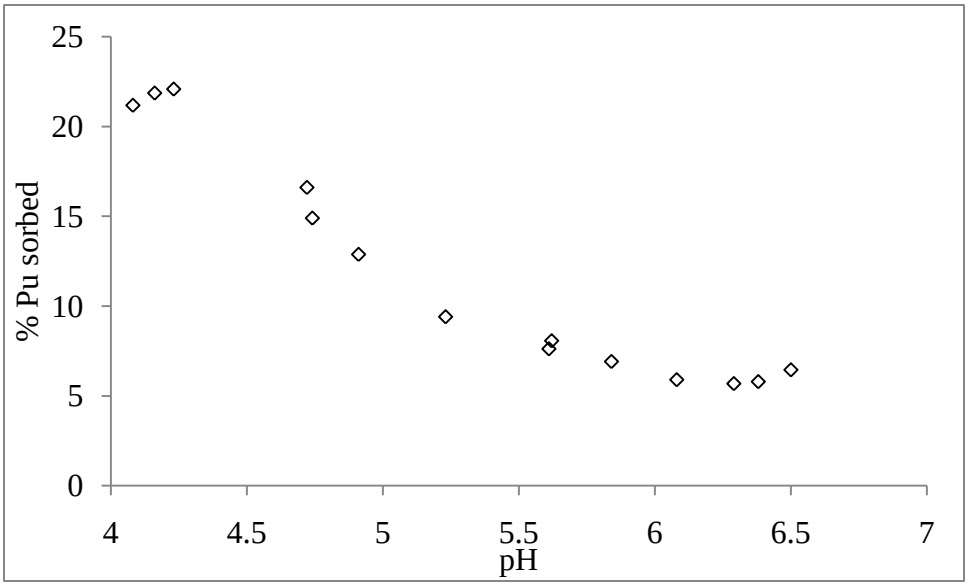


Figure 17: Percent Pu associated with the vial wall (likely due to HA sorption) as a function of pH. Data based on the 4.35E-8 M Pu data set and Equation 25.

## TERNARY SORPTION

The influence of HA on Pu sorption to gibbsite was explored by generating a series of sorption isotherms at pH 4 and 6.

Gibbsite (available from Ward's Scientific) was purified by suspending 10 g of gibbsite in a 180 mL centrifuge bottle filled with approximately 180 mL 0.1 M NaOH. This suspension was mixed for one hour, and then centrifuged for 20 minutes at 8000 rotations $min^{-1}$ using a Sorvall Evolution RC centrifuge with a SLA-1500 Super-lite fixed-angle rotor. This centrifugation procedure was developed to leave particles less than 100 nm in the supernatant. The NaOH supernatant was then decanted and the solution was replaced with 0.1 M HCl, mixed for 1 hour, and then centrifuged again using the parameters outlined above. The HCl was decanted and replaced with ultra-pure MQ-water. This suspension was mixed for approximately 1 hour, centrifuged, and the

aqueous phase was decanted. The solids were washed with MQ-water an additional four times using the procedure described above. The final wet solids were transferred to a glass petri dish and dried in an oven at 105 °C. After drying, the solids were lightly ground with a mortar and pestle to break up large aggregates and then stored in a glass vial. Ultimately, a sufficient quantity of purified gibbsite was suspended in 0.1 M NaCl to yield a 120 g gibbsite/L stock solution (I = 0.1 M). A stir bar was included to ensure the sample remained homogeneous.

A $^{242}$Pu-HA stock solution was prepared by heating 0.5 mL of a $^{242}$Pu stock solution to dryness at approximately 230°C in a 30 mL Teflon vessel. To this, 20 mL of a 10 mg C/L HA solution was added. The resulting solution was mixed well using careful agitation, and then adjusted to pH 5. The $^{242}$Pu concentration in this Pu-HA stock solution was confirmed to be 3.39E-6 M using both ICP-MS and Liquid Scintillation Counting (LSC). LSC measurements were corrected for trace levels of other Pu isotopes (please see Table B-1 in Appendix B for isotope distribution).

Appropriate quantities of gibbsite, HA, and 0.1 M NaCl were added to cleaned 15 mL polypropylene vials to yield 20 samples, each containing 12 mL total volume, with 10 g/L gibbsite and 10 mg C/L HA. The ionic strength was 0.1 M with NaCl. Ten of these suspensions were adjusted to pH 4 and the remaining ten samples were adjusted to pH 6. The pH of each solution was adjusted to within 0.1 pH units of the desired pH using a minimum amount of either 0.1 N HCl or 0.1 N NaOH. A Thermo Fisher Orion Ross Sure-Flow semi-micro electrode that had been calibrated using pH 4, 7, and 10 buffers was used for all pH measurements. After pH adjustments, the gibbsite-HA

suspensions were allowed to equilibrate for 24 hours on an orbital shaker at 25 °C in the absence of light. An appropriate volume of Pu-HA working solution was then spiked into the gibbsite-HA solutions described above, to yield duplicate samples (at both pH 4 and 6) containing 1, 5, 10, 15, or 20 ppb Pu. These solutions were then re-adjusted to the appropriate pH as described above, and placed back on the orbital shaker at 25 °C in the absence of light.

Homogenous aliquots (1.5 mL) were removed after 24 hours. Aliquots were centrifuged at 8000 rotations $min^{-1}$ for 30 min using an F2402H rotor on an Allegra X-22R centrifuge. This centrifugation procedure is designed to leave particles less than 100 nm in the supernatant. After centrifugation, 1.0 mL of the supernatant was extracted and diluted to 10 mL with 0.01 M EDTA. The concentration of $^{242}Pu$ in each sample was determined using ICP-MS as described previously.

The final sampling event (approximately 2 weeks) used a modified sampling procedure. This was done to examine what influence, if any, HA colloids played in the system. It was theorized that HA could aggregate sufficiently to be removed from solution using the centrifugation procedure described above, thereby artificially enhancing the concentration of Pu associated with the "solid phase". The centrifugation parameters were modified to allow the system to be fractionated into < 1500 nm, < 100 nm, and < 3 kDa (nominally considered to be 1-5 nm) size fractions. The desired fractionation was achieved using the following procedure. Solutions were centrifuged for 5 minutes at 1000 rotations $min^{-1}$ using a C1015 rotor on the Allegra X-22R centrifuge. This step served as a pre-filtration step, and was designed to leave particles smaller than

1500 nm in the aqueous phase. Homogenous 1.0 mL aliquots were then removed and diluted with 9 mL 0.01M EDTA for quantification using ICP-MS. The remaining sample was then centrifuged for an additional 20 minutes at 8000 rotations $min^{-1}$. From this, a 1.0 mL aliquot of the supernatant was removed and prepared for quantification using the ICP-MS as described above. Theoretically, particles larger than 100 nm were removed during this centrifugation step. Finally, an additional 2.0 mL of the supernatant was removed from each centrifuged sample and passed through a 3 kDa Amicon ultra-4 centrifugal filter. Approximately 0.5 mL of the solution was used to pre-equilibrate each filter. The filtrate was then discarded and filtration resumed. Approximately 1.0 mL of the filtrate was collected and prepared for quantification of the $^{242}Pu$ concentration using ICP-MS.

CHAPTER FIVE

## RESULTS AND DISCUSSION

The modeling approach used to determine the conditional Pu-HA stability constant is summarized in Figure 18. Humic acid titration data served as input data for the proton-binding model. The HA titration data was modeled assuming that proton-binding to the HA can be described by a discrete spectrum of pKa values. The number of accessible proton-binding sites at each discrete pKa value was calculated from model output and served as input data, in addition to metal partitioning data, in subsequent metal-binding models. Finally, the conditional stability constant for the Pu-HA complex was determined using this metal-binding model.

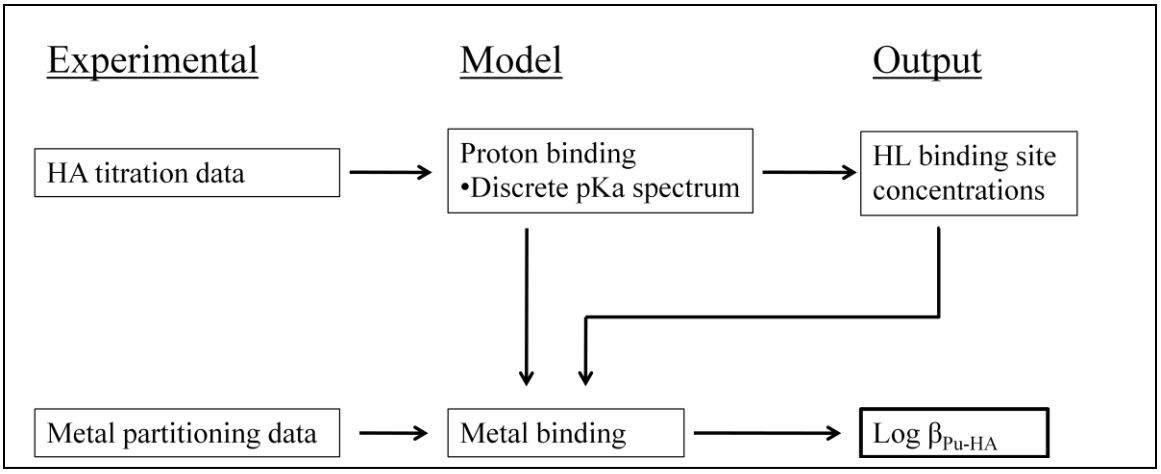


Figure 18: Flow diagram describing the modeling approach used in this work.

PROTON BINDING MODELING

Titrations of Leonardite HA were carried out as described in Chapter Four of this thesis. Figure 19 shows the complete HA titration data (*i.e.*, cycles 1-5). For clarity,

Figure 20 shows only the last 2 cycles (*i.e.*, Cycle 4 and Cycle 5), which exhibited the least hysteresis.

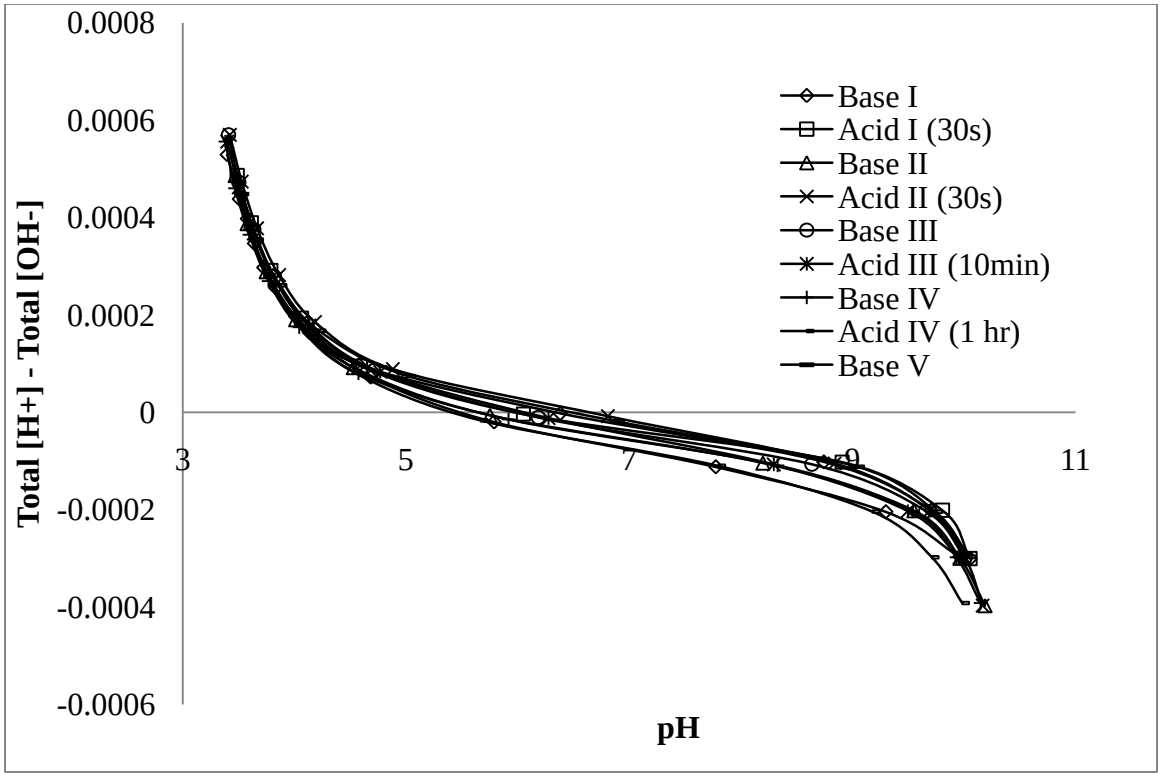


Figure 19: HA titration data (complete). HA concentration: 50 mg C/L, I = 0.1M NaCl. Note: lines are intended to guide the eye and do not represent a model fit.

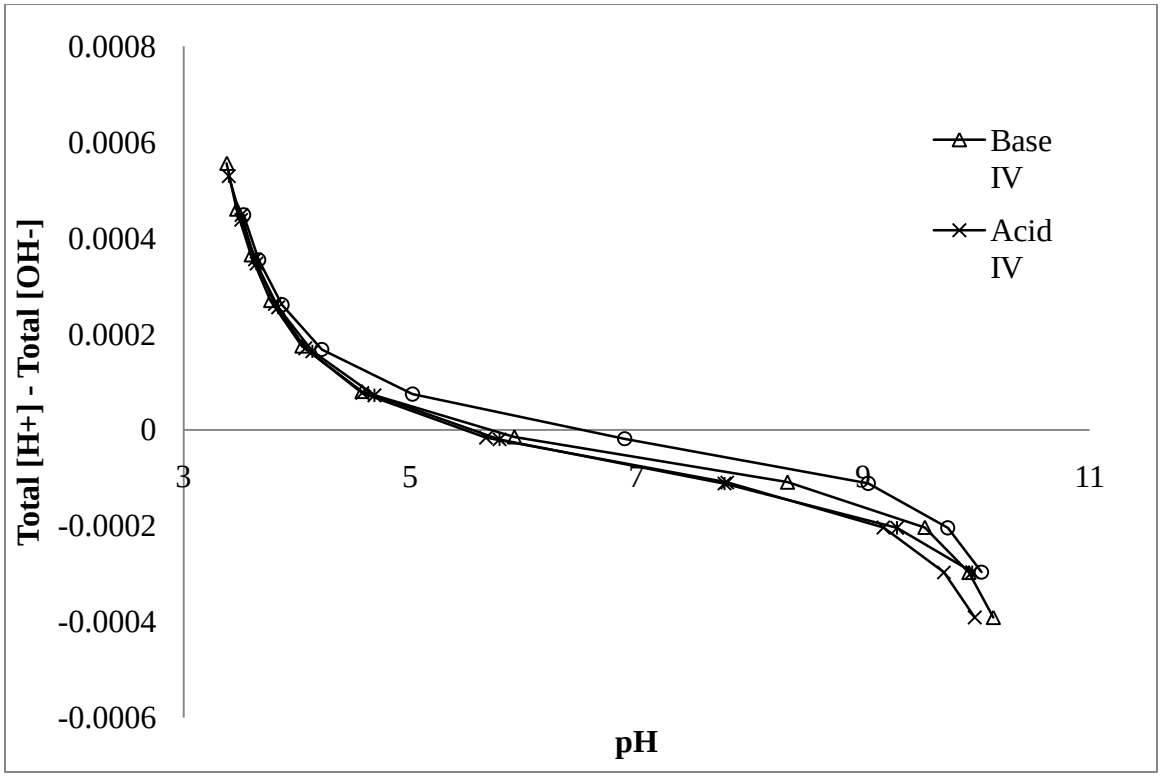


Figure 20: HA titration data (cycles 4 and 5). HA concentration: 50 mg C/L, I = 0.1M NaCl. Note: lines are intended to guide the eye and do not represent a model fit.

Due to the limited hysteresis, these titration curves (Cycles 4 and Cycle 5) were used in initial efforts to model proton-binding to HA. Ultimately, the binding site concentrations determined using the Base IV data were used in Pu-HA stability constant models. The Base IV dataset was selected for inclusion in metal-HA binding models since it is representative (*i.e.*, approximates the average) of all cycles, and exhibited limited hysteresis (when compared with the corresponding Acid IV curve).

Titration data were modeled using FITEQL assuming the proton-binding sites can be represented by a spectrum of discrete pKa values. Initial modeling efforts focused on determining the most appropriate combination of pKa values for accurately representing the experimental data. In the end, four proton-binding sites, with pKa values of 3, 5, 7,

and 9 (referred to herein as HL1, HL2, HL3, and HL4, respectively), provided the most reasonable fit to the experimental data. Modeling the data assuming pKa values of 2, 4, 6, and 9 did provide a better fit (weighted sum of squares: 0.108 *versus* 0.289). However, consideration of the pH range of HA titration data suggests that the latter set of pKa values may be less appropriate as the inclusion of a pKa 2 site, significantly, and perhaps artificially, skews the distribution of binding sites to the low end of the spectrum. The uncertainty in a pKa 2 site is driven by the fact that this site is well outside of the pH range of HA titration data.

Figure 21 shows the Base IV curve with model fit. The table imbedded in Figure 21 contains the proton-binding site concentrations determined using FITEQL. FITEQL model output reports the concentration of species (*e.g.*, proton-binding sites) in [mol/L]. Therefore, Equation 26 was used to adjust the binding site concentrations to a measurable quantity, mg C (determined using TOC).

$$\left\{ \frac{[HLx]_{model}}{C_{HA,\ titration}\left(\frac{mgC}{L}\right)} \right\} = C_{HLx}\left(\frac{mol}{mg\ C}\right) \qquad (26)$$

The concentration of HLx (mol/mg C) was then scaled to the HA concentrations used in the complexation studies using Equation 27, and served as input data for subsequent Pu- and Th-HA complexation models.

$$C_{HLx}\left(\frac{mol}{mg\ C}\right) * C_{HA,\ complexation}\left(\frac{mg\ C}{L}\right) = C_{HLx,\ complexation}\left(\frac{mol}{L}\right) \qquad (27)$$

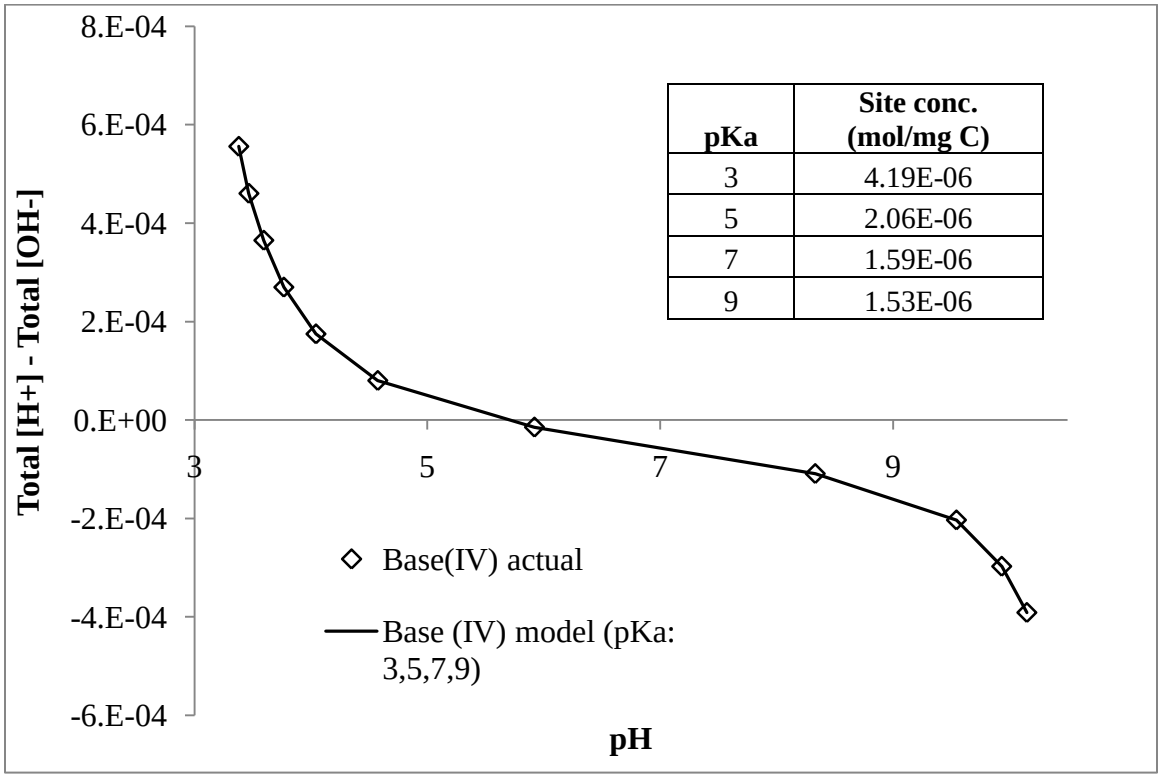


Figure 21: HA base (IV) titration data with model fit. Model fit generated using FITEQL assuming a discrete pKa spectrum of 3, 5, 7, and 9.

During later modeling efforts, the influence of titration hysteresis on total proton-binding site concentrations and the resultant conditional Pu-HA stability constant, was examined using the acid (*i.e.*, base – acid) curves shown in Figure 22, which were generated using different times between additions, and found to be minimal. These results indicate that future titrations (for studies of this type) can be conducted without being overly concerned with the time between acid or base additions. The results of these modeling efforts are summarized in Table 3 (proton binding site concentrations) and Table 6 (corresponding Pu-HA stability constants).

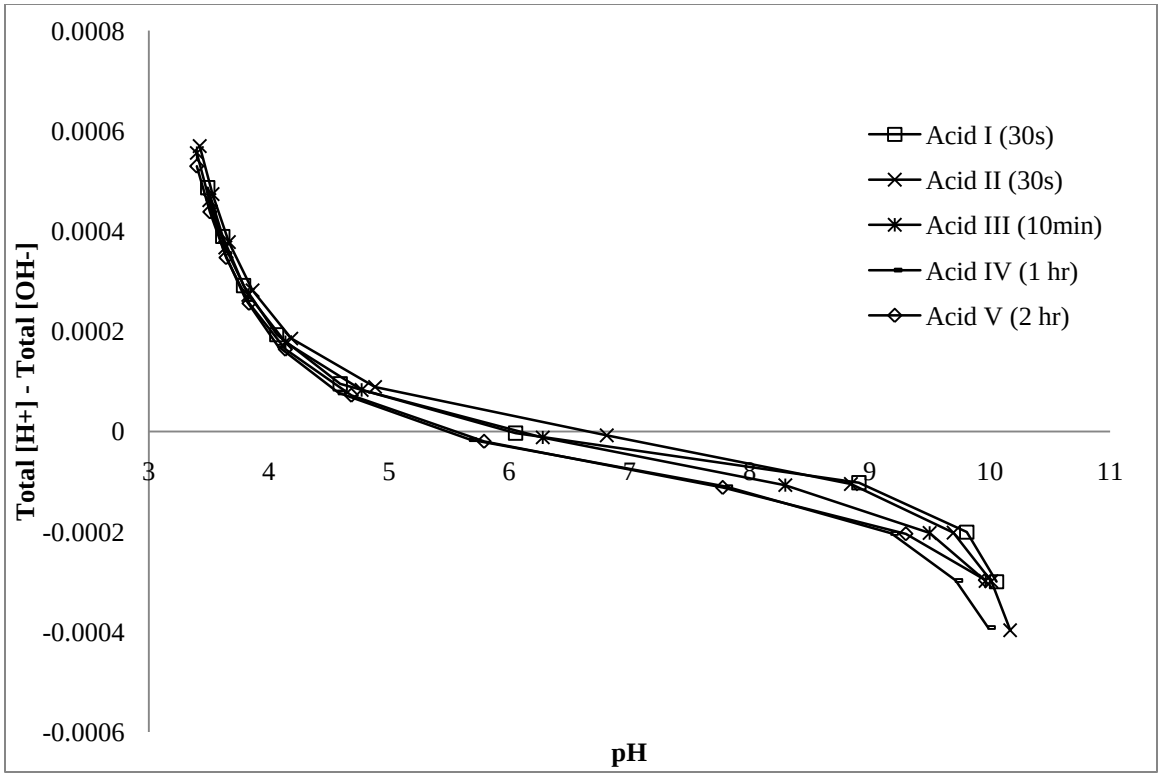


Figure 22: HA titration data (acid only). HA concentration: 50 mg C/L, I = 0.1 M NaCl. Note: lines are intended to guide the eye and do not represent a model fit.

Table 3: Influence of titration hysteresis on resultant binding site concentrations (as modeled using FITEQL assuming a discrete pKa spectrum of 3, 5, 7, and 9).

| | | **Site conc. (mol/mg C)** | | | | |
|---|---|---|---|---|---|---|
| | Time between additions | HL1 | HL2 | HL3 | HL4 | Total binding site conc. (mol/mg C) |
| Acid(I) | 30 seconds | 6.24E-06 | 1.98E-06 | 1.29E-06 | 8.72E-07 | 1.04E-05 |
| Acid(II) | 30 seconds | 6.10E-06 | 1.98E-06 | 1.50E-06 | 1.96E-06 | 1.16E-05 |
| Acid(III) | 10 minutes | 4.21E-06 | 2.25E-06 | 2.00E-06 | 1.39E-06 | 9.86E-06 |
| Acid(IV) | 1 hour | 6.05E-06 | 2.38E-06 | 1.57E-06 | 2.77E-06 | 1.28E-05 |
| Acid(V) | 2 hours | 3.68E-06 | 2.81E-06 | 1.93E-06 | 1.09E-06 | 9.51E-06 |

Westall *et al.* (1995), using a discrete pKa spectrum of 4, 6, 8, and 10, reported a total proton-binding site concentration of 1.01E-5 (mol/mg C) for Leonardite HA. This value corresponds very well with the total binding site concentrations shown in Table 3.

The average total binding site concentration for the five Acid curves in Table 3 is 1.08E-5 (mol/mg C).

## PLUTONIUM-HA COMPLEXATION and MODELING STUDIES

Pre-modeling analysis of the Pu-EDTA speciation over the pH range of this study (Figure 23) using reported stability constants (Table 4) indicate that EDTA forms exceptionally strong complexes with Pu.

As an aside, please note that the stability constants selected for inclusion in Table 4 are the best available constants for the various species needed to model the systems of interest. The constants from Boukhalfa et al. (2004), the Nuclear Energy Agency – Thermochemical Database Project (NEA-TDB), Neck and Kim (2001), and the NIST Standard Reference Database 6 Version 7.0, were corrected to 0.1 M ionic strength as needed. The only stability constants determined as part of this work are the conditional Pu- and Th-HA constants and the four pKa values assigned to the assumed proton-binding sites on the HA.

The partitioning of Pu and Th between HA and EDTA was examined using the experimental conditions outlined in Chapter Four. An initial study using 2.60E-7 M Pu, 10 mg C/L HA, and 1E-5 M EDTA confirmed that these experimental conditions provide the necessary distribution of Pu-HA and Pu-EDTA species for stability constant determination. The data from this experiment appear in Figure 24 and show that greater than 50% of the total Pu is complexed by HA, rather than EDTA, across the entire pH range of interest.

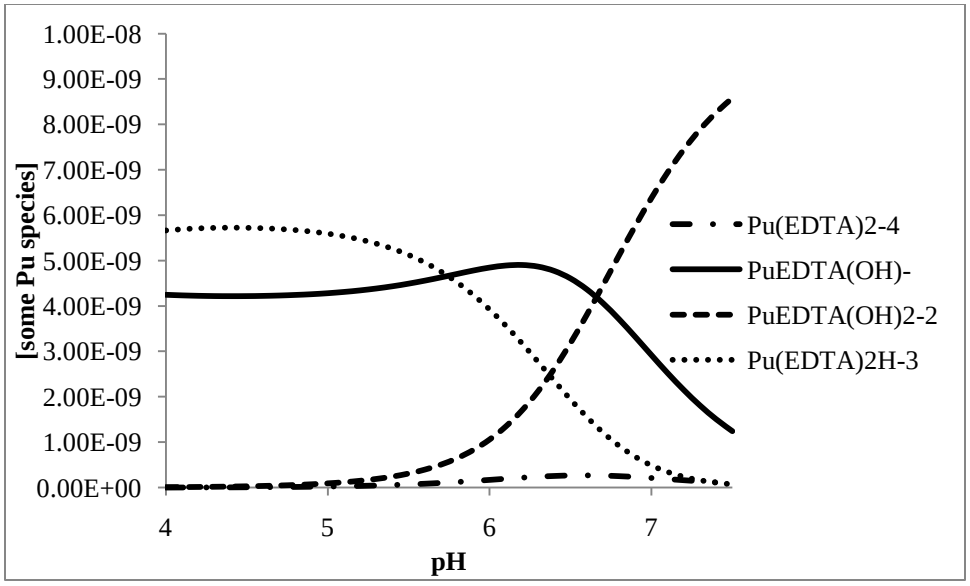


Figure 23: 1E-8 M Pu speciation in the presence of 1E-5 M EDTA. For clarity only the dominant species are depicted. Speciation modeled using FITEQL and the applicable stability constants in Table 4.

The potential exists for perturbing equilibrium when using UF for studies of this type. In these experiments, the separation resulted in the concentration of HA in the retentate. This could theoretically lead to a disruption of the equilibrium between metal bound to HA and metal bound to EDTA, resulting in an increased concentration of Pu bound to HA over the amount bound in the equilibrium system. This would occur during the time required for centrifugation. During separations the times required to separate the samples varied considerably (± approximately 30 minutes) due to variations in flow rate through the filter assemblies. This information, coupled with the consistency observed in the datasets shown in Figure 24, Figure 25, and Figure 26 (especially the consistency between samples pulled from the same vials in the 4.35E-8 M Pu and 4.90 E-8 M Th datasets), indicate that the metal partitioning kinetics do not appear to play an appreciable role over the timescale of these separations.

The 2.60E-7 M Pu (Figure 24), 4.35E-8 M Pu (Figure 25), and 4.90E-8 M Th (Figure 26) datasets were modeled independently, and then globally (Pu only) using FITEQL. In addition to $[M]_{total}$, [M-HA] (as determined using Equation 25), and the [EDTA], the binding-site concentrations determined previously (*i.e.*, [HL1], [HL2], [HL3], and [HL4]) served as input data for the An-HA models (an example input matrix appears in Appendix C). Using this approach, the conditional Pu- and Th-HA stability constants were calculated over the pH range 4 – 7.

Parameter optimization in FITEQL is performed by minimizing the weighted sum of squares (WSOS) of the difference functions Y for all Group II components (Group II components are used as the basis species for optimization) over all *m* data points:

$$WSOS = \sum_{m} \left[ \frac{Y_{II}^2(m)}{s_{Y_{II}(m)}^2} \right] \tag{28}$$

where $Y_{II(m)}$ represents the difference function and $S_{YII(m)}$ is an estimate of the experimental error associated with $Y_{II(m)}$ (Herbelin and Westall, 1999). The value of $S_{YII(m)}$ can be calculated using Equation 29:

$$s_{Y(m)}^2 = \left( \frac{\partial Y}{\partial T_{I,II}} \right)\Bigg|_m^2 s_{T_{I,II(m)}}^2 + \left( \frac{\partial Y}{\partial X_{II,III}} \right)\Bigg|_m^2 s_{X_{II,III(m)}}^2 \tag{29}$$

where $S_T$ and $S_x$ are estimates of the error associated with the experimentally measured values $T_{I,II}$ (total analytical concentration of a component) and $X_{II,III}$ (free concentration of a component) (Herbelin and Westall, 1999). In this work, 5% relative error and 0% absolute error were presumed to be valid for the entire set of serial data.

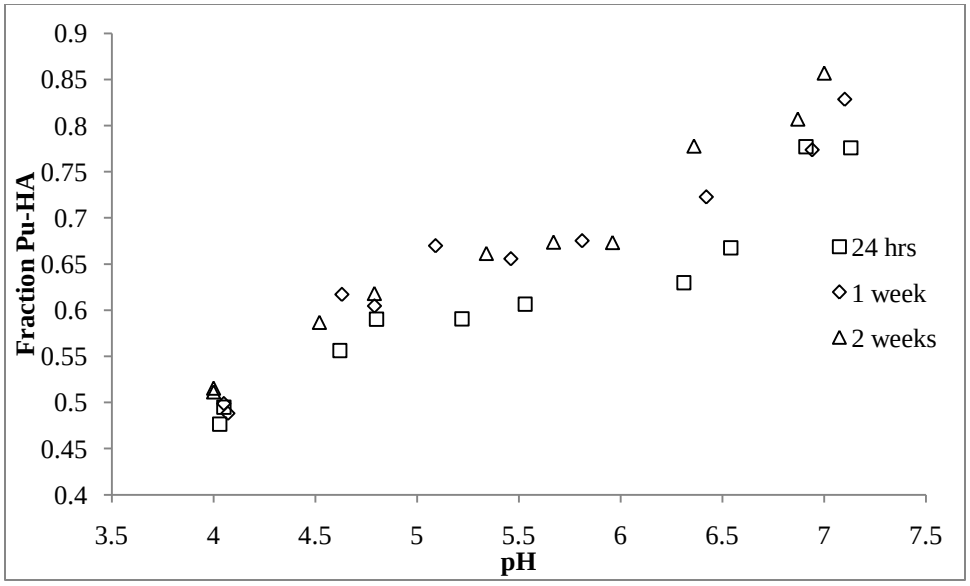


Figure 24: Pu fraction bound to HA *versus* pH after 24 hours, 1 week, or 2 weeks in the system containing 2.60E-7 M Pu.

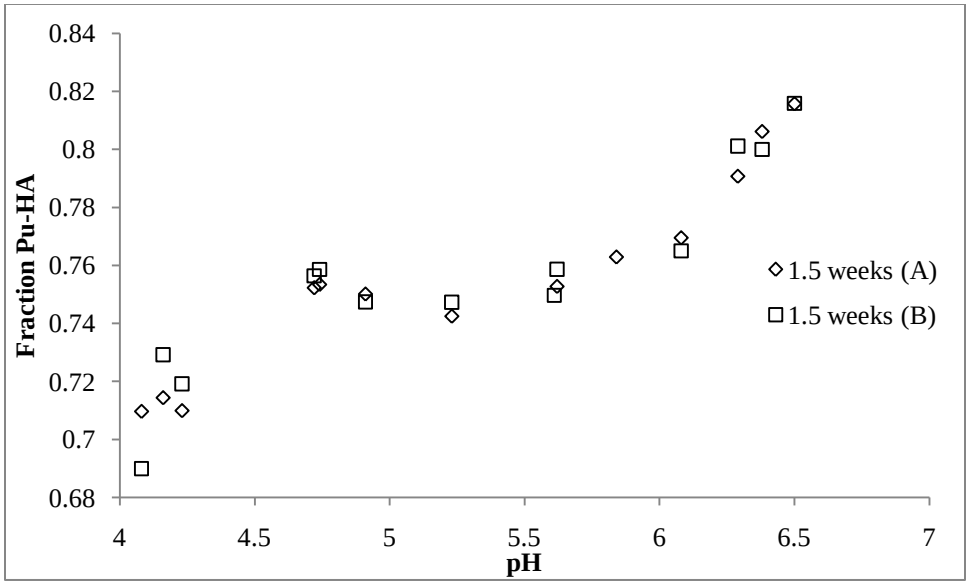


Figure 25: Pu fraction bound to HA *versus* pH after 1.5 weeks in the system containing 4.35E-8 M Pu.. A and B represent samples from the same vial.

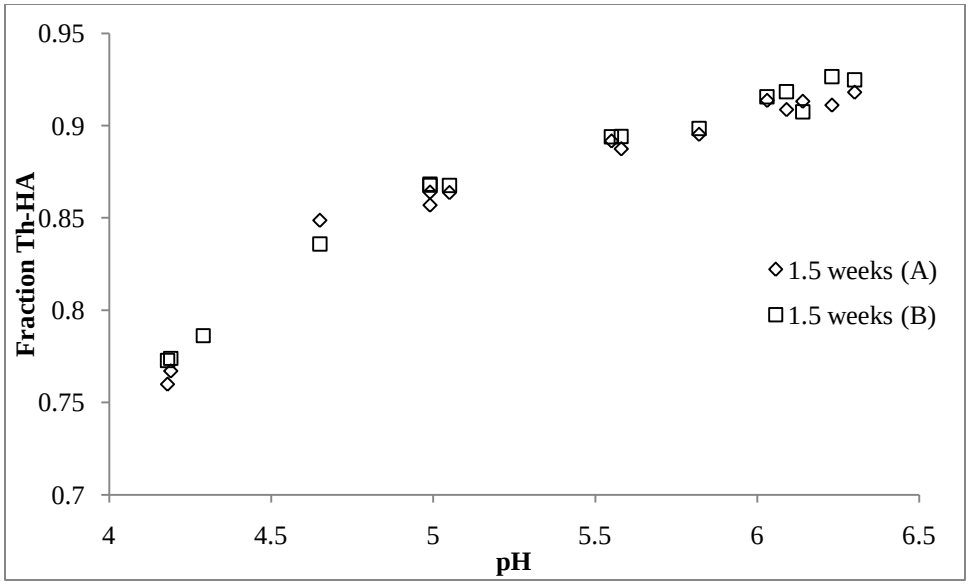


Figure 26: Th fraction bound to HA *versus* pH after 1.5 weeks in the system containing 4.90E-8 M Th. A and B represent samples from the same vial.

Table 4: Critically selected stability constants used in this study. For simplicity, the HA binding sites are represented by Lx, and EDTA by $Y^{4-}$.

| Reaction | Constant | Boukhalfa *et al.*(2004) (I = 0.1M $NaNO_3$, T = 298.15K) | NEA-TDB (I = 0M) | This study* (I = 0.1M NaCl, T = 298.15K) |
|---|---|---|---|---|
| $HL1 \leftrightarrow H^+ + L1^-$ | pKa | | | 3.00 |
| $HL2 \leftrightarrow H^+ + L2^-$ | pKa | | | 5.00 |
| $HL3 \leftrightarrow H^+ + L3^-$ | pKa | | | 7.00 |
| $HL4 \leftrightarrow H^+ + L4^-$ | pKa | | | 9.00 |
| $Pu^{4+} + H_2O \leftrightarrow Pu(OH)^{3+} + H^+$ | Log $\beta_{11}$ | -1.41 | 0.60 | -0.04 |
| $Pu^{4+} + 2H_2O \leftrightarrow Pu(OH)_2^{2+} + 2H^+$ | Log $\beta_{12}$ | -3.72 | 0.60 | -0.47 |
| $Pu^{4+} + 3H_2O \leftrightarrow Pu(OH)_3^{+} + 3H^+$ | Log $\beta_{13}$ | | -2.3 | -3.58 |
| $Pu^{4+} + 4H_2O \leftrightarrow Pu(OH)_4(aq) + 4H^+$ | Log $\beta_{14}$ | | -8.5 | -9.78 |
| $Y^{4-} + H^+ \leftrightarrow YH^{3-}$ | Log $K_{011}$ | 9.52 | | 9.52 |
| $YH^{3-} + H^+ \leftrightarrow YH_2^{2-}$ | Log $K_{012}$ | 6.13 | | 6.13 |
| $YH_2^{2-} + H^+ \leftrightarrow YH_3^-$ | Log $K_{013}$ | 2.69 | | 2.69 |
| $YH_3^- + H^+ \leftrightarrow YH_4$ | Log $K_{014}$ | 2.0 | | 2.0 |
| $YH_4 + H^+ \leftrightarrow YH_5^+$ | Log $K_{015}$ | 1.5 | | 1.5 |
| $YH_5^+ + H^+ \leftrightarrow YH_6^{2+}$ | Log $K_{016}$ | 0 | | 0 |

Table 4 continued…

| Reaction | Constant | Boukhalfa *et al.*(2004) (I = 0.1M NaNO3, T = 298.15K) | NEA-TDB (I = 0M) | This study* (I = 0.1M NaCl, T = 298.15K) |
|---|---|---|---|---|
| $Pu^{4+} + Y^{4-} \leftrightarrow Pu(Y)$ | Log $\beta_{11}$ | 24.20 (0.1M KCl) | | 24.20 |
| $Pu^{4+} + Y^{4-} + H_2O \leftrightarrow [Pu(Y)(OH)]^{-} + H^{+}$ | Log $\beta_{111}$ | 21.95 | | 21.95 |
| $Pu^{4+} + Y^{4-} + 2H_2O \leftrightarrow [Pu(Y)(OH)_2]^{2-} + 2H^{+}$ | Log $\beta_{112}$ | 15.29 | | 15.29 |
| $Pu^{4+} + 2Y^{4-} \leftrightarrow [Pu(Y)_2]^{4-}$ | Log $\beta_{120}$ | 35.39 | | 35.39 |
| $Pu^{4+} + 2Y^{4-} + H^{+} \leftrightarrow [Pu(Y)_2H]^{3-}$ | Log $\beta_{121}$ | 42.75 | | 42.75 |
| $Pu^{4+} + 2Y^{4-} + 2H^{+} \leftrightarrow [Pu(Y)_2H_2]^{2-}$ | Log $\beta_{122}$ | Not included | | Not included |
| $Pu^{4+} + 2Y^{4-} + 3H^{+} \leftrightarrow [Pu(Y)_2H_3]^{-}$ | Log $\beta_{123}$ | 47.39 | | 47.39 |
| | | | | |
| $Th^{4+} + H_2O \leftrightarrow Th(OH)^{3+} + H^{+}$ | Log $\beta_{11}$ | | | -2.84[a] |
| $Th^{4+} + 2H_2O \leftrightarrow Th(OH)_2^{2+} + 2H^{+}$ | Log $\beta_{12}$ | | | -7.07[a] |
| $Th^{4+} + 3H_2O \leftrightarrow Th(OH)_3^{+} + 3H^{+}$ | Log $\beta_{13}$ | | | -12.28[a] |
| $Th^{4+} + 4H_2O \leftrightarrow Th(OH)_4(aq) + 4H^{+}$ | Log $\beta_{14}$ | | | -18.78[a] |
| | | | | |
| $Th^{4+} + Y^{4-} \leftrightarrow Th(Y)$ | Log $\beta_{11}$ | | | 23.20[b] |
| $Th^{4+} + Y^{4-} + H^{+} \leftrightarrow [Th(H)(Y)]^{+}$ | Log $\beta_{111}$ | | | 25.20[b] |
| $Th^{4+} + Y^{4-}\ H_2O \leftrightarrow [Th(OH)(Y)]^{-} + H^{+}$ | Log $\beta_{111}$ | | | 16.16[b] |
| $2Th^{4+} + 2Y^{4-}\ 2H_2O \leftrightarrow [Th_2(OH)_2(Y)_2]^{2-} + 2H^{+}$ | Log $\beta_{222}$ | | | 36.58[b] |

* The stability constants used in this study were corrected to 0.1 M ionic strength using the Davies equation as needed.

[a] Neck and Kim (2001)

[b] NIST Standard Reference Database 6 Version 7.0

Initial models attempted to describe metal binding to HA using the following reaction:

$$An^{4+} + HL \leftrightarrow AnL^{3+} + H^{+} \quad (30)$$

Note that $An^{4+}$ represents $Th^{4+}$ or $Pu^{4+}$, which were generalized as M in Equation 25. Similarly, L is used to represent HA. The reaction shown in Equation 30 failed to capture the pH dependence of the An-HA complexation data depicted in Figure 24, Figure 25, and Figure 26. The inability of the reaction shown in Equation 30 to capture the pH dependence of the experiment data is illustrated in Figure 27.

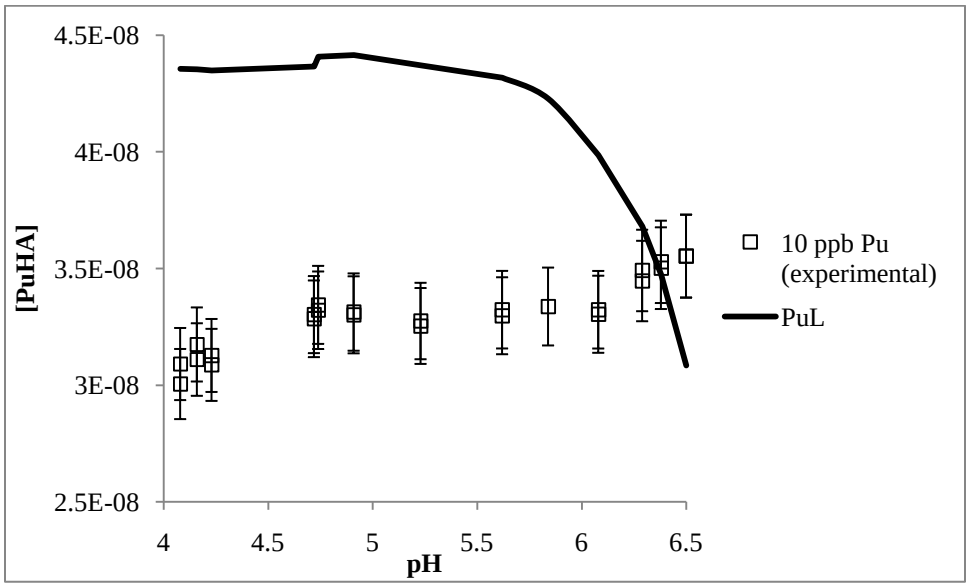


Figure 27: Concentration of 4.35E-8 M Pu bound to HA with model fit based on the reaction shown in Equation 30 (logK: 19.41, WSOS: 13.25, HL3 basis). Error bars depict the assumed 5% error.

The assumption that the metal is at least partially hydrolyzed (Equation 31) captures the pH dependence of the experimental data. It is important to note that this speciation is merely a theoretical mathematical construct which captures the pH dependence of the experimental data and may not represent the actual species formed.

Spectroscopic techniques are required to verify this species but the concentrations of Pu used in this work prohibit such characterization. The corresponding stability constant is shown in Equation 32.

$$An^{4+} + HL + xH_2O \leftrightarrow An(OH)_xL^{(4-x)} + (x+1)H^+ \quad (31)$$

$$\beta_{11x} = \frac{\left[An(OH)_xL^{4-x}\right]\left[H^+\right]^{(x+1)}}{\left[An^{z+}\right][HL]\ a_{H_2O}} \quad (32)$$

Using the approach outlined in Equation 31, with x = 1, 2, 3, or 4, each dataset was modeled independently using each of the four basis species individually (*i.e.*, HL1, HL2, HL3, and HL4). The results from these modeling efforts are summarized in Table 5. The discrepancy in model fit with extent of metal hydrolysis (Equation 31), as well as the variation in model fit for different binding sites at constant metal hydrolysis, was examined using the 4.35E-8 M Pu dataset. The results appear in Figure 28 and Figure 29. For comparison between model results based on Equation 30 (no metal hydrolysis) and Equation 31 (metal hydrolysis assumed), the model fit for a Pu-L species (Figure 27) is shown in Figure 28.

Figure 28 shows significant variability in the model fit obtained for varying extents of Pu hydrolysis. Models incorporating the first hydrolysis product of Pu, $Pu(OH)^{3+}$, significantly over-fit the experimental data at low pH and exhibit decreasing Pu-HA complex formation with increasing pH (while still over-fitting the experimental data over nearly the entire pH range). Similarly, assuming no hydrolysis (Equation 30) results in a model fit similar to that described for $Pu(OH)^{3+}$. The second hydrolysis product of Pu, $Pu(OH)_2^{2+}$, does a much better job of fitting the experimental data. This

species captures the subtle pH dependence of the data, while only slightly over-fitting at high pH. As expected based on Equation 32, the third and fourth hydrolysis products of Pu show major pH dependence and over-fit the experimental data over nearly the entire pH range. Based on the data in Table 5 and corresponding plots in Figure 28, the assumption that Pu is present as $Pu(OH)_2^{2+}$ provides the best model fit.

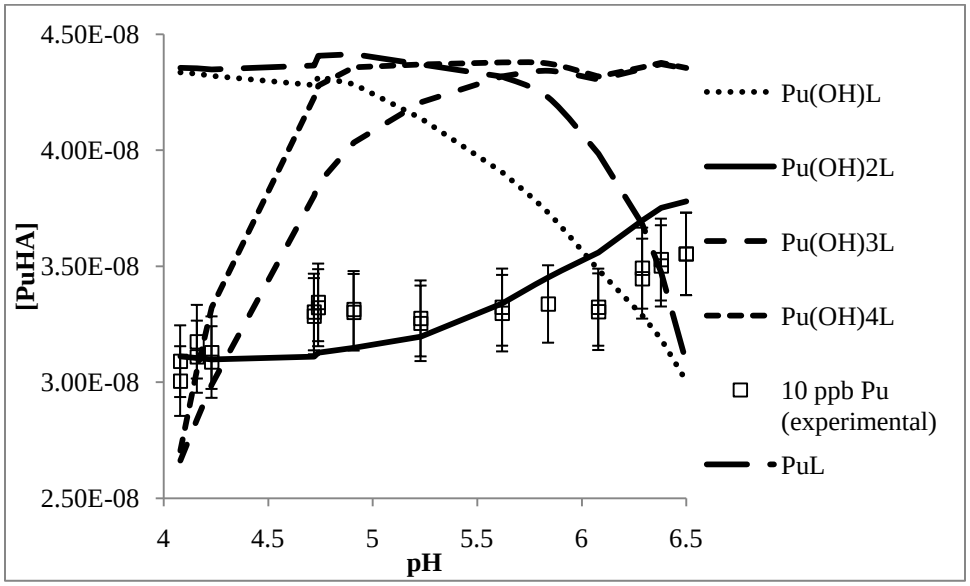


Figure 28: Model fit to 4.35E-8 M Pu dataset for varying extents of metal hydrolysis (HL3 basis).

Similarly, the influence of proton-binding site on the resulting Pu-HA stability constant was examined. Figure 29 shows that the HL3 (pKa 7) and HL4 (pKa 9) binding sites provide reasonable fits to the data, while the HL1 (pKa 3) and HL2 (pKa 5) sites over-predict Pu-HA complex formation (over the majority of the pH range considered). Furthermore, the HL1 and HL2 binding sites fail to capture the pH dependence of the experimental data, instead predicting decreasing Pu-HA complex formation with increasing pH. Overall, the HL3 binding site provides the best fit to the 4.35E-8 M Pu data.

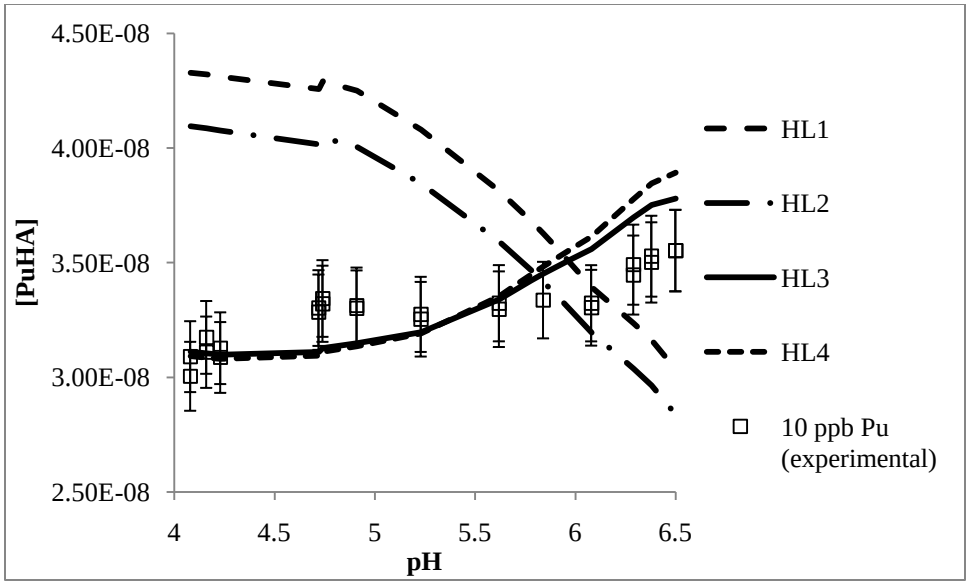


Figure 29: Model fit to 4.35E-8 M Pu dataset using HL1, HL2, HL3, and HL4 binding sites. Pu assumed to be present as $Pu(OH)_2L^+$.

Figure 30 and Figure 31 show the experimental data for 2.60E-7 M Pu (2 week) with a model fit based on an HL1 (pKa 3) or HL3 (pKa 7) basis, respectively. Despite the less precise model fit (when compared with the data in Figure 30), the data in Figure 31 allow easier comparison between the 4.35E-8 M and 2.60E-7 M Pu models and the global Pu fit described later, since the proton-binding site used is the same. Figure 32 and Figure 33 show the experimental data for 4.35E-8 M Pu and 4.90E-8 M Th, respectively, with the corresponding best model fit.

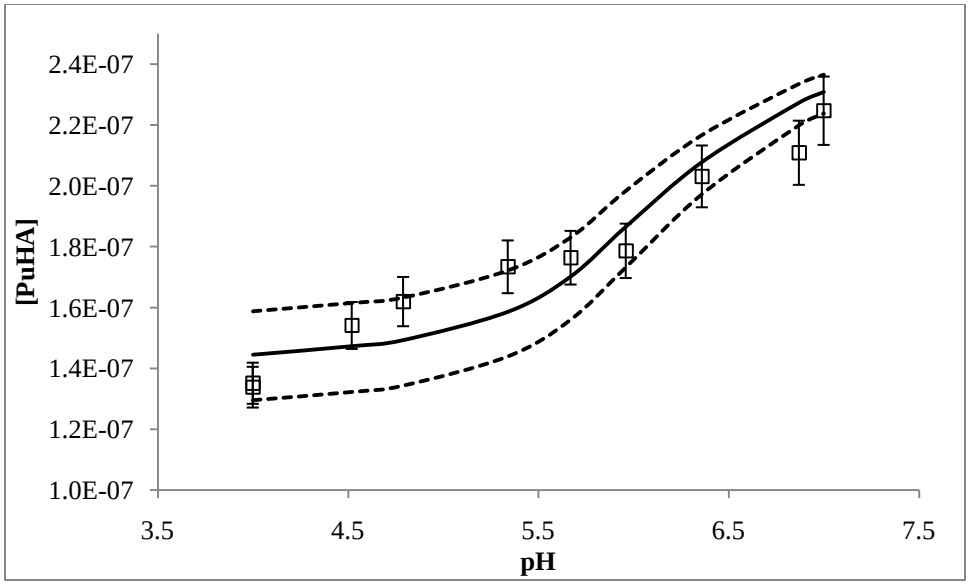


Figure 30: Concentration of 2.60E-7 M Pu bound to HA (log K: 3.181, WSOS: 0.6645, HL1 basis). Dashed lines represent ±1 σ error in the calculated stability constant. Error bars depict the assumed 5% error.

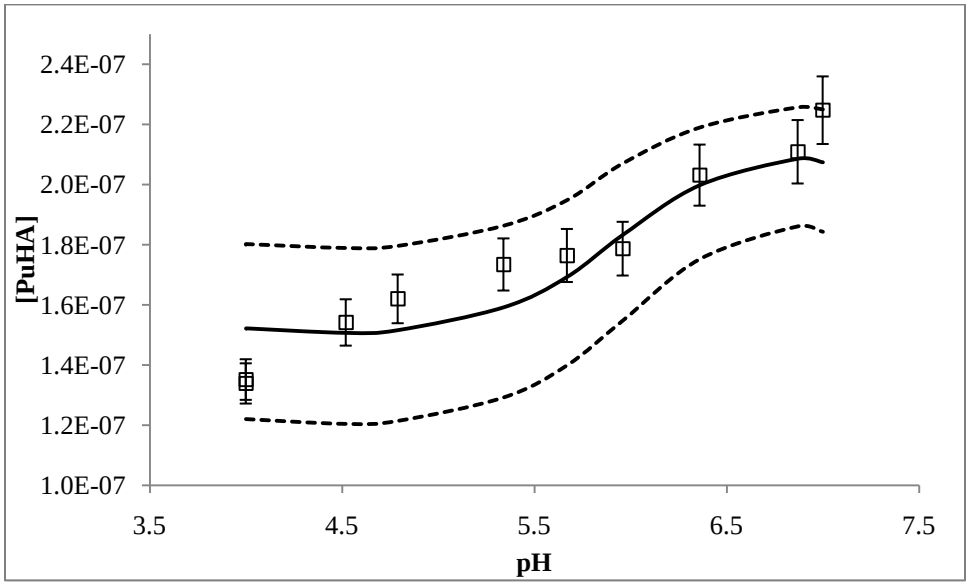


Figure 31: Concentration of 2.60E-7 M Pu bound to HA (log K: 6.615, WSOS: 0.9043, HL3 basis). Dashed lines represent ±1 σ error in the calculated stability constant. Error bars depict the assumed 5% error.

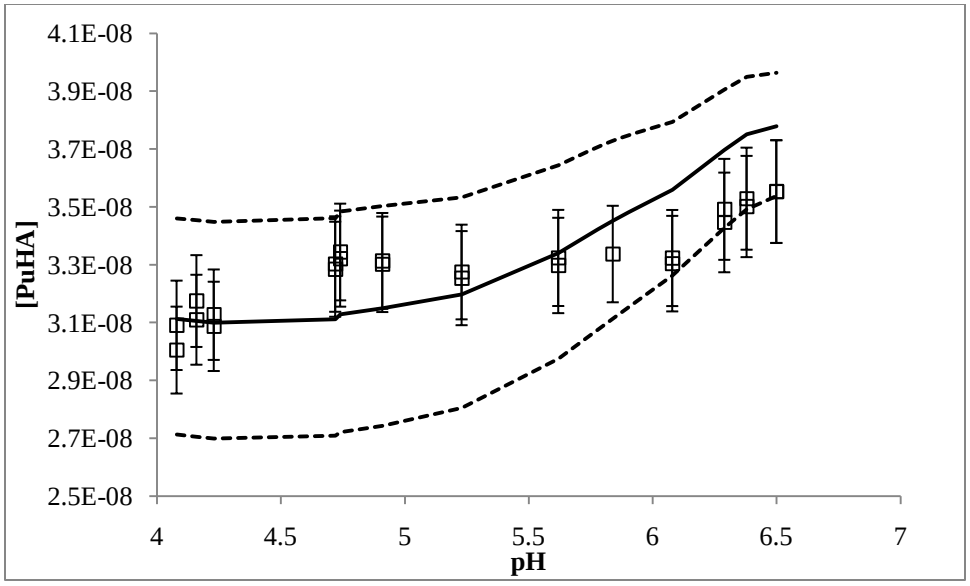


Figure 32: Concentration of 4.35E-8 M Pu bound to HA (logK: 6.841, WSOS: 0.4505, HL3 basis). Dashed lines represent ±1 σ error in the calculated stability constant. Error bars depict the assumed 5% error.

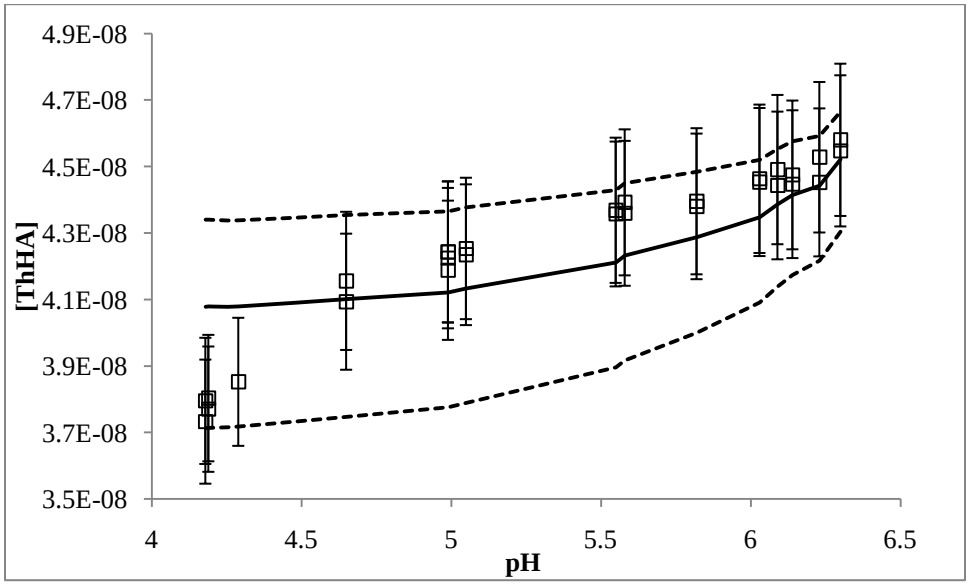


Figure 33: Concentration of 4.90E-8 M Th bound to HA (logK: 4.629, WSOS: 0.2817, HL1 basis). Dashed lines represent ±1 σ error in the calculated stability constant. Error bars depict the assumed 5% error.

After modeling each dataset individually, the 4.35E-8 M and 2.60E-7 M Pu data sets were combined, and a global fit was achieved. To simplify the data presentation the experimental data, with global model fit is divided between A (4.35E-8 M Pu) and B (2.60E-7 M Pu) sections in Figure 34.

Although the model fit deteriorates somewhat when both datasets are modeled simultaneously, as reflected in the increased WSOS value (0.4505 (4.35E-8 M Pu) and 0.6645 (2.60E-7 M Pu) *versus* 1.366 (global)), the resultant Pu-HA stability constants are reasonably similar, 6.84, 3.18 (HL1 basis), and 6.76, respectively. The calculated stability constants and corresponding WSOS values are summarized in Table 5.

Qualitatively, when the data are modeled globally, the 4.35E-8 M Pu dataset (Figure 34A) is under-fit at low pH (*i.e.*, less than approximately pH 5.8) and over-fit at high-pH. In contrast, the 2.60E-7 M Pu dataset (Figure 34B) is over-fit, to varying extents across nearly the entire pH spectrum (the highest pH data point is slightly under-fit). An interesting point to note is the inability of the models, including the 4.35E-8 M Pu only model shown in Figure 32, to capture the experimental data from approximately pH 4.3 – 5.3 in the 4.35E-8 M Pu datasets. This could indicate inadequacies in the body of knowledge surrounding Pu-EDTA speciation and the corresponding stability constants.

Despite the variation in model fit (as reflected in the WSOS value) shown in Table 5, the calculated stability constants are relatively similar. Furthermore, the calculated Pu-HA stability constants are largely independent of the binding site used (*e.g.*, HL1 *versus* HL4), indicating that the energetics of proton-binding are minimal in comparison to those associated with An binding to the same sites.

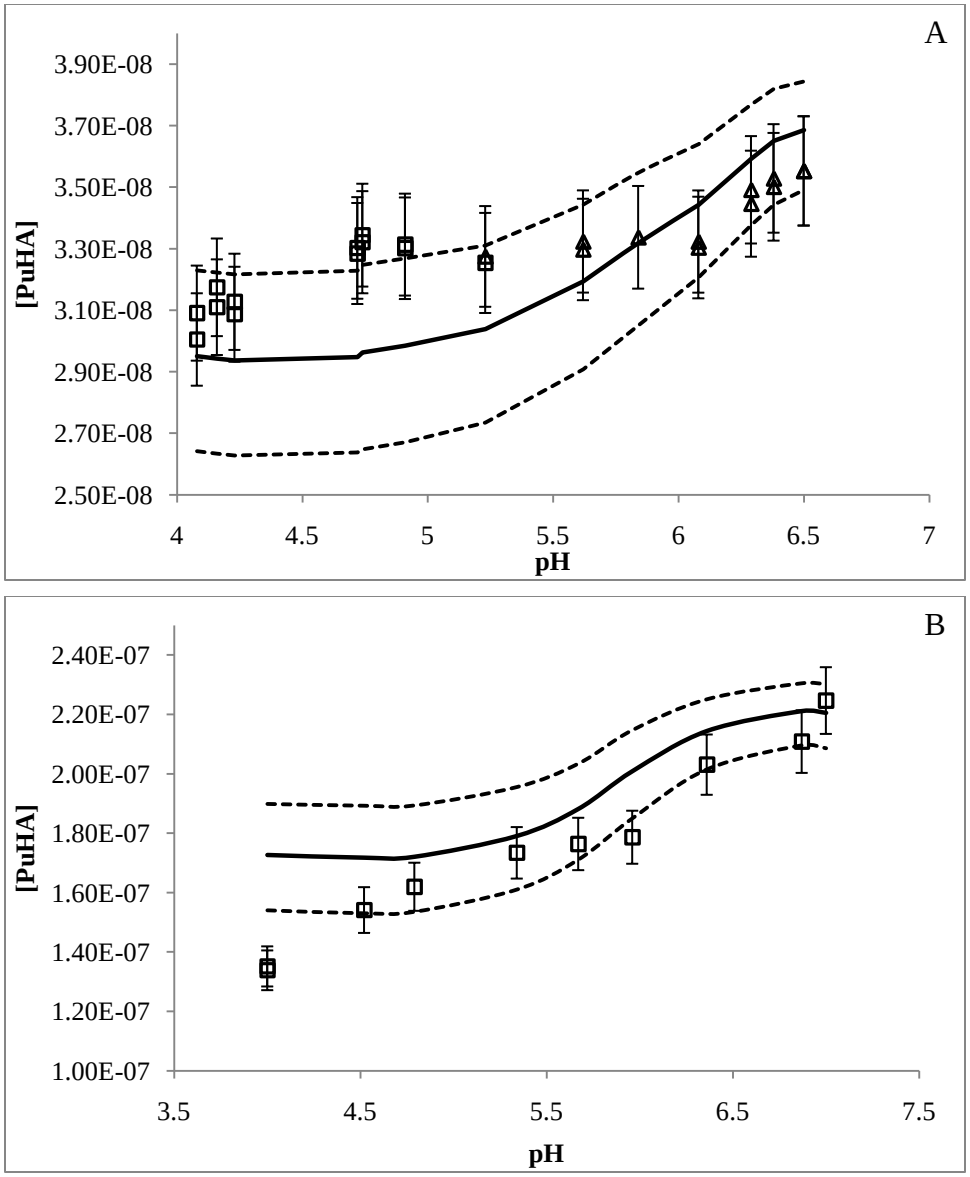


Figure 34: Concentration of 4.35E-8 M Pu (A) and 2.60E-7 M Pu (B**)** bound to HA with global fit (logK: 6.764, WSOS: 1.366, HL3 basis). Dashed lines represent ±1 σ error in the calculated stability constant. Error bars depict the assumed 5% error.

Table 5: Calculated stability constants and corresponding weighted sum of squares values. Numbers in bold represent the best fit for the dataset of interest.

HL1 basis

| | 10 ppb Pu | | 63 ppb (2 week) | | Pu(global) | | 11 ppb Th | |
|---|---|---|---|---|---|---|---|---|
| | K | WSOS | K | WSOS | K | WSOS | K | WSOS |
| $K(An(OH)L^{+2})$ | 15.88 | 13.08 | 16.85 | 38.20 | 16.55 | 20.86 | no convergence | |
| $K(An(OH)2L^{+})$ | 9.35 | 10.21 | 9.56 | 34.12 | 9.42 | 16.57 | **4.63** | **0.28** |
| K(An(OH)3L) | 3.43 | 0.75 | **3.18** | **0.66** | 3.34 | 1.62 | 0.19 | 1.49 |
| $K(An(OH)4L^{-1})$ | -0.83 | 8.00 | -1.06 | 15.05 | -0.91 | 9.97 | -3.97 | 2.21 |

HL2 basis

| | 10 ppb Pu | | 63 ppb (2 week) | | Pu(global) | | 11 ppb Th | |
|---|---|---|---|---|---|---|---|---|
| | K | WSOS | K | WSOS | K | WSOS | K | WSOS |
| $K(An(OH)L^{+2})$ | 14.19 | 12.96 | 15.16 | 38.17 | 14.84 | 20.81 | no convergence | |
| $K(An(OH)2L^{+})$ | 7.58 | 7.50 | 7.69 | 31.19 | 7.61 | 13.79 | 3.51 | 0.64 |
| K(An(OH)3L) | 2.45 | 5.60 | 2.20 | 9.32 | 2.37 | 1.62 | -0.63 | 2.08 |
| $K(An(OH)4L^{-1})$ | -1.58 | 9.86 | -1.71 | 20.14 | -1.62 | 9.97 | -4.80 | 2.38 |

HL3 basis

| | 10 ppb Pu | | 63 ppb (2 week) | | Pu(global) | | 11 ppb Th | |
|---|---|---|---|---|---|---|---|---|
| | K | WSOS | K | WSOS | K | WSOS | K | WSOS |
| $K(An(OH)L^{+2})$ | 12.87 | 10.72 | 13.34 | 36.14 | 13.04 | 18.09 | 8.06 | 0.39 |
| $K(An(OH)2L^{+})$ | **6.84** | **0.45** | 6.62 | 0.90 | **6.76** | **1.37** | 3.58 | 1.44 |
| K(An(OH)3L) | 2.56 | 7.84 | 2.32 | 14.58 | 2.48 | 9.76 | -0.57 | 2.20 |
| $K(An(OH)4L^{-1})$ | -1.50 | 10.16 | -1.61 | 20.84 | -1.54 | 12.75 | -4.74 | 2.41 |

Table 5: cont…

| HL4 basis | 10 ppb Pu | | 63 ppb (2 week) | | Pu(global) | | 11 ppb Th | |
|---|---|---|---|---|---|---|---|---|
| | K | WSOS | K | WSOS | K | WSOS | K | WSOS |
| $K(An(OH)L^{+2})$ | 12.78 | 10.24 | 13.01 | 34.19 | 12.86 | 16.62 | no convergence | |
| $K(An(OH)2L^{+})$ | 6.85 | 0.71 | 6.61 | 0.85 | 6.77 | 1.62 | 3.60 | 1.45 |
| K(An(OH)3L) | 2.58 | 7.86 | 2.34 | 14.64 | 2.49 | 9.79 | -0.55 | 2.20 |
| $K(An(OH)4L^{-1})$ | -1.49 | 10.17 | -1.60 | 20.84 | -1.53 | 12.75 | -4.73 | 2.41 |

Note: molar concentrations are 4.35E-8 M (10 ppb), 2.60E-7 M (63 ppb), and 4.90E-8 M (11 ppb).

The best-fit modeling result for the global dataset (log β = 6.76, WSOS = 1.366) was selected as the most accurate representation of the experimental data. The reaction for which this stability constant is valid appears in Equation 33:

$\text{Log } \beta_{112} = 6.76 \pm 0.14$ $\qquad Pu^{4+} + HL3 + 2H_2O \leftrightarrow Pu(OH)_2L3^{+} + 3H^{+}$ (33)

or alternatively, as a complexation reaction:

$\text{Log } \beta'_{112} = 41.36$ $\qquad Pu^{4+} + L3^{-} + 2OH^{-} \leftrightarrow Pu(OH)_2L3^{+}$ (34)

For completeness, the variation in log $\beta_{112}$ as a function of pH was examined; the results appear in Figure 35. While the calculated stability constants do vary over the pH range of interest, the inclusion of the assumed 5% error, coupled with the understanding that the data points in Figure 35 were determined by modeling at most two data points (only one in the case of the 2.60E-7 M Pu data set), further validates the calculated Pu-HA stability constant.

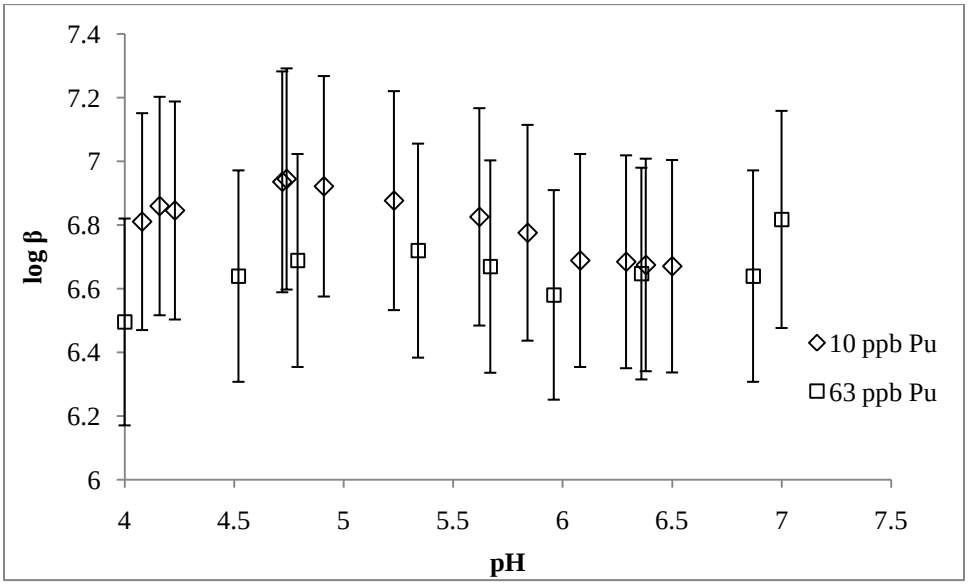


Figure 35: Variation in log $\beta_{112}$ as a function of pH. Note that each 10 ppb Pu data point represents two experimental data points.

Since the conditional Pu-HA stability constant was determined *via* competition reactions with EDTA, it is important to note the influence of the Pu-EDTA stability constants on the resulting Pu-HA constant. For example, when only Pu-EDTA and $[Pu(EDTA)_2]^{4-}$ are considered, the calculated Pu-HA stability constant is reduced to $\log \beta_{112} = 4.731$ (WSOS = 5.620). Comparison of this WSOS value (5.620), with comparable values shown in Table 5, indicates that modeling the Pu-EDTA speciation by assuming the system can be described using only $\log\beta_{11}$ and $\log\beta_{12}$ values, provides a poor fit to the experimental data. While every effort has been made to select the best available stability constants, these constants are subject to refinement. Many of the problems that plague Pu-HA complexation studies are present in analogous Pu-EDTA studies (*e.g.*, precipitation and hydrolysis). Similar to the modeling effort described in this work, where the inclusion of a hydrolyzed species was essential for accurately predicting experimental data, species such as $[Pu(EDTA)(OH)]^-$ and $[Pu(EDTA)(OH)_2]^{2-}$ play a dominant role in systems containing both Pu and EDTA, yet are not yet well understood (Boukhalfa *et al.*, 2004 and Meyer *et al.*, 2007). Therefore, every effort must be made to utilize the best available constants for studies of this nature, as these constants represent a tremendous source of potential error.

## COMPARISION WITH LITERATURE

There is some debate in the literature regarding Pu-EDTA speciation and the corresponding stability constants. Meyer *et al.* (2007) published stability constants for a similar set of Pu-EDTA species to those considered by Boukhalfa *et al.* (2004). Boukhalfa *et al.* (2004) included the species $[Pu(EDTA)_2H_3]^-$ while Meyer *et al.* (2007)

included $[Pu(EDTA)_2H_2]^{2-}$ instead. Meyer *et al*. (2007) used an iterative process of excluding data points, based on the theoretical solubility of $Pu(OH)_4(am)$, which resulted in a truncated dataset (deemed insufficient for inclusion in this study). However, for comparison purposes, the Meyer *et al.* (2007) Pu-EDTA stability constants were used to model the global Pu data. The resulting Pu-HA stability constant (HL3 basis) of 6.72 (WSOS = 1.746) is in reasonable agreement with the value of log $\beta$ = 6.76 ±0.14 (WSOS = 1.366) calculated based on the Pu-EDTA stability constants from Boukhalfa *et al.* (2004).

As discussed previously, Banik *et al.* (2007) reported a conditional stability constant for Pu-HA complexes over the pH range: 1.8 - 3. Despite differences in the conceptual model used to describe proton-binding by the HA, and calculate the resulting binding site concentrations (discrete pKa spectrum (this work) *versus* normalization to a loading capacity term (Banik *et al.*, 2007)), the Pu-HA stability constant determined as part of this study (log$\beta$ = 6.76±0.14) is roughly comparable with the values reported by Banik *et al.* (2007) (6.4 – 8.4 over the pH range 1.8 – 3). As mentioned previously (Chapter Three), Banik *et al.* (2007) normalized the calculated Pu-HA stability constant to a LC term, which is comparable to the degree of HA ionization (Kim and Czerwinski, 1996). The fact that the degree of HA ionization is intrinsically included in our proton-binding model, coupled with the fact that Banik *et al.* (2007) assumed that Pu was present as $Pu(OH)_2^{2+}$, makes the comparison of the resulting Pu-HA stability constants possible (for stability constants determined for the species $Pu(OH)_2L^{+}$).

Comparison of the Th-HA stability constant determined as part of this research is more challenging. The Th- and Pu-HA stability constants summarized in Table 5 can be compared. The stability constants for Th and Pu complexation with large organic ligands, that exhibit similar functionality to HA, were compiled, and are plotted in Figure 36 Also, the Th- and Pu-HA stability constants (HL3 binding site) determined as part of this research are shown in the same figure. This comparison shows excellent agreement between the Pu(IV)- and Th(IV)-HA stability constants determined as part of this work and values for Th(IV) and Pu(IV) complexation with other organic ligands.

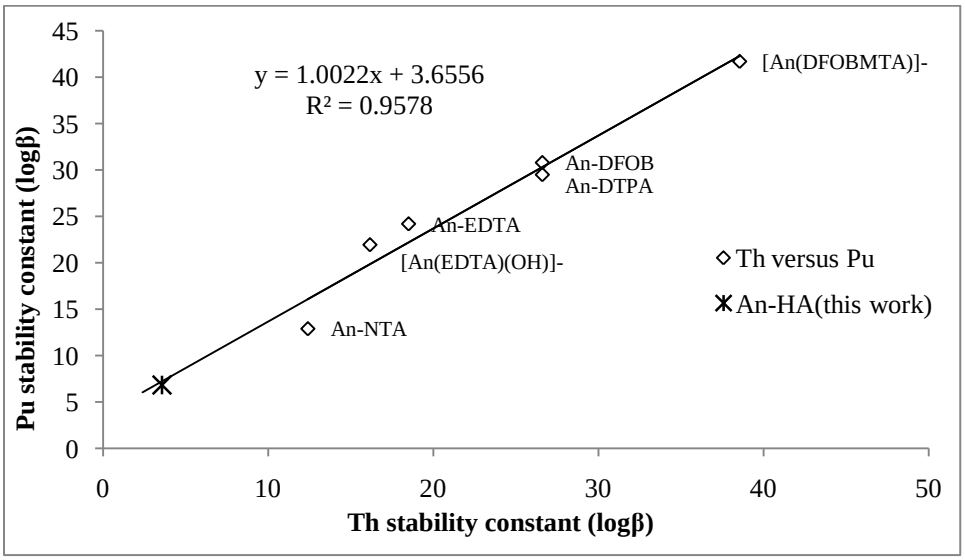


Figure 36: Plot of Th-ligand stability constants *versus* the corresponding Pu-ligand constants. The star corresponds to the stability constants determined for the 4.90E-8 M Th- and 4.35E-8 M Pu-HA datasets assuming an HL3 basis.

Rough comparisons can also be drawn between the Th-HA stability constants determined by Reiller *et al.* (2003) and the ones determined in this work. Reiller *et al.* (2003) calculated a conditional Th-HA stability constant of 16.8 at pH ≈ 7 (10 mg/L HA) *via* competition sorption studies with silica. Unfortunately, differences in the conceptual model used to describe metal- and proton-binding by the HA (*i.e.*, discrete pKa spectrum

(this work) *versus* ignoring the energetics of proton-binding (Reiller *et al.*, 2003)) preclude comparison beyond simply stating that Reiller *et al.* (2003) found the Th-HA complex to be favorable, which is consistent with the findings of this study.

## SENSITIVITY ANALYSIS

As part of the sensitivity analysis, the effect of titration hysteresis on the resultant binding site concentrations, and Pu-HA stability constant, was examined and found to be minimal. Recall, during HA titrations, the back (base – acid) titrations were conducted using varying times between acid additions. These curves were modeled independently, and the calculated binding site concentrations were used as input data in five separate Pu-HA stability constant models (all other system conditions were held constant). Building on the results from previous Pu-HA modeling efforts, the HL3 binding site was selected as the basis species to model the global (*i.e.*, 4.35E-8 M Pu and 2.60E-7 M Pu) Pu data. The results from these tests are summarized in Table 6. Given the inherent error in studies of this type (assumed to be 5%), the calculated stability constants are reasonably similar, indicating that titration hysteresis does not have a profound impact on the ultimate stability constant.

Table 6: Influence to titration hysteresis on total proton-binding site concentration and subsequent Pu-HA stability constant.

| | Time between additions | Total binding site conc. (mol/mg C) | $\log K(Pu(OH)_2L^+)$ | WSOS |
|---|---|---|---|---|
| Acid(I) | 30 seconds | 1.04E-05 | 6.86 | 1.302 |
| Acid(II) | 30 seconds | 1.16E-05 | 6.79 | 1.316 |
| Acid(III) | 10 minutes | 9.86E-06 | 6.66 | 1.319 |
| Acid(IV) | 1 hour | 1.28E-05 | 6.77 | 1.375 |
| Acid(V) | 2 hours | 9.51E-06 | 6.68 | 1.321 |

SPECTIATION ANALYSIS USING NEWLY DERIVED CONSTANTS

Using the conditional stability constant for the Pu-HA complex, determined as part of this study ($\log \beta_{112} = 6.76 \pm 0.14$), a series of speciation diagrams were generated to compare HA with other organic ligands. Figure 37 shows the predicted speciation under conditions similar to those of the initial Pu-HA-EDTA complexation experiments. The model output shown in these figures is consistent with the partitioning behavior observed experimentally.

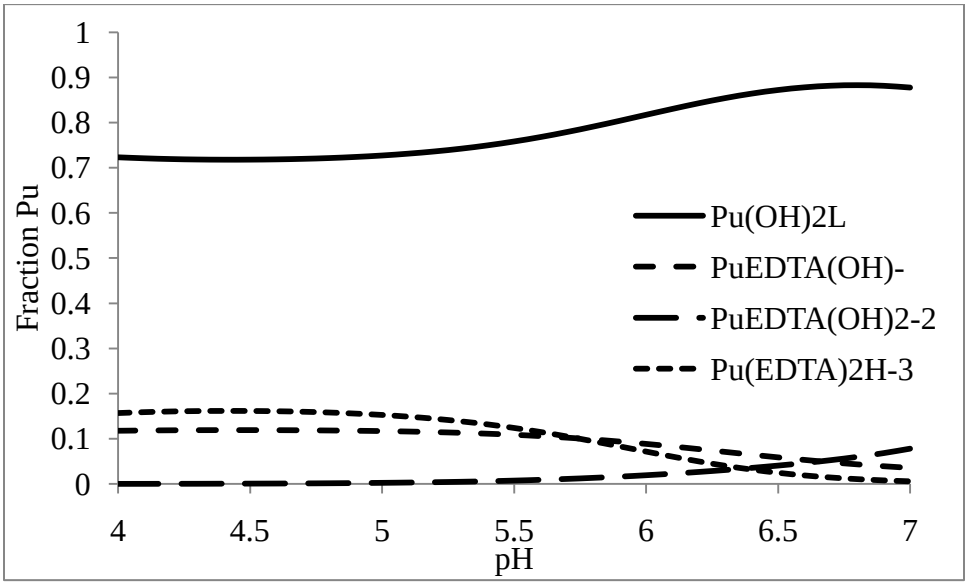


Figure 37: Speciation diagram generated assuming 1E-8M Pu(IV), 1E-5M EDTA, and 2E-5M HA (roughly equivalent to 10 mg C/L using the HL2 site only). Pu-HA is represented by the species $Pu(OH)_2L$. For clarity only the dominant species are shown.

Similarly, the speciation was modeled assuming equal concentrations of oxalate and HA (1E-5M), and 1E-8M Pu. Again, the strength of the Pu-HA complex was reflected in the model output, with 100% of the Pu complexed with the HA over the pH range 4-7. Modification of the model input to assume 1E-2M oxalate and 1E-6M HA,

resulted in the same distribution of Pu between the two ligands (*i.e.*, 100% complexed with HA).

Finally, the competition between DFO-B (a commercially available siderophore known to form strong complexes with Pu(IV)) and HA was examined, and found to be consistent with the fact that DFOB forms exceptionally favorable complexes with tetravalent actinides (Boukhalfa *et al.*, 2007). This system was modeled using Pu(IV)(DFO-B) stability constants from Boukhalfa *et al.* (2007). When DFOB is present at an equal or greater concentration than Pu, the model predicts that all of the Pu will be complexed with DFOB.

The speciation studies described above should have implications for future studies. These modeling results indicate that HA forms strong complexes with both Pu and Th and is capable of out-competing small organic ligands (*e.g.,* oxalate), and to a lesser extent EDTA, when present in sufficient concentrations. However, when present at concentrations greater than that of the metal, DFOB dominates over HA. This suggests that DFOB and other similar ligands are not suitable for Pu-HA complexation studies that are based on competition reactions.

## BINARY SORPTION

Sorption of Pu(IV) and Pu(V) to gibbsite (in the absence of HA) was examined and found to be consistent with the known sorption behavior of tetra- and pentavalent actinides in binary, metal – mineral systems (*i.e.,* increasing metal sorption with increasing pH). The data from this experiment appears in Figure 38. It is important to note that these samples were spiked with an aliquot of an appropriate Pu working solution

containing the actinide in the oxidation state of interest. However, previous studies have shown that during equilibration Pu undergoes redox reactions such that weakly bound Pu(V) undergoes surface mediated reduction to Pu(IV) and sorbed Pu(IV) undergoes oxidative dissolution to aqueous Pu(V) (Powell *et al.*, 2008, Kaplan *et al.*, 2007, Powell *et al.*, 2006, Powell *et al.*, 2005, and Powell *et al.*, 2004). Over 300 days Powell *et al.* (2008) observed a decrease in Pu sorption in the initially Pu(IV) system and an increase in sorption in the initially Pu(V) system. After 300 days, partitioning in the initially Pu(IV) dataset remained constant, while the initially Pu(V) dataset appeared to be converging towards the Pu(IV) dataset. This is consistent with the conceptual model of surface mediated Pu(V) reduction to Pu(IV). Due to the long equilibration times necessary to observe these reactions, their consequences are limited in the data shown in Figure 38. However, many studies of Pu(IV) sorption have shown that aqueous Pu is predominantly Pu(V) despite starting the experiments with pure Pu(IV) (Banik *et al.*, 2009, Powell *et al.*, 2008). Therefore, in the initially Pu(IV) system, the aqueous Pu is likely Pu(V) and greater than 90% is sorbed across the pH range 3-10, with greater than 99% sorption above pH 7.5. The increase in Pu sorption in the Pu(IV) system corresponds with the sorption edge of Pu(V). This is consistent with the assumption that the aqueous Pu in the initially Pu(IV) system, is likely Pu(V).

Recall, Pu(V) exists as the dioxy cation, $PuO_2^+$. Therefore, the lower solid-phase affinity of Pu(V) is to be expected, due to the lower effective charge of the actinide. The Pu(V) sorption edge at approximately pH 6.8 is a result of the overall surface charge on

the mineral becoming increasingly more negative, thereby increasing the energetic favorability of cation sorption.

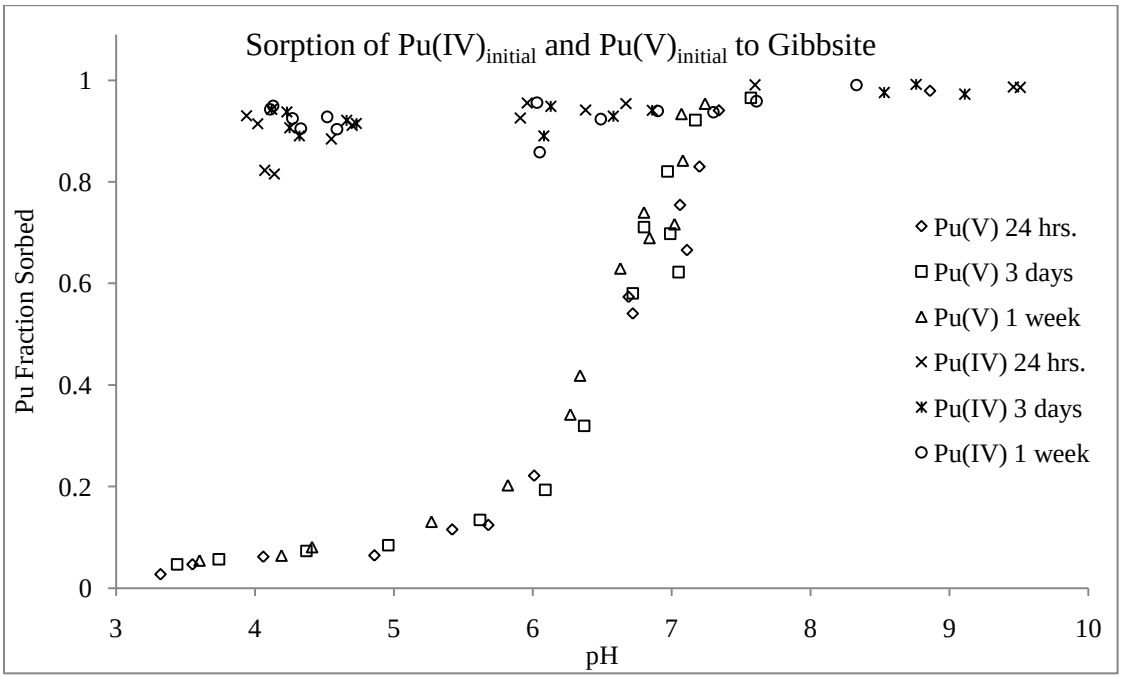


Figure 38: Pu(IV) and Pu(V) sorption to gibbsite. Concentration α-$Al(OH)_3$ = 10 g/L, ionic strength 0.1M (NaCl), $[^{238}Pu]_{total}$ = 1.3E-10 (1000 dpm/mL), exposed to the atmosphere.

When the differing experimental conditions are considered (*i.e.*, ionic strength, solid-phase concentration, and the presence (this study) or absence of $CO_2(g)$), rough comparisons can be made with the Pu(IV) and Pu(V) sorption data in Figure 12 (Powell *et al.*, 2008). Comparison of the Pu(IV) data in each study shows very similar sorption behavior (*i.e.*, strong sorption across the entire pH spectrum of interest). Examination of the Pu(V) sorption data shows that while the overall trend for pentavalent Pu is similar in both datasets, the pH of the sorption edges, are not. The Pu(V) sorption edge in the Powell *et al.* (2008) data is around pH 7.8, approximately 1 pH unit higher than this

study. The differences between the sorption edges of these two datasets are likely due to the difference in solid-phase (gibbsite) concentration. Sorption studies in this work used a gibbsite concentration of 10 g/L, which translates into 19 $m^2$ $L^{-1}$; in contrast, Powell *et al.* (2009) used 10 $m^2$ $L^{-1}$ gibbsite.

Pu(IV) and (V) sorption to gibbsite was examined in the absence of HA and found to be consistent with previous studies examining Pu sorption to gibbsite. The results from these experiments will serve to inform and provide a comparison for the ternary, Pu-HA-gibbsite experiments that follow.

## TERNARY SORPTION

Using the binary, Pu-gibbsite data as a reference, a series of sorption isotherms for the ternary, Pu-HA-gibbsite system were generated and the data were compared. As mentioned in Chapter Four, two different sampling procedures were used to fractionate the aqueous phase into < 100 nm and < 3 kDa (nominally considered to be 1-5 nm) size fractions. The data from these sampling events can be found in Figure 39.

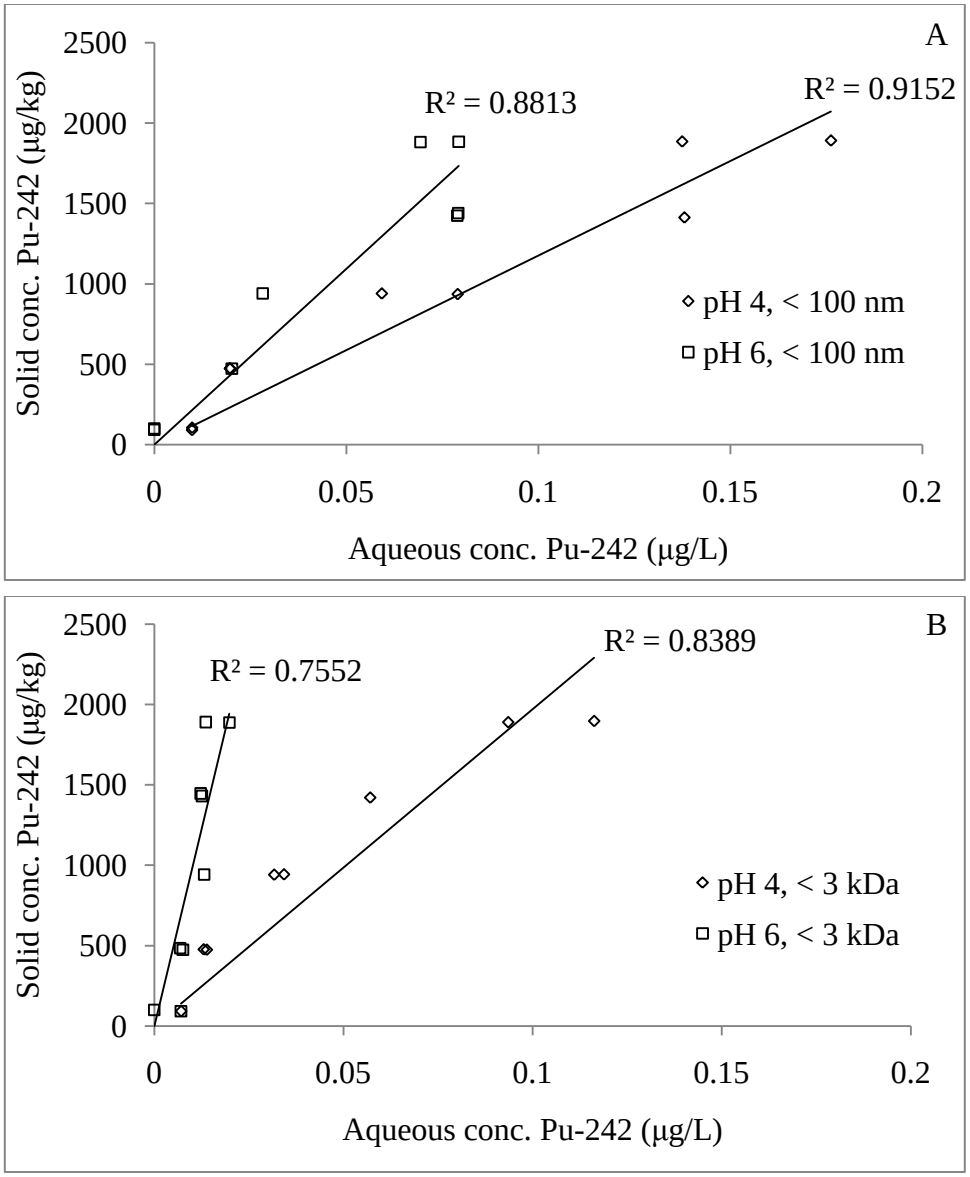


Figure 39: $^{242}$Pu sorption to 10 g/L gibbsite in the presence of 10 mg C/L HA; A (100 nm size fraction) and B (3 kDa (1-5 nm) size fraction).

The solid-water distribution coefficient ($K_d$) is a measure of the extent to which a species is associated with the solid phase. It is defined as the concentration of a substance associated with the solid phase over the concentration of the substance in the aqueous phase. For the systems of interest in this work, the $K_d$ can be defined as:

$$K_d = \frac{C_{Pu,\ gibbsite}}{C_{Pu,\ aq}} \quad (35)$$

where $C_{Pu,\ gibbsite}$ (μg/kg) is the concentration of Pu associated (*i.e.,* sorbed) with the solid phase, and $C_{Pu,\ aq}$ (μg/L) is the concentration of Pu in the aqueous phase. Therefore, the resulting distribution coefficient ($K_d$) has units of (L/kg). The concentration of Pu sorbed ($C_{Pu,\ gibbsite}$) was determined using Equation 36:

$$C_{Pu,gibbsite} = \left(C_{Pu,T} - C_{Pu,aq}\right)\left(\frac{V_T}{C_{gibbsite,stock} * V_{gibbsite,stock}}\right) \quad (36)$$

where $C_{Pu,T}$ represents the total concentration of Pu in the system (μg/L), $V_T$ (L) denotes the total sample volume, $C_{gibbsite,stock}$ is the concentration of the gibbsite stock solution (kg/L), and $V_{gibbsite,\ stock}$ (L) is the volume of gibbsite stock solution added to each sample.

Based on the conditional Pu-HA stability constant calculated as part of this work, and the concentrations of Pu and HA used, the assumption can be made that all of the aqueous Pu is associated with HA. $K_d$ values for the binary (Pu-gibbsite) system were calculated from data at pH 4 and 6 and compared to those calculated for the ternary system at the same pH values (Table 7). Note that since the ternary sorption isotherms shown in Figure 39 were plotted with units of μg/kg on the y-axis, and μg/L on the x-axis, the $K_d$ (L/kg) is simply the slope of the trend lines.

Table 7. Kd comparison for the binary and ternary systems.

| | **$K_d$ values (L/kg)** | | | |
|---|---|---|---|---|
| | **Ternary** | | **Binary** | |
| **size fraction** | **pH 4** | **pH 6** | **pH 4** | **pH 6** |
| < 100 nm | 14,500 | 22,500 | 1,000 | 2,000 |
| < 3 kDa | 25,000 | 86,000 | N/A | N/A |

Two important conclusions can be drawn from the data in Table 7. First, increased sorption of Pu is observed in the ternary system relative to the binary system; indicating that HA influences the sorption behavior of Pu. Second, increased sorption is observed at low pH (pH 4) indicating ligand facilitated sorption specifically (Type B complexes, Equation 13). Therefore, the assumption that the increased solubility observed for Pu associated with HA will result in enhanced transport, may not be correct under these conditions. In fact, the data in this study indicate that the presence of HA may decrease Pu transport, through the formation of Type B ternary surface complexes. Further research is needed to ascertain what impact HA will have in the broader context of Pu fate and transport.

It is noteworthy that some aqueous phase activity remains in the ternary systems (depicted in Figure 39 B, the filtered fraction). Cursory consideration of this data might lead to the incorrect conclusion that HA, and therefore Pu, is passing through the centrifugal filters. In an effort to describe this remaining aqueous phase activity, the system was modeled using the conditional Pu-HA stability constant determined as part of this work ($\log\beta = 6.76 \pm 0.14$), coupled with the reaction shown in Equation 37:

$\log \beta = 3.439$ $\quad Pu^{4+} + 1.5H_2O + 0.25O_2(g) \leftrightarrow PuO_2^+ + 3H^+$ (37)

The concentration of oxygen gas fugacity was assumed to be 5.25E-15 atm at pH 4 and 3.52E-13 atm at pH 6. These values are based on $E_H$ measurements of solutions under conditions similar to those used in this study, which were corrected using:

$\log K = 20.78$ $\quad O_2(g) + 4H^+ + 4e^- \leftrightarrow 2H_2O$ (38)

Based on the inputs described above, the model predicts 0.80% of the total Pu will be present as Pu(V) at pH 4, and 2.46% Pu(V) at pH 6. These fractions account for more than the 0.4% ($1\sigma = 0.16$) (pH 4) and 0.16% ($1\sigma = 0.21$) (pH 6) observed in the aqueous phase of the ternary system. Based on these results, the aqueous phase Pu shown in Figure 39 may be $Pu(V)O_2^+$.

# CHAPTER SIX

## CONCLUSIONS

The over-arching purpose of this research has been to examine the influence of HA on Pu geochemical behavior through a series of laboratory studies. While the system conditions have been simplified relative to environmental conditions (*e.g.,* purified gibbsite was used in lieu of natural soil suspensions), this data will serve to inform future studies under more environmentally relevant conditions.

The conditional stability constant for the Pu-HA complex was determined over the pH range 4-7 using a hybrid ultra-filtration/equilibrium dialysis ligand exchange approach. Using stability constants for the various Pu-EDTA species from Boukhalfa *et al.* (2004), Pu hydrolysis constants from the NEA-TDB, and Th-EDTA and Th hydrolysis constants from the NIST Standard Reference Database 6 (Version 7.0), the Pu-HA stability constant was calculated to be 6.76 (± 0.14). This number is consistent with the Pu-HA stability constants ranging from 6.4 to 8.4 over the pH range: 1.8 – 3 reported by Banik *et al.* (2007) and discussed previously (Chapter Three and Chapter Five).

Another important finding during the complexation studies, involved the influence of titration hysteresis on the final Pu-HA stability constant. While every effort should be made to conduct titrations in a fashion that is consistent with the current body of knowledge surrounding proton-binding by HAs, the amount of error that is present in studies of this nature (assumed to be 5% in this work) makes the contribution from titration hysteresis appear minimal. Cycling the HA, and then selecting the curve that

exhibits the least hysteresis (Base IV), provided acceptable binding site concentrations for this work.

Binary (Pu-gibbsite) sorption studies were conducted for both initially Pu(IV) and initially Pu(V) systems. The results were found to be consistent with both the known sorption behavior of tetra- and penta-valent actinides and a previous study performed by Powell *et al.* (2008) under similar conditions.

A series of ternary (Pu-HA-gibbsite) sorption isotherms were generated at pH 4 and 6. The results were then compared to the binary system using the solid – water distribution coefficient. The results of this comparison indicate that the assumption that the increased solubility observed for Pu complexed with HA will result in enhanced transport is inappropriate. In contrast, the formation of ternary surface complexes (Type A and Type B) appears to be important, and may cause a decrease in aqueous Pu concentrations. The influence of HA on Pu in more realistic representations of environmental systems must be examined before definitive conclusions can be drawn regarding the role of HA in Pu transport.

# CHAPTER SEVEN

## PROPOSED FUTURE WORK

While the research in this thesis represents an improvement in the body of knowledge surrounding Pu-HA complexation, the role of HA in ternary, Pu-HA-gibbsite systems, and the inferences that can be drawn from these data regarding the behavior of these species in natural systems, there is still work to be done. Specifically, the primary focuses of future efforts in this area of research can be summarized as follows.

First, spectroscopic studies aimed at examination of the structure of both the aqueous Pu-HA and Pu-EDTA species, as well as the same species associated with the solid-phase, would offer tremendous insight into the systems of interest. Knowledge of the structure of these species, would simplify and improve the modeling effort by constraining the species considered (such as the differing opinion of the presence of $[Pu(EDTA)_2H_3]^-$ versus $[Pu(EDTA)_2H_2]^{2-}$ as shown by Boukhalfa *et al.* (2004) and Meyer *et al.* (2007), respectively).

As mentioned in Chapter Five, the stability constants selected for the An-reference ligand species (An-EDTA in this work) and An-hydrolysis constants are of the utmost importance as they scale the calculated Pu-HA stability constant. Therefore, further refinement of these numbers would aid in improving the fit to the experimental data contained in this thesis.

Finally, the speciation of Pu in the presence of EDTA is quite complex. EDTA was selected as the reference ligand for these studies due to its ability to limit Pu hydrolysis at higher pH values than had been explored previously (*e.g.*, Banik et al.,

2007). However, other organic ligands such as citrate or oxalate might work well for studies of this type. It is important to note, however, that based on the speciation model for a system containing Pu, HA, and oxalate shown in Chapter Five, the use of oxalate as a reference ligand might not provide the distribution of Pu between the two ligands necessary for calculating a Pu-HA stability constant (*e.g.*, Equation 14). Therefore, citrate might be an acceptable ligand to consider based on a comparison of Pu-citrate and Pu-oxalate $\log\beta_{11}$ values of 8.30 and 15.6, respectively (Clark *et al.*, 2006).

# APPENDICES

# Appendix A

## COMPLEXATION SCOPING STUDIES

As mentioned previously, the filtration requirements for these studies are two-fold. First, HA must be excluded from passing through the filter. Second, the Pu-EDTA complex must be able to pass through the filter unhindered (*i.e.,* 100% recovery of Pu-EDTA is required). Initial scoping experiments were conducted to ensure that these criteria were met.

### HUMIC ACID FILTRATION

The ability of various filter assemblies to effectively remove HA was studied using UV-Visible spectroscopy and TOC analysis. UV–Vis spectroscopic measurements were performed on a Cary 50 single-beam spectrophotometer using a 1 cm quartz cell. This instrument was used instead of an available Cary 300 dual-beam spectrophotometer because it exhibited superior stability over the timescale of these experiments. This is shown clearly in Figure A-1, Figure A-2, Figure A-3, and Figure A-4 which were generated by running the same 2 mg HA/L standard repeatedly. Based on the data in Figure A-1, the Cary 50 achieved steady-state after approximately 80 minutes. In contrast, the data in Figure A-2 indicate that at least two hours was required to achieve equilibrium for the Cary 300. After a suitable warm-up period (100 min for the Cary 50 and 120 min for the Cary 300) the standard deviation between data points collected over 20 minutes was calculated for each instrument. Based on these datasets the Cary 50 was used after a two hour warm-up in these experiments.

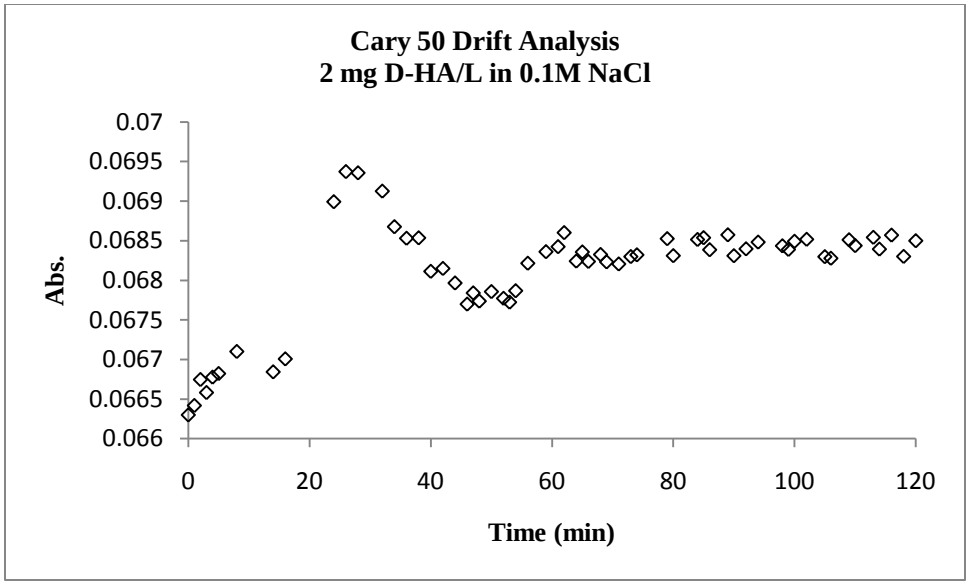


Figure A-1: Cary 50 drift analysis. 2 mg HA/L in 0.1 M NaCl analyzed repeatedly.

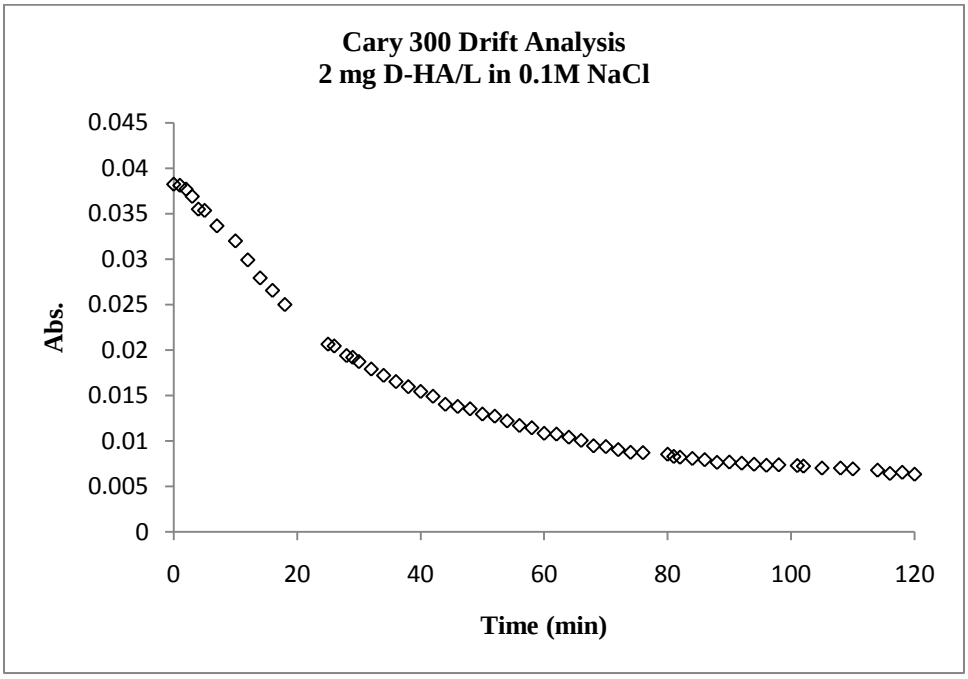


Figure A-2: Cary 300 drift analysis. 2 mg HA/L in 0.1 M NaCl analyzed repeatedly.

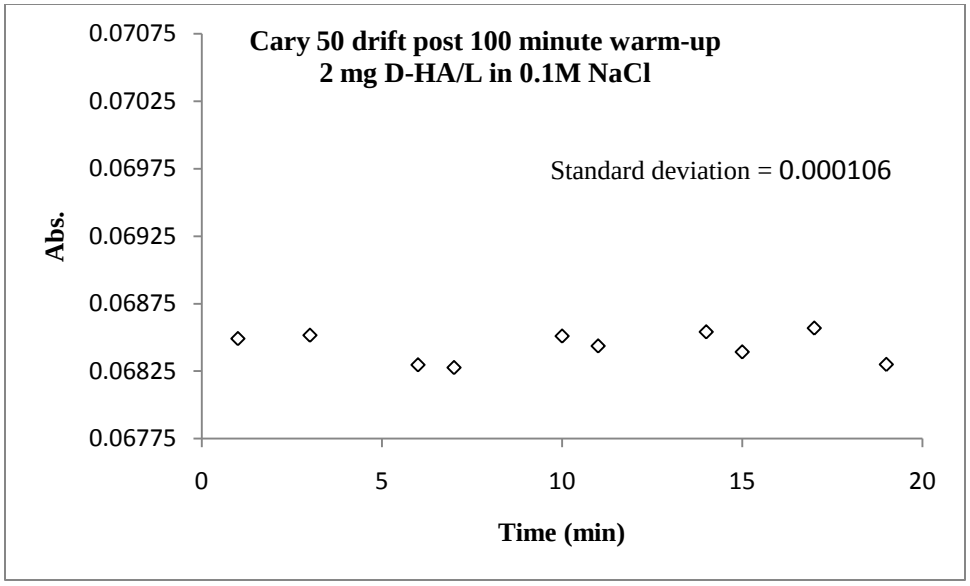


Figure A-3: Cary 50 drift post 100 minute warm-up. 2 mg HA/L in 0.1 M NaCl.

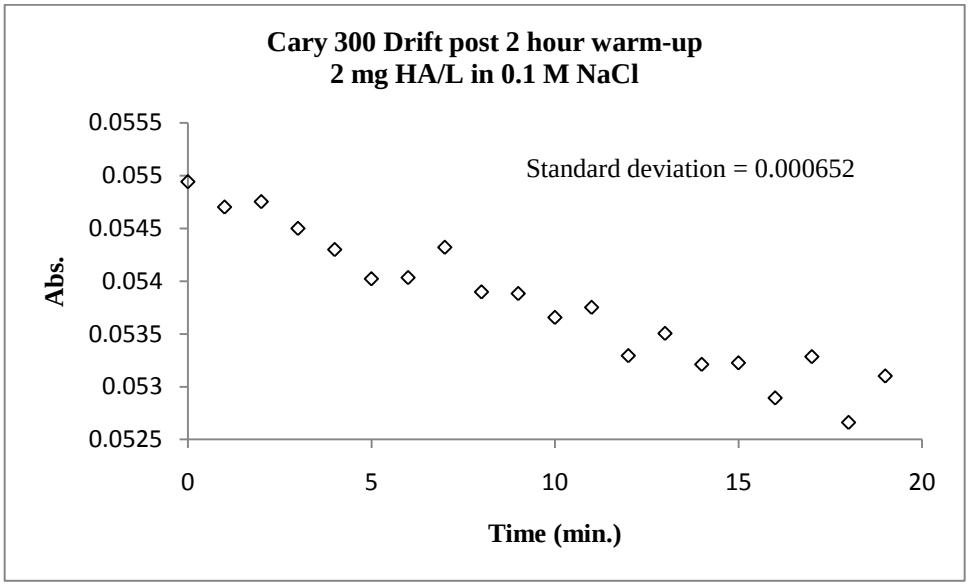


Figure A-4: Cary 300 drift post 2 hour warm-up. 2 mg HA/L in 0.1 M NaCl.

Initial HA exclusion studies using polyethersulfone-based membranes were confounded by organic carbon leaching from the filters that showed an absorbance at 254 nm. This problem was remedied by switching to Amicon Ultra 4 filters which use regenerated cellulose membranes. Although carbon was released from these filters, it did

not exhibit an absorbance at 254 nm allowing the absence of HA in the filtrate to be confirmed using UV-Vis spectroscopy. Furthermore, the total concentration of organic carbon leached from the filters was sufficiently low, constant, and exhibited a different carbon/nitrogen (C/N) ratio than Leonardite HA to allow for its use in confirming the absence of HA in the filtrate.

HA exclusion from the filtrate was confirmed by running triplicate samples as follows. Filters were pre-washed with approximately 2 mL 0.1M NaCl or 2 mL 0.01M EDTA (for C/N ratio experiments). The samples were then centrifuged at 3000 rotations $min^{-1}$ using a swing-bucket rotor in a Beckman GS-6 centrifuge. The filtrate and retentate were discarded and replaced with a solution containing 10 mg C/L HA (I = 0.1M NaCl). After pre-equilibration with approximately 1.0 mL of this solution, the filtrate was again discarded, and centrifugation resumed. The final filtrate was collected and analyzed using UV-Vis or TOC as appropriate. Additionally, blanks and filtrate from the wash and equilibration steps were analyzed. The presence or absence of HA in the filtrate was determined by measuring the absorbance at 254 nm using UV-Vis. Additional studies in the presence of EDTA (the reference ligand for these studies) used TOC to differentiate between HA and EDTA by virtue of their different C/N ratios. EDTA has a C/N ratio of 4.29% (w/w) while Leonardite HA has a C/N = 51.88% (w/w) (IHSS, 2010). The nominal C/N ratio of the material(s) being leached from the filter assemblies themselves was found to be 5.6 % (w/w). The average C/N ratio of filtrate after washing with 0.01 M EDTA was 8.9 % (w/w). Analysis of filtrate collected both in the presence and absence of EDTA indicates that 3 kDa Amicon Ultra-4 filters reject

greater than 99% of the dialyzed Leonardite HA at the concentrations used in these studies.

## PLUTONIUM-EDTA RECOVERY

Scoping experiments were also conducted to insure that the Pu-EDTA complex could pass through the selected filters unhindered. The results from these initial experiments showed that when the membranes were pre-equilibrated/washed with approximately 2 mL 0.01M EDTA, greater than 99% of the Pu was recovered (experiments conducted in the absence of HA). The Pu concentration in both filtered and un-filtered samples was quantified using LSC. The results are reported in decays per minute (dpm) per mL: the average for duplicate, filtered samples was 119.80 dpm/mL compared with 119.77 for duplicate un-filtered samples. If this pre-equilibration step with EDTA was not conducted, greater than 99% recovery of Pu was not achieved. This is likely due to some fraction of the initial EDTA becoming associated with the membrane. These Pu-EDTA experiments led to the development of the following filter-washing procedure that was used throughout these studies. Filters were pre-equilibrated with approximately 2.0 mL 0.01M EDTA prior to use in separations. The filtrate and retenate were then discarded and replaced with the appropriate sample.

## Pu-EDTA QUANTIFICATION USING ICP-MS

The use of EDTA as a reference ligand, coupled with our desire to quantify the Pu concentration using ICP-MS, led to a variety of problems. Generally, ICP-MS analysis of dissolved metals is performed in 2% $HNO_3$. The low pH of this solution keeps metals

(*e.g.*, Pu) from hydrolyzing and precipitating inside the instrument and associated tubing. In contrast, EDTA readily precipitates, and thereby co-precipitates Pu, at low pH. Since the complexation studies in this thesis require the presence of both species, experiments were conducted to address this problem. Eventually it was determined that using 0.01M EDTA to dilute samples, internal standards, external standards, and as the ICP-MS wash solution, effectively solubilizes Pu, thereby allowing the concentration to be fully quantified using ICP-MS. A representative ICP-MS calibration curve appears in Figure A-5.

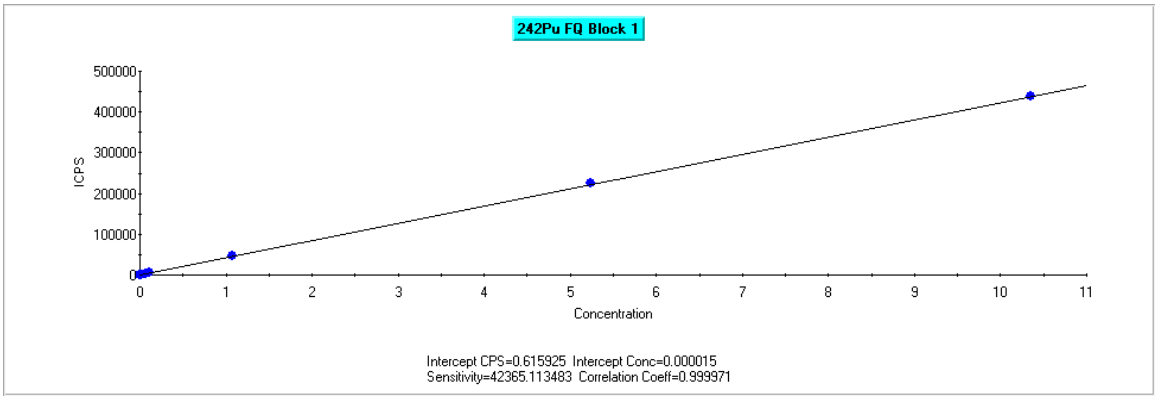


Figure A-5: Representative ICP-MS calibration curve. Calibration performed using 0.01, 0.05, 0.1, 1, 5, and 10 ppb Pu standards in 1E-5 M EDTA.

## Appendix B

## $^{242}$PLUTONIUM ISOTOPE DISTRIBUTION

Table B-1: Isotope distribution for the NIST traceable $^{242}$Pu stock solution used in this work.

| Isotope | % | relative abundance |
|---|---|---|
| **Pu-238** | 0.00419 | 0.0000419 |
| **Pu-239** | 0.00478 | 0.0000478 |
| **Pu-240** | 0.01974 | 0.0001974 |
| **Pu-241** | 0.02466 | 0.0002466 |
| **Pu-242** | 99.94623 | 0.9994623 |
| **Pu-244** | 0.0004 | 0.000004 |

## Appendix C

## FITEQL INPUT MATRIX

Table C-1: Species, Log K, and Stoichiometry Matrix A from FITEQL. Note: the sum0 component is a dummy variable used to represent the total Pu bound to HA.

| # | Id | Name | Log K | Pu++++ | EDTA4- | HL1 | HL2 | HL3 | HL4 | sum0 | H+ | H2O |
|---|---|---|---|---|---|---|---|---|---|---|---|---|
| 1 | 1 | H+ | 0 | 0 | 0 | 0 | 0 | 0 | 0 | 0 | 1 | 0 |
| 2 | 2 | Pu++++ | 0 | 1 | 0 | 0 | 0 | 0 | 0 | 0 | 0 | 0 |
| 3 | 3 | EDTA4- | 0 | 0 | 1 | 0 | 0 | 0 | 0 | 0 | 0 | 0 |
| 4 | 4 | HL1 | 0 | 0 | 0 | 1 | 0 | 0 | 0 | 0 | 0 | 0 |
| 5 | 5 | HL2 | 0 | 0 | 0 | 0 | 1 | 0 | 0 | 0 | 0 | 0 |
| 6 | 6 | HL3 | 0 | 0 | 0 | 0 | 0 | 1 | 0 | 0 | 0 | 0 |
| 7 | 7 | HL4 | 0 | 0 | 0 | 0 | 0 | 0 | 1 | 0 | 0 | 0 |
| 8 | 8 | L1 | -3 | 0 | 0 | 1 | 0 | 0 | 0 | 0 | -1 | 0 |
| 9 | 9 | L2 | -5 | 0 | 0 | 0 | 1 | 0 | 0 | 0 | -1 | 0 |
| 10 | 10 | L3 | -7 | 0 | 0 | 0 | 0 | 1 | 0 | 0 | -1 | 0 |
| 11 | 11 | L4 | -9 | 0 | 0 | 0 | 0 | 0 | 1 | 0 | -1 | 0 |
| 12 | 12 | Pu(OH)2L | 6.764 | 1 | 0 | 0 | 0 | 1 | 0 | 1 | -3 | 2 |
| 13 | 13 | EDTAH--- | 9.52 | 0 | 1 | 0 | 0 | 0 | 0 | 0 | 1 | 0 |
| 14 | 14 | EDTAH2-- | 15.65 | 0 | 1 | 0 | 0 | 0 | 0 | 0 | 2 | 0 |
| 15 | 15 | EDTAH3- | 18.34 | 0 | 1 | 0 | 0 | 0 | 0 | 0 | 3 | 0 |
| 16 | 16 | EDTAH4(aq) | 20.34 | 0 | 1 | 0 | 0 | 0 | 0 | 0 | 4 | 0 |
| 17 | 17 | EDTAH5+ | 21.84 | 0 | 1 | 0 | 0 | 0 | 0 | 0 | 5 | 0 |
| 18 | 18 | EDTAH6++ | 21.84 | 0 | 1 | 0 | 0 | 0 | 0 | 0 | 6 | 0 |
| 19 | 19 | PuEDTA(aq) | 24.2 | 1 | 1 | 0 | 0 | 0 | 0 | 0 | 0 | 0 |
| 20 | 20 | Pu(EDTA)2-4 | 35.39 | 1 | 2 | 0 | 0 | 0 | 0 | 0 | 0 | 0 |

Table C-1 continued…

| # | Id | Name | Log K | Pu++++ | EDTA4- | HL1 | HL2 | HL3 | HL4 | sum0 | H+ | H2O |
|---|---|---|---|---|---|---|---|---|---|---|---|---|
| 21 | 21 | PuEDTA(OH)- | 4 | 1 | 1 | 0 | 0 | 0 | 0 | 0 | -1 | 1 |
| 22 | 22 | PuEDTA(OH)2-2 | 15.29 | 1 | 1 | 0 | 0 | 0 | 0 | 0 | -2 | 2 |
| 23 | 23 | Pu(EDTA)2H-3 | 42.75 | 1 | 2 | 0 | 0 | 0 | 0 | 0 | 1 | 0 |
| 24 | 24 | Pu(EDTA)2H3- | 47.39 | 1 | 2 | 0 | 0 | 0 | 0 | 0 | 3 | 0 |
| 25 | 25 | OH- | -14 | 0 | 0 | 0 | 0 | 0 | 0 | 0 | -1 | 1 |
| 26 | 26 | PuOH+++ | -0.04 | 1 | 0 | 0 | 0 | 0 | 0 | 0 | -1 | 1 |
| 27 | 27 | Pu(OH)2++ | -0.47 | 1 | 0 | 0 | 0 | 0 | 0 | 0 | -2 | 2 |
| 28 | 28 | Pu(OH)3+ | -3.58 | 1 | 0 | 0 | 0 | 0 | 0 | 0 | -3 | 3 |
| 29 | 29 | Pu(OH)4(aq) | -9.78 | 1 | 0 | 0 | 0 | 0 | 0 | 0 | -4 | 4 |

# Appendix D

## EXPERIMENTAL DATA

### HUMIC ACID TITRATION DATA

Table D-1: Initial conditions and titrant concentrations used in humic acid titration.

| Stock solution concentrations: | |
|---|---|
| HA soln. Volume: | 25 mL |
| [NaOH] | 0.1004 M |
| [HCl] | 0.0999 M |
| Conc. DOC | 0.0499 g/L |

Table D-2: HA titration data.

| NaOH added (mL) | HCl added (mL) | pH |
|---|---|---|
| 0 | 0.1 | 3.578 |
| 0 | 0 | 3.578 |
| 0.025 | 0 | 3.725 |
| 0.025 | 0 | 4.01 |
| 0.025 | 0 | 4.577 |
| 0.025 | 0 | 6.382 |
| 0.025 | 0 | 8.745 |
| 0.025 | 0 | 9.705 |
| 0.025 | 0 | 10.058 |
| 0 | 0 | 10.055 |
| 0 | 0.025 | 9.807 |
| 0 | 0.025 | 8.909 |
| 0 | 0.025 | 6.052 |
| 0 | 0.025 | 4.592 |
| 0 | 0.025 | 4.063 |
| 0 | 0.025 | 3.788 |
| 0 | 0.025 | 3.614 |
| 0 | 0.025 | 3.488 |
| 0 | 0 | 3.47 |
| 0.025 | 0 | 3.577 |
| 0.025 | 0 | 3.748 |
| 0.025 | 0 | 4.012 |
| 0.025 | 0 | 4.529 |
| 0.025 | 0 | 5.753 |
| 0.025 | 0 | 8.199 |
| 0.025 | 0 | 9.553 |

Table D-2 continued…

| | | |
|---|---|---|
| 0.025 | 0 | 9.965 |
| 0.025 | 0 | 10.19 |
| 0 | 0 | 10.168 |
| 0 | 0.025 | 10.012 |
| 0 | 0.025 | 9.696 |
| 0 | 0.025 | 8.842 |
| 0 | 0.025 | 6.81 |
| 0 | 0.025 | 4.882 |
| 0 | 0.025 | 4.185 |
| 0 | 0.025 | 3.862 |
| 0 | 0.025 | 3.666 |
| 0 | 0.025 | 3.529 |
| 0 | 0.025 | 3.422 |
| 0 | 0 | 3.409 |
| 0.025 | 0 | 3.502 |
| 0.025 | 0 | 3.636 |
| 0.025 | 0 | 3.82 |
| 0.025 | 0 | 4.117 |
| 0.025 | 0 | 4.708 |
| 0.025 | 0 | 6.186 |
| 0.025 | 0 | 8.637 |
| 0.025 | 0 | 9.658 |
| 0.025 | 0 | 10.011 |
| 0 | 0 | 9.963 |
| 0 | 0.025 | 9.497 |
| 0 | 0.025 | 8.296 |
| 0 | 0.025 | 6.277 |
| 0 | 0.025 | 4.77 |
| 0 | 0.025 | 4.135 |
| 0 | 0.025 | 3.826 |
| 0 | 0.025 | 3.636 |
| 0 | 0.025 | 3.502 |
| 0 | 0.025 | 3.399 |
| 0 | 0 | 3.38 |
| 0.025 | 0 | 3.467 |
| 0.025 | 0 | 3.595 |
| 0.025 | 0 | 3.767 |

Table D-2 continued…

| | | |
|---|---|---|
| 0.025 | 0 | 4.043 |
| 0.025 | 0 | 4.574 |
| 0.025 | 0 | 5.92 |
| 0.025 | 0 | 8.332 |
| 0.025 | 0 | 9.545 |
| 0.025 | 0 | 9.934 |
| 0.025 | 0 | 10.15 |
| 0 | 0 | 9.986 |
| 0 | 0.025 | 9.713 |
| 0 | 0.025 | 9.179 |
| 0 | 0.025 | 7.8 |
| 0 | 0.025 | 5.669 |
| 0 | 0.025 | 4.578 |
| 0 | 0.025 | 4.075 |
| 0 | 0.025 | 3.806 |
| 0 | 0.025 | 3.629 |
| 0 | 0.025 | 3.51 |
| 0 | 0 | 3.529 |
| 0.025 | 0 | 3.661 |
| 0.025 | 0 | 3.869 |
| 0.025 | 0 | 4.22 |
| 0.025 | 0 | 5.021 |
| 0.025 | 0 | 6.895 |
| 0.025 | 0 | 9.045 |
| 0.025 | 0 | 9.747 |
| 0.025 | 0 | 10.044 |
| 0 | 0 | 9.962 |
| 0 | 0.025 | 9.3 |
| 0 | 0.025 | 7.776 |
| 0 | 0.025 | 5.79 |
| 0 | 0.025 | 4.685 |
| 0 | 0.025 | 4.136 |
| 0 | 0.025 | 3.834 |
| 0 | 0.025 | 3.643 |
| 0 | 0.025 | 3.508 |
| 0 | 0.025 | 3.399 |

COMPLEXATION DATA

Table D-3: 4.35E-08 M Pu-HA complexation data (1.5 weeks).

| Pu-Total[M] | Pu-HA [M] | log[H+] |
|---|---|---|
| 4.35E-08 | 3.09E-08 | -4.23 |
| 4.35E-08 | 3.11E-08 | -4.16 |
| 4.36E-08 | 3.09E-08 | -4.08 |
| 4.37E-08 | 3.28E-08 | -4.72 |
| 4.41E-08 | 3.32E-08 | -4.74 |
| 4.42E-08 | 3.31E-08 | -4.91 |
| 4.38E-08 | 3.30E-08 | -5.62 |
| 4.38E-08 | 3.25E-08 | -5.23 |
| 4.32E-08 | 3.32E-08 | -6.08 |
| 4.37E-08 | 3.34E-08 | -5.84 |
| 4.36E-08 | 3.45E-08 | -6.29 |
| 4.35E-08 | 3.55E-08 | -6.50 |
| 4.38E-08 | 3.53E-08 | -6.38 |
| 4.35E-08 | 3.13E-08 | -4.23 |
| 4.35E-08 | 3.17E-08 | -4.16 |
| 4.36E-08 | 3.00E-08 | -4.08 |
| 4.37E-08 | 3.30E-08 | -4.72 |
| 4.41E-08 | 3.34E-08 | -4.74 |
| 4.42E-08 | 3.30E-08 | -4.91 |
| 4.38E-08 | 3.32E-08 | -5.62 |
| 4.38E-08 | 3.27E-08 | -5.23 |
| 4.32E-08 | 3.30E-08 | -6.08 |
| 4.36E-08 | 3.49E-08 | -6.29 |
| 4.35E-08 | 3.55E-08 | -6.50 |
| 4.38E-08 | 3.50E-08 | -6.38 |

Table D-4: 4.90E-08 M Th-HA complexation data (1.5 weeks).

| Th-Total[M] | Th-HA[M] | log[H+] |
|---|---|---|
| 4.91E-08 | 3.73E-08 | -4.18 |
| 4.91E-08 | 3.77E-08 | -4.19 |
| 4.90E-08 | 4.16E-08 | -4.65 |
| 4.89E-08 | 4.19E-08 | -4.99 |
| 4.89E-08 | 4.22E-08 | -4.99 |
| 4.90E-08 | 4.23E-08 | -5.05 |
| 4.89E-08 | 4.36E-08 | -5.55 |
| 4.91E-08 | 4.36E-08 | -5.58 |
| 4.90E-08 | 4.47E-08 | -6.14 |
| 4.89E-08 | 4.38E-08 | -5.82 |
| 4.87E-08 | 4.45E-08 | -6.03 |
| 4.89E-08 | 4.45E-08 | -6.23 |
| 4.95E-08 | 4.55E-08 | -6.30 |
| 4.89E-08 | 4.44E-08 | -6.09 |
| 4.91E-08 | 3.79E-08 | -4.18 |
| 4.91E-08 | 3.80E-08 | -4.19 |
| 4.90E-08 | 3.85E-08 | -4.29 |
| 4.90E-08 | 4.09E-08 | -4.65 |
| 4.89E-08 | 4.24E-08 | -4.99 |
| 4.89E-08 | 4.24E-08 | -4.99 |
| 4.90E-08 | 4.25E-08 | -5.05 |
| 4.89E-08 | 4.37E-08 | -5.55 |
| 4.91E-08 | 4.39E-08 | -5.58 |
| 4.90E-08 | 4.45E-08 | -6.14 |
| 4.89E-08 | 4.40E-08 | -5.82 |
| 4.87E-08 | 4.46E-08 | -6.03 |
| 4.89E-08 | 4.53E-08 | -6.23 |
| 4.95E-08 | 4.58E-08 | -6.30 |
| 4.89E-08 | 4.49E-08 | -6.09 |

Table D-5: 2.60E-07 M Pu-HA complexation data (24 hours).

| Pu-Total[M] | Pu-HA [M] | log[H+] |
|---|---|---|
| 2.62E-07 | 1.25E-07 | -4.03 |
| 2.62E-07 | 1.30E-07 | -4.05 |
| 2.63E-07 | 1.46E-07 | -4.62 |
| 2.62E-07 | 1.55E-07 | -5.22 |
| 2.62E-07 | 1.55E-07 | -4.80 |
| 2.62E-07 | 1.59E-07 | -5.53 |
| 2.61E-07 | 1.64E-07 | -6.31 |
| 2.65E-07 | 1.77E-07 | -6.54 |
| 2.62E-07 | 2.03E-07 | -7.13 |
| 2.61E-07 | 2.03E-07 | -6.91 |

Table D-6: 2.60E-07 M Pu-HA complexation data (1 week).

| Pu-Total[M] | Pu-HA [M] | log[H+] |
|---|---|---|
| 2.62E-07 | 1.31E-07 | -4.05 |
| 2.62E-07 | 1.28E-07 | -4.07 |
| 2.63E-07 | 1.62E-07 | -4.63 |
| 2.62E-07 | 1.76E-07 | -5.09 |
| 2.62E-07 | 1.58E-07 | -4.79 |
| 2.62E-07 | 1.72E-07 | -5.46 |
| 2.61E-07 | 1.89E-07 | -6.42 |
| 2.65E-07 | 1.79E-07 | -5.81 |
| 2.62E-07 | 2.17E-07 | -7.1 |
| 2.61E-07 | 2.02E-07 | -6.94 |

Table D-7: 2.60E-07 M Pu-HA complexation data (2 weeks).

| Pu-Total[M] | Pu-HA [M] | log[H+] |
|---|---|---|
| 2.62E-07 | 1.34E-07 | -4.00 |
| 2.62E-07 | 1.35E-07 | -4.00 |
| 2.63E-07 | 1.54E-07 | -4.52 |
| 2.62E-07 | 1.73E-07 | -5.34 |
| 2.62E-07 | 1.62E-07 | -4.79 |
| 2.62E-07 | 1.76E-07 | -5.67 |
| 2.61E-07 | 2.03E-07 | -6.36 |
| 2.65E-07 | 1.79E-07 | -5.96 |
| 2.62E-07 | 2.25E-07 | -7.00 |
| 2.61E-07 | 2.11E-07 | -6.87 |

SORPTION DATA

BINARY

Table D-8: Data describing Pu(IV) sorption to gibbsite.

| [Pu](total) | pH | [Pu](24 hrs) | pH | [Pu](3 days) | pH | [Pu](1 week) |
|---|---|---|---|---|---|---|
| 1.09E-10 | 3.94 | 7.67E-12 | 4.12 | 6.27E-12 | 4.13 | 5.53E-12 |
| 1.10E-10 | 4.02 | 9.41E-12 | 4.23 | 6.88E-12 | 4.11 | 6.29E-12 |
| 1.08E-10 | 4.07 | 1.91E-11 | 4.25 | 1.01E-11 | 4.27 | 8.13E-12 |
| 1.09E-10 | 4.14 | 2.02E-11 | 4.32 | 1.20E-11 | 4.33 | 1.04E-11 |
| 1.04E-10 | 4.55 | 1.21E-11 | 4.66 | 8.26E-12 | 4.52 | 7.52E-12 |
| 1.07E-10 | 4.70 | 9.44E-12 | 4.73 | 9.08E-12 | 4.59 | 1.03E-11 |
| 1.06E-10 | 5.91 | 7.85E-12 | 6.08 | 1.16E-11 | 6.05 | 1.50E-11 |
| 1.07E-10 | 5.96 | 4.77E-12 | 6.13 | 5.47E-12 | 6.03 | 4.69E-12 |
| 1.07E-10 | 6.38 | 6.26E-12 | 6.58 | 7.58E-12 | 6.49 | 8.16E-12 |
| 1.11E-10 | 6.67 | 5.09E-12 | 6.86 | 6.56E-12 | 6.90 | 6.73E-12 |
| 1.03E-10 | 7.60 | 9.39E-13 | 8.76 | 8.39E-13 | 8.33 | 9.83E-13 |
| 1.05E-10 | 9.46 | 1.39E-12 | 9.11 | 2.87E-12 | 7.61 | 4.33E-12 |
| 1.09E-10 | 9.51 | 1.53E-12 | 8.53 | 2.63E-12 | 7.30 | 6.82E-12 |

Table D-9: Data describing Pu(V) sorption to gibbsite.

| [Pu](total) | pH | [Pu](24 hrs) | pH | [Pu](3 days) | pH | [Pu](1 week) |
|---|---|---|---|---|---|---|
| 1.10E-10 | 3.32 | 1.07E-10 | 3.44 | 1.05E-10 | 3.60 | 1.04E-10 |
| 1.09E-10 | 3.55 | 1.04E-10 | 3.74 | 1.03E-10 | 4.19 | 1.02E-10 |
| 1.10E-10 | 4.06 | 1.03E-10 | 4.37 | 1.02E-10 | 4.41 | 1.01E-10 |
| 1.09E-10 | 4.86 | 1.02E-10 | 4.96 | 1.00E-10 | 5.27 | 9.48E-11 |
| 1.09E-10 | 5.42 | 9.68E-11 | 5.62 | 9.50E-11 | 5.82 | 8.72E-11 |
| 1.12E-10 | 5.68 | 9.78E-11 | 6.09 | 9.03E-11 | 6.27 | 7.35E-11 |
| 1.11E-10 | 6.01 | 8.62E-11 | 6.37 | 7.57E-11 | 6.34 | 6.44E-11 |
| 1.19E-10 | 6.69 | 5.08E-11 | 6.72 | 5.03E-11 | 6.63 | 4.42E-11 |
| 1.10E-10 | 6.72 | 5.06E-11 | 7.05 | 4.19E-11 | 6.84 | 3.42E-11 |
| 1.09E-10 | 7.06 | 2.68E-11 | 6.80 | 3.19E-11 | 6.80 | 2.84E-11 |
| 9.99E-11 | 7.11 | 3.34E-11 | 6.99 | 3.05E-11 | 7.02 | 2.83E-11 |
| 1.11E-10 | 7.20 | 1.89E-11 | 6.97 | 2.03E-11 | 7.08 | 1.75E-11 |
| 1.09E-10 | 7.34 | 6.46E-12 | 7.17 | 8.85E-12 | 7.07 | 7.21E-12 |
| 1.09E-10 | 8.86 | 2.25E-12 | 7.57 | 4.07E-12 | 7.24 | 5.01E-12 |

TERNARY

Table D-10: Stock solution concentrations.

| | |
|---|---|
| $^{242}$Pu stock solution concentration: | 3.38E-06 M |
| Concentration gibbsite stock solution: | 119.97 g/L |

Table D-11: Ternary, Pu-HA-gibbsite, sample preparation

| Sample | Gibbsite soln (g) | HA soln (g) | 0.1 M NaCl (g) | Pu-HA-ws (g) | Pu 242 conc. [M] | Conc. Gibbsite (g/L) |
|---|---|---|---|---|---|---|
| Pu-HA-Gibb-4-1 | 1.0804 | 1.0102 | 10.0243 | 0.0170 | 4.7207E-09 | 10.6391 |
| Pu-HA-Gibb-4-2 | 1.0728 | 0.9927 | 9.9871 | 0.0146 | 4.0840E-09 | 10.6418 |
| Pu-HA-Gibb-4-3 | 1.0728 | 0.9874 | 9.9281 | 0.0747 | 2.0901E-08 | 10.6446 |
| Pu-HA-Gibb-4-4 | 1.0666 | 1.0108 | 9.8998 | 0.0746 | 2.0892E-08 | 10.5929 |
| Pu-HA-Gibb-4-5 | 1.0695 | 0.9942 | 9.8723 | 0.1482 | 4.1351E-08 | 10.5824 |
| Pu-HA-Gibb-4-6 | 1.0705 | 0.9953 | 9.8839 | 0.1480 | 4.1249E-08 | 10.5805 |
| Pu-HA-Gibb-4-7 | 1.0693 | 1.0052 | 9.7680 | 0.2233 | 6.2421E-08 | 10.6000 |
| Pu-HA-Gibb-4-9 | 1.0676 | 0.9998 | 9.7344 | 0.2968 | 8.2777E-08 | 10.5589 |
| Pu-HA-Gibb-4-10 | 1.0629 | 1.0035 | 9.7630 | 0.2970 | 8.2643E-08 | 10.4883 |
| Pu-HA-Gibb-6-1 | 1.0674 | 1.0004 | 9.9925 | 0.0146 | 4.0843E-09 | 10.5889 |
| Pu-HA-Gibb-6-2 | 1.0644 | 1.0091 | 10.0188 | 0.0156 | 4.3477E-09 | 10.5196 |
| Pu-HA-Gibb-6-3 | 1.0418 | 1.0054 | 9.9143 | 0.0740 | 2.0771E-08 | 10.3700 |
| Pu-HA-Gibb-6-4 | 1.0647 | 1.0144 | 9.9451 | 0.0741 | 2.0675E-08 | 10.5343 |
| Pu-HA-Gibb-6-5 | 1.0652 | 1.0062 | 9.8864 | 0.1472 | 4.1086E-08 | 10.5435 |
| Pu-HA-Gibb-6-7 | 1.0669 | 1.0144 | 9.8031 | 0.2238 | 6.2468E-08 | 10.5606 |
| Pu-HA-Gibb-6-8 | 1.0489 | 1.0162 | 9.8066 | 0.2224 | 6.2150E-08 | 10.3945 |
| Pu-HA-Gibb-6-9 | 1.0658 | 1.0021 | 9.7248 | 0.2953 | 8.2570E-08 | 10.5681 |
| Pu-HA-Gibb-6-10 | 1.0676 | 0.9988 | 9.6930 | 0.2954 | 8.2743E-08 | 10.6046 |

Table D-12: Aqueous phase Pu concentration in the ternary system: Pu-HA-gibbsite.

| Aqueous Pu concentration [M] | | | |
|---|---|---|---|
| < 100 nm (2 weeks) | < 1500 nm (3 weeks) | < 100 nm (3 weeks) | 3 kDa (3 weeks) |
| 8.39E-11 | 2.04E-10 | 4.07E-11 | 1.63E-10 |
| 4.10E-11 | 1.63E-10 | 4.06E-11 | 2.93E-11 |
| 2.87E-10 | 6.49E-10 | 8.14E-11 | 5.73E-11 |
| 2.74E-10 | 6.91E-10 | 8.14E-11 | 5.39E-11 |
| 2.86E-10 | 1.50E-09 | 2.45E-10 | 1.42E-10 |
| 3.26E-10 | 1.98E-09 | 3.26E-10 | 1.31E-10 |
| 6.93E-10 | 2.64E-09 | 5.70E-10 | 2.36E-10 |
| 7.76E-10 | 2.92E-09 | 5.68E-10 | 3.86E-10 |
| 2.61E-09 | 2.94E-09 | 7.28E-10 | 4.80E-10 |
| 4.07E-11 | 3.49E-10 | 0.00E+00 | 2.91E-11 |
| 4.24E-11 | 2.44E-10 | 0.00E+00 | 0.00E+00 |
| 5.51E-10 | 1.50E-09 | 1.62E-10 | 2.82E-11 |
| 8.17E-11 | 1.42E-09 | 8.35E-11 | 3.12E-11 |
| 4.49E-10 | 2.77E-09 | 1.17E-10 | 5.45E-11 |
| 4.08E-10 | 4.93E-09 | 3.26E-10 | 5.19E-11 |
| 1.32E-09 | 5.54E-09 | 3.27E-10 | 5.05E-11 |
| 4.92E-10 | 6.85E-09 | 3.27E-10 | 5.61E-11 |
| 4.83E-10 | 6.08E-09 | 2.86E-10 | 8.20E-11 |

REFERENCES


1. Andre C, Choppin, GR. Reduction of Pu(V) by humic acid. Radiochim Acta 2000; 88: 613-16.
2. Argonne National Laboratory E. Human health fact sheet: Plutonium. Argonne, IL: Argonne National Laboratory; 2005.
3. Banik NL, Buda RA, Burger S, Kratz JV, Trautmann N. Speciation and interactions of plutonium with humic substances and kaolinite in aquifer systems. J Alloys Compd 2007;444(445):522-5.
4. Boukhalfa H, Reilly SD, Smith WH, Neu MP. EDTA and Mixed-Ligand Complexes of Tetravalent and Trivalent Plutonium. Inorg. Chem. 2004; 43(19):5823.
5. Boukhalfa H, Reilly SD, Neu MP. Complexation of Pu(IV) with the Natural Siderophore Desferrioxamine B and the Redox Properties of Pu(IV)(siderophore) Complexes. Inorg. Chem. 2007; 46(3):1026.
6. Buda RA, Banik NL, Kratz JV, Trautmann N. Studies of the ternary systems humic substances - kaolinite - Pu(III) and Pu(IV). Radiochim Acta 2008; 96: 657-65.
7. Buffle J, Greter FL, Haerdi W. Measurement of complexation properties of humic and fulvic acids in natural-waters with lead and copper ion-selective electrodes. Anal Chem 1977;49(2):216-22.
8. Choppin GR. Actinide speciation in the environment. Radiochimica Acta 2003; 91: 645–649.

9. Clark DL, Hecker SS, Jarvinen GD, Neu MP, editors. The Chemistry of the Actinide and Transactinide Elements. 3rd ed. Netherlands: Springer; 2006. Volume 2 - Plutonium.
10. Ephraim JH, Xu H. The binding of cadmium by an aquatic fulvic-acid - a comparison of ultrafiltration with ion-exchange distribution and ion-selective electrode techniques. Sci Total Environ 1989; 81-2:625-34.
11. Glaus MA, Hummel W, Vanloon LR. Equilibrium dialysis ligand-exchange - adaptation of the method for determination of conditional stability-constants of radionuclide fulvic-acid complexes. Anal Chim Acta 1995; 10: 303(2-3):321-31.
12. Hebert HJ. Nuclear waste won't be going to Nevada's Yucca Mountain, Obama official says. Chicago Tribune March 6, 2009.
13. Herbelin, A, Westall, JC. 1999. FITEQL: A computer program for determination of chemical equilibrium constants from experimental data [computer program], v. 4.0. Dep. of Chemistry, Oregon State University, Corvallis, OR
14. [Internet]: International Humic Substances Society (IHSS) cited 2010. Available from: http://ihss.gatech.edu/ihss2/
15. Kaplan, DI, Powell, BA, Duff, M., Demirkanli, DI, Denham, M, Fjeld, RA, Molz, FJ. Influence of sources on plutonium mobility and oxidation state transformations in vadose zone sediments. Env. Sci. Tech. 2007, 41, 7417-7423.
16. Kersting AB, Efurd DW, Finnegan DL, Rokop DJ, Smith DK, Thompson JL. Migration of plutonium in ground water at the Nevada Test Site. Nature 1999; 397(6714)- 59.

17. Kim JI, Czerwinski KR. Complexation of metal ions with humic acid: metal ion charge neutralization model. Radiochimica Acta 1996; 73: 5-10.
18. Meyer M, Burgat R, Faure S, Batifol B, Hubinois JC, Chollet H, Guilard R. Thermodynamic studies of actinide complexes. 1. A reappraisal of the solution equilibria between plutonium(IV) and ethylenediaminetetraacetic acid (EDTAH(4)) in nitric media. Comptes Rendus Chimie. 2007; 10: 929-947.
19. Millipore. Amicon® Ultra-4 centrifugal filter manual. 2010.
20. Neck V, Altmaier M, Seibert A, Yun JI, Marquardt CM, Fanghaenel T. Solubility and redox reactions of Pu(IV) hydrous oxide: Evidence for the formation of $PuO_{2+x}$(s, hyd). Radiochim Acta 2007; 95(4):193-207.

12. Neck V, Kim JI. Solubility and hydrolysis of tetravalent actinides. Radiochim Acta 2001; 89(1):1-16.
13. Orlandini KA, Penrose, WR, Nelson, DM. Pu(V) as the stable form of oxidized plutonium in natural waters. Marine chemistry 1986; 18: 49-57.
14. Powell BA, Rao L, Nash KL. Effect of 1-hydroxyethane-1,1-diphosphonic acid (HEDPA) on partitioning of Np and Pu to synthetic boehmite. Sep. Sci. Tech., 2010; 45: 1-11.
15. Powell BA, Zavarin MK, Kersting AB, Zhao P. Development of a composite non-electrostatic surface complexation model describing plutonium sorption to aluminosilicates. Lawrence Livermore National Laboratory 2008. Report LLNL-TR-408276.

16. Powell BA, Duff MC, Kaplan DI, Bertsch PM, Coates JT, Eng P, Fjeld RA, Hunter DB, Newville M, Rivers ML, Serkiz SM, Sutton SR, Triay IR, Vaniman DT. Plutonium oxidation and subsequent reduction by Mn(IV) minerals in Yucca Mt. tuff. Env. Sci. Tech. 2006; 40(11): 3508-3514.

17. Powell BA, Fjeld RA, Kaplan DI, Coates JT, Serkiz SM. $Pu(V)O_2^+$ Adsorption and reduction on synthetic goethite and hematite Env. Sci. Tech. 2005; 39(7): 2107-2114.

18. Powell BA, Fjeld RA, Kaplan DI, Coates JT, Serkiz SM. $Pu(V)O_2^+$ Adsorption and reduction on synthetic magnetite ($Fe_3O_4$). Env. Sci. Tech. 2004; 38: 6016-6024.

19. Reiller P, Moulin V, Casanova F, and Dautel C. On the study of Th(IV)-humic acid interactions by competition sorption studies with silica and determination of global interaction constants. Radiochim Acta 2003; 91: 513-524.

20. Righetto L, Bidoglio G, Azimonti G, Bellobono IR. Competitive actinide interactions in colloidal humic-acid mineral oxide systems. Environ Sci Technol. 1991; 25(11):1913-9.

21. Ritchie JD, Perdue EM. Proton-binding study of standard and reference fulvic acids, humic acids, and natural organic matter. Geochim Cosmochim Acta. 2003; 67(1):85-96.

22. Roberts KA, Santschi PH, Honeyman BD. Pu(V) reduction and enhancement of particle-water partitioning by exopolymeric substances. Radiochim Acta 2008; 96(9-11):739-45.

23. Santschi PH, Roberts KA, Guo LD. Organic mature of colloidal actinides transported in surface water environments. Environ Sci Technol 2002; 36(17):3711-9.
24. Schafer T, Artinger R, Dardenne K, Bauer A, Schuessler W, Kim JI. Colloid-borne americium migration in Gorleben groundwater: Significance of iron secondary phase transformation. Environ Sci Technol 2003; 37(8):1528-34.
25. Schindler PW. Co-adsorption of metal-ions and organic-ligands - formation of ternary surface complexes. Rev Mineral 1990; 23:281-307.
26. Silva RJ, Nitsche H. Actinide environmental chemistry. Radiochimica Acta 1995; 70(71):377.
27. Soderholm L, Almond PM, Skanthakumar S, Wilson RE, Burns PC. The structure of the plutonium oxide nanocluster [Pu38O56Cl54(H2O)(8)](14-). Angew Chem 2008; 47(2):298-302.
28. Sposito G. Soil organic matter. In: The Chemistry of Soils. Oxford University Press; 1989.
29. Stevenson IL, Schnitzer M. Transmission electron-microscopy of extracted fulvic and humic acids. Soil Sci 1982; 133(3):179-85.
30. Stumm W. Chemistry of the Solid-Water Interface: Processes at the Mineral-Water and Particle-Water Interface in Natural Systems. Wiley, 1992.
31. United States Department of Energy: Nevada Operations Office. United States nuclear tests: July 1945 through september 1992. Las Vegas, Nevada: United States Department of Energy; 2000. Report nr DOE/NV--209-REV 15.

32. Van Loon LR, Granacher S, Harduf H. Equilibrium dialysis—ligand exchange: A novel method for determining conditional stability constants of radionuclide—humic acid complexes. Analytica Chimica Acta 1992; 268(2):235-46.

33. Wang XK, Rabung T, Geckeis H. Effect of pH and humic acid on the adsorption of cesium onto gamma-$Al_2O_3$. J Radioanal Nucl 2003; 258(1):83-7.

34. Westall JC, Jones JD, Turner GD, Zachara JM. Models for association of metal-ions with heterogeneous environmental sorbents .1. Complexation of Co(II) by Leonardite humic-acid as a function of pH and $NaClO_4$ concentration. Environ Sci Technol 1995; 29(4):951-9.